Brunel UNIVERSITY WEST LONDON

ANALYSIS OF TELOMERE MAINTENANCE IN ARTEMIS DEFECTIVE HUMAN CELL LINES

A thesis submitted for the degree of doctorate of philosophy

by

Hemad Yasaei

Division of Biosciences
School of Health Sciences and Social Care
September 2009

Abstract

Telomeres are physical ends of chromosomes consisting of $(TTAGGG)_n$ DNA sequence and a specialized set of proteins that protect chromosomal ends from degradation and from eliciting DNA damage response. These specialized set of proteins, known as shelterin, directly bind to telomeric DNA. In addition, some DNA double-strand break (DSB) repair proteins such as, DNA-PKcs and KU70/80, play active roles in telomere maintenance. Mouse knock-out experiments have revealed that deletion of either DNA-PKcs or Ku70/80 resulted in elevated levels of telomeric fusion, indicative of dysfunctional telomeres. Artemis protein is involved in DNA DSB repair through non-homologous end joining (NHEJ) and it is phosphorylated by DNA-PKcs. Human cells defective in Artemis have been identified and shown to be radiosensitive and patients with an Artemis defective gene suffer from radiosensitive severe-combined immune deficiency syndrome (RS-SCID). Mouse cells defective in Artemis have elevated levels of telomeric fusion.

We have demonstrated in this thesis that Artemis defective human cell lines show a mild telomeric dysfunction phenotype detectable at the cytological level. The nature of telomere dysfunction phenotype appears to be similar to that observed in DNA-PKcs defective cells as exemplified by the presence of IR induced chromatid telomeric fusions. We have also shown that (a) DNA damage occurring within the telomeric DNA is difficult to repair or irreparable in older cells and that (b) Artemis defective older cells show higher proportion of DNA damage at telomeres than their normal counterparts. Finally, we have demonstrated that inhibition of DNA-PKcs causes (a) an increase in telomeric fusions in Artemis defective cell lines relative to both normal cell lines after inhibition and Artemis cell lines before inhibition and (b)

elevated levels of DNA damage at telomeres following exposure of cells to radiation relative to both irradiated normal cells exposed to a DNA-PKcs inhibitor and irradiated Artemis defective cells but not exposed to the DNA-PKcs inhibitor. These results suggest that the effects of Artemis and DNA-PKcs on telomeres are cumulative. We have also performed (a) experiments to examine telomere function in Artemis defective cell lines after knocking down DNA-PKcs levels by RNAi and b) preliminary experiments to knock-down Artemis in DNA-PKcs defective cells. Taken together, our results suggest that the Artemis defect causes mild telomere dysfunction phenotype in human cells.

Publications:

- Defective Artemis causes mild telomere dysfunction (Yasaei H. and Slijepcevic P.), 2010, Genome Integrity (*in press*)

- Inhibition of kinase activity of DNA-protein kinase causes telomere shortening in mouse lymphoma cells but not in Artemis defective human cells. (Yasaei H. and Slijepcevic P. 2010) (working title, manuscript in preparation)

Acknowledgement

My deepest gratitude must firstly be conveyed to Dr. Predrag Slijepcevic, whose excellent supervision, support, guidance from day one has enabled me to submit this thesis. He believed in my ability and showed me the way and trained me to become a scientist. I am grateful for his encouragement in the loneliest of times, been the shining light that illuminated the path towards my success.

I must also thank my second supervisor, Dr. Christopher Parris, whom offered guidance, help and encouragement with his positive thinking and great sense of humour, and to be there for me whenever I needed a quick discussion or a friendly chat. I also must thank, Professor Robert Newbold, the Director of the Brunel Institute of Cancer Genetics, for which I performed all my research within BICGP. Also I must say a special thanks to Dr. Terry Roberts, for his expert advice on molecular biology and real-time qPCR, and plus being a great friend. My thanks also goes to Mrs. Rana Hassan, for her help on molecular biology and those little skills she showed me that have made a huge difference in my research. I also must thank Mrs. Christine Newton for her training in the tissue culture lab.

The work presented in this thesis was supported by RISC-RAD grant awarded to Dr. Predrag Slijepcevic under European Commission framework 6.

Finally, I would like to thank my family for their perpetual love and support, specially my wife, Ghazaleh, whose love, support and encouragement was like a scaffold that supported me during the final years of my research. For those reasons and more I dedicate this thesis to my beautiful wife, Ghazaleh Movasaghi.

Abbreviations

ATM	Ataxia telangastia mutated protein
BME	beta-mercaptoethanol
BSA	Bovine serum albumin
CA	Chromosomal aberration
ChIP	Chromatin immuneprecipitation
cDNA	complementary DNA
DDR	DNA damage response
DEPC	Diethyl pyrocarbonate
DMEM	Dulbecco modified eagle medium
DMSO	Dimethylsulfoxide
DNA	Deoxyribonucleic acid
DNA-PK	DNA-protein kinase
DNA-PKcs	DNA-protein kinase catalytic-subunit
DNA-PKcsi	DNA-protein kinase catalytic-subunit inhibitor
DSB	Double strand breaks
dsDNA	double stranded DNA
DTT	Dithiothreitol
DW	Distilled water
ES	Embryonic stem cells
FACS	Fluorescence activated cell sorting
FCS	Fetal calf serum
FISH	Fluorescence in-situ hybridization
FITC	Fluorescein isothiocynate
gDNA	genomic DNA
Gy	Gray
HR	Homologous recombination
HRP	Horseradish peroxidase
IF	Immunofluorescence
IF-TIF	Immunofluorescence-Telomere dysfunction induced foci
IPA	Iso propyl alcohol
IR	Ionising Radiation
LOF	Loss of function
LY-R	Radioresistant mouse lymphoma cells
LY-S	radio-sensitive mouse lymphoma cells
MCS	Missing chromatid signal
Myb	A human proto-oncogene
miRNA	microRNA
NHEJ	Non-homologous end joining
NICGM	National Institute of General Medical Sciences
PBS	Phosphate buffer saline
PCR	Polymerase chain reaction

PD	population doubling
PI	Propidium iodide
piRNA	Piwi-interacting RNA
PNA	Peptide nucleic acid
POT1	Protection of telomeres 1
PVDF	Polyvinylidene fluoride
Q-FISH	Quantitative in-situ hybridization
RAP1	Repressor activator protein 1
RISC	RNAi silencing complex
RNA	Ribonucleic acid
RNAi	Ribonucleic acid interference
RPM	Revolution per minute
RS-SCID	Radiosensitive severe-combined immunodeficiency syndrome
RT-PCR	Reverse transcriptase-polymerase chain reaction
SCID	Severe-combined immunodeficiency syndrome
SD	Standard deviation
SDS	Sodium dodecyl sulphate
SEM	Standard error of mean
siRNA	Short interfering ribonucleic acid
SQ	Serine/threonine motif sites
SSC	Sodium chloride sodium citric acid
ssDNA	single stranded DNA
T-loop	Telomeric-loop
TBE	Tris-borate-EDTA
TBST	Tris-buffered saline tween-20
Telo-FISH	Telomeric fluorescence in-situ hybridization
TEMED	Tetramethylethylenediamine
TFI	Telomeric fluorescence intensity
TIF	Telomere dysfunction induced foci
TIN2	TRF1-interacting factor
TPP1	Tripeptidyl peptidase I
TRF1	Telomeric repeat binding factor 1
TRF2	Telomeric repeat binding factor 2
UV	Ultra violet

Table of Contents

List of Tables

List of Figures

Chapter 1 : General Introduction

1.1 Telomere structure and function

Telomeres are specialized structures found at the end of most eukaryotic and all of mammalian chromosomes. The combined action of telomeric DNA, telomere associated proteins, and telomerase, facilitate the protection, degradation, and in some cases fusion of mammalian chromosomal ends (de Lange, 2006). The highly conserved DNA component of telomeres in humans was first described by Moyzis and colleagues in 1988. They showed telomeres to be comprised of a tandem of guanine-rich repeats of $(TTAGGG)_n$ (Moyzis et al., 1988). Human telomeres were found to be 10kb long at birth and gradually shorten with cell division (de Lange et al., 1990), although human telomere length may vary between 2kb – 30kb in telomerase positive human cell lines (de Lange, 2006). With each cell cycle, in telomerase-negative cell lines, telomere length gets shorter at a rate of 50-300bp/population doubling (Huffman et al., 2000). James Watson was the first to observe the problem with replicating telomeres and called it the "end replication problem" (Watson, 1972) (Figure 1.1). However it was a Russian scientist that linked the end replication problem to telomere shortening (Olovnikov, 1973). Olovnikov then linked cellular aging to telomere shortening and called it marginotomy (Olovnikov, 1973). It is now understood that telomere shortening is a major cause of replicative senescence in human cells lacking telomerase activity. It was shown in 1997 that telomeres of many eukaryotes including mammals have a 3´ overhang (Makarov et al., 1997). In his paper, Makarov proposed a new model for telomere replication that extended Watson's and Olivnokov's end replication problem and proposed that there is a much greater degradation at the 5´ of the lagging strand that leaves a long 3'

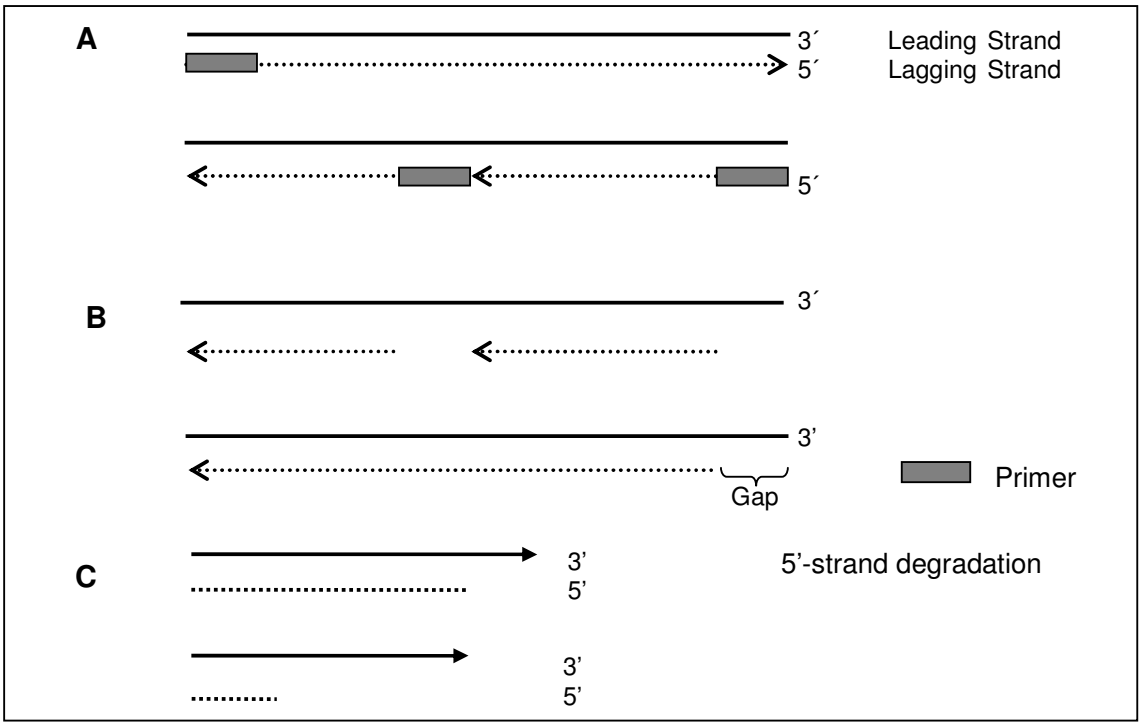

Figure 1.1 Conventional end replication problem
A| The end replication problem applies to the lagging strand of DNA during replication processes. The leading strand is replicated in a continuous fashion. **B**| Formation of an Okazaki fragment in the lagging strand and subsequent degradation of primers leaves a gap of around 8-12bp in the 5´ end of lagging strand that cannot be replicated and is lost during cell division. **C**| Revised model predicts a greater degradation at 5' end of both DNA strands (lagging and leading), leaving a long 3' overhang at both ends. This revised model was first proposed by (Makarov et al., 1997).

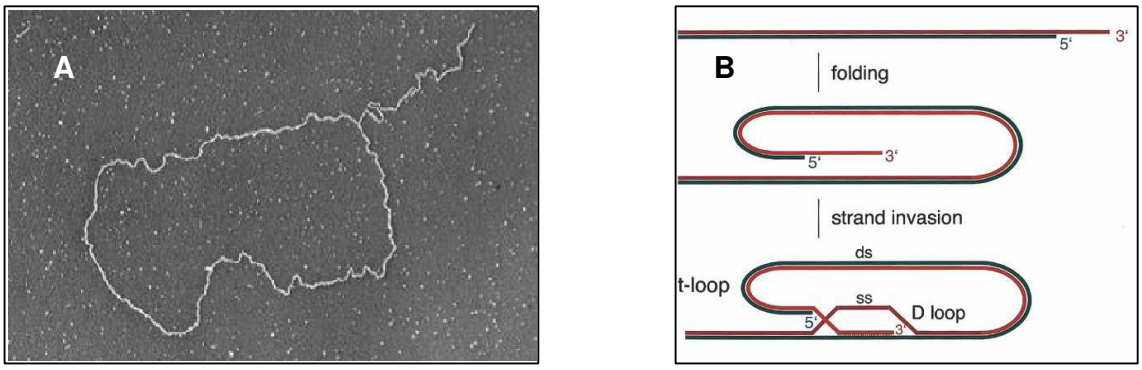

Figure 1.2 T-Loop Structure
A| Electron Microscopy image of purified human telomeres revealing the lariat structure known as T-loop. (Griffith et al., 1999) B| The 3´overhang of single stranded DNA invades the dsDNA forming a larger T-loop and smaller D-Loop(de Lange, 2005).

overhang (Makarov et al., 1997) composed of TTAGGG repeats and it could be several hundred nucleotides long (Wright et al., 1997). The long 3' overhang (50-300bp) has a crucial function and it was shown in 1999 to form a telomeric loop (t-loop) by folding back and invading the double stranded DNA (dsDNA) (Griffith et al., 1999). The formation of a t-loop hides the 3´ overhang from telomerase and from DNA repair and degradation activities (Figure 1.2) (Blasco, 2007).

1.2 Proteins associated with mammalian telomeres

Factors associated with human telomeric DNA are divided into three groups: 1. Nucleosomes, 2. Proteins directly bound to t-loops and D-loops known as shelterin, 3. Other factors, namely DNA-damage response proteins found to function elsewhere in the cell but also found to be associated with telomere maintenance.

1.2.1 Shelterin

There are six proteins that were found to be directly associated with telomeric DNA at the end of the human chromosome and they are known by a collective name shelterin (de Lange 2006). Two of these proteins, telomere repeat factor 1 (TRF1) and telomere repeat factor 2 (TRF2) are directly bound to the double stranded telomeric DNA. Protection of telomeres 1 (POT1) binds to single stranded, TTAGGG repeats of telomeric DNA. The protein interaction between TRF1, TRF2, and POT1 holds together and protects the t-loop formation of the telomere (de Lange, 2006). TRF1 and TRF2 complexes regulate telomere length and function (de Lange, 2002). Inhibition of TRF2 in human culture cells causes telomere dysfunction (de Lange, 2002). By depleting TRF2, the cell perceives telomere sites as DNA damage sites. Depending on cell types, depletion of TRF2 induces either apoptosis or triggers senescence by activating ATM and p53 (de Lange, 2002). For example, inhibition of

TRF2 in primary fibroblast initiates senescence via p53 activation and/or p16/Rb inhibition, whilst in primary lymphocytes TRF2 inhibition causes cellular apoptosis via ATM/p53 activation (de Lange, 2002). The three protein complexes of TRF1, TRF2, and POT1 have a strong affinity to bind only to the telomeric DNA due to five DNA-binding domains that recognize TTAGGG repeats of telomeric DNA (de Lange, 2005). Three other members of shelterin are TIN2, Rap1, and TPP1. TIN2 interacts directly with TRF1 and TRF2 to regulate telomere length and it is also shown to bind to POT1 through TPP1 (de Lange, 2006). TIN2 also stabilizes TRF2 to bind with telomeric DNA and can be lethal to a cell when both TRF2 and TIN2 are depleted and show telomere deprotection phenotype (Kim et al., 2004).

Human Rap1 is a TRF2 interacting protein that contains a conserved MYB DNA binding domain which is necessary for it to bind with telomeric DNA. Because of a weak positive charge Rap1 is unable to bind directly to telomeric DNA and hence interacts with TRF2 (Li et al., 2000). TRF2's and Rap1's protein interaction regulates telomere length and also affects telomere length heterogeneity (Li et al., 2000). TPP1 is the most recently identified telomere binding protein that interacts with POT1 and TIN2, and helps in the recruitment of POT1 to telomeres (Ye et al., 2004).

1.2.2 Nucleosome

Besides proteins that are directly associated with telomeric DNA, nucleosomes were also found to bind to telomeres (Tommerup et al., 1994). Modified versions of histone proteins were found associated with heterochromatin. Several of histone proteins including, heterochromatic protein 1 (HP1), isoforms of HP1 (HP1α), histone 3 trimethylated at lysine 9 (H3-K9), and histone 4 trimethylated at lysine 20 (H4-K20), suppressor of variegation 3-9 homologue (SUV39H), suppressor of variegation

4-20 homologue (SUV4-20H), and histone methyltransferases (HMTases) are found at heterochromatin near the telomeric ends of chromosomes (Blasco, 2005). The retinoblastoma (RB) family of proteins were also found to be required for the trimethylation of H4-K20 at both telomeres and centromeres (Gonzalo et al., 2005, Blasco, 2005). The novel role of the RB-family of proteins, apart from its function in cellular proliferation, is in histone modification which interacts directly with SUV4-20H HMTases that regulate telomeric and pericentric heterochromatin. Hence the novel role of the RB-family of proteins in chromatin remodelling, chromosome segregation, and telomere length control (Blasco, 2005). Loss of the RB-family of proteins leads to the abnormal elongation of telomeres (Gonzalo et al., 2005). The abnormal elongation of telomeres can be explained by the loss of the heterochromatin at telomeres that leads to a less compact chromatic structure. This in turn, results in abnormal telomere elongation due to an increased access of telomerase or other telomere-elongating activities to the telomere (Blasco, 2005).

1.3 Telomere length regulation

Normal somatic cells cannot elongate their telomeres so the telomere length eventually gets shorter in each cell cycle until it reaches critical length when cells stop dividing and enter the senescence state. Telomeric proteins mentioned above have a role in protecting telomeres. The telomerase enzyme (an enzyme responsible for elongating telomeric DNA) is present in germ line cells, cancer cells, and immortal cell lines but it is usually below the level of detection in somatic cells (Greider and Blackburn, 1985). However, Masutomi et al 2003, found a small quantity of telomerase enzyme in primary presenescence cells that exhibited hTERT (a ribonucleoprotien that functions with telomerase to maintain telomeric DNA length)

activity in S-phase and argued that telomere shortening on its own cannot trigger senescence and cells need the bimodal action of hTERT depletion and telomere shortening (Masutomi et al., 2003).

Shelterin proteins sense telomere length through their ability to bind and accumulate at telomeric binding sites with their TTAGGG binding motifs. They protect and prevent the access of the telomerase enzyme to the telomeric sites and hence prevent telomere elongation. A model proposed by de Lange explains the telomere length homeostasis and the role shelterin plays in telomere end protection (see Figure 1.3, de Lange 2006). Telomere length homeostasis therefore is affected by all components of shelterin.

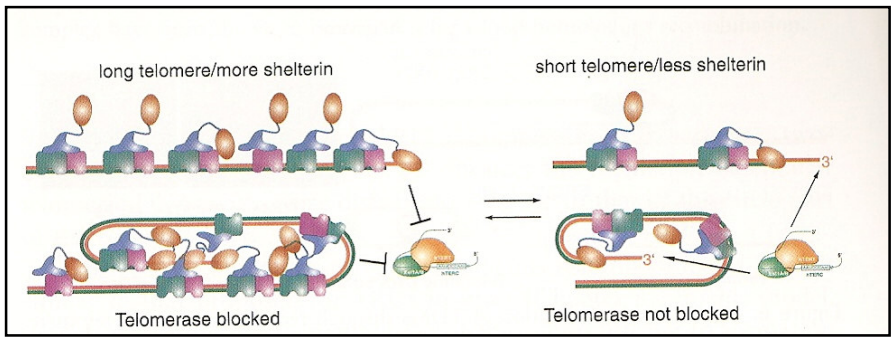

Figure 1.3 Telomere length homeostasis.
Long telomeres will contain more shelterin with the binding of POT1 to the 3' overhang. This blocks the access of telomerase whereas shorter telomeres will have less shelterin proteins and therefore easier access for the telomerase enzyme (de Lange, 2006).

Tankyrase is a protein involved in telomere maintenance but it is not part of the shelterin complex . It has a modulating effect on TRF1 and causes the release of TRF1 from telomeric DNA (Mattuli, 2007, de Lange, 2006). Overexpression of tankyrase also reduces the amount of POT1 on telomeres and hence explains the induction of telomere elongation in cells with excess tankyrase expression in the

nucleus. Tankyrase 1 has an ankyrin domain and a catalytic domain of the poly(ADP-ribose) polymerases (PARPs) with an amino terminus motif similar to that of TRF1 (Smith et al., 1998, Smith and de Lange, 2000).

Several other non-shelterin proteins affect telomere length regulation in human cells, including Nijmegan breakage syndrome 1 (Nbs1) and Est1A/SMG6 (*Ever Shorter Telomeres, EST*) that mediate telomere elongation (de Lange, 2006). However, in mouse cell lines, a deficiency in DNA-PK causes altered telomere length (Hande et al., 1999) and mouse cells lacking all three of the Rb-family of proteins are shown to have longer telomere length than normal. Other factors affecting telomere length are PARP1, Rad54, Rad51D, Suv39h1/2, heterogeneous nuclear ribonucleoprotein (hnRNP) and A1/UP1 (see for review de Lange, 2006).

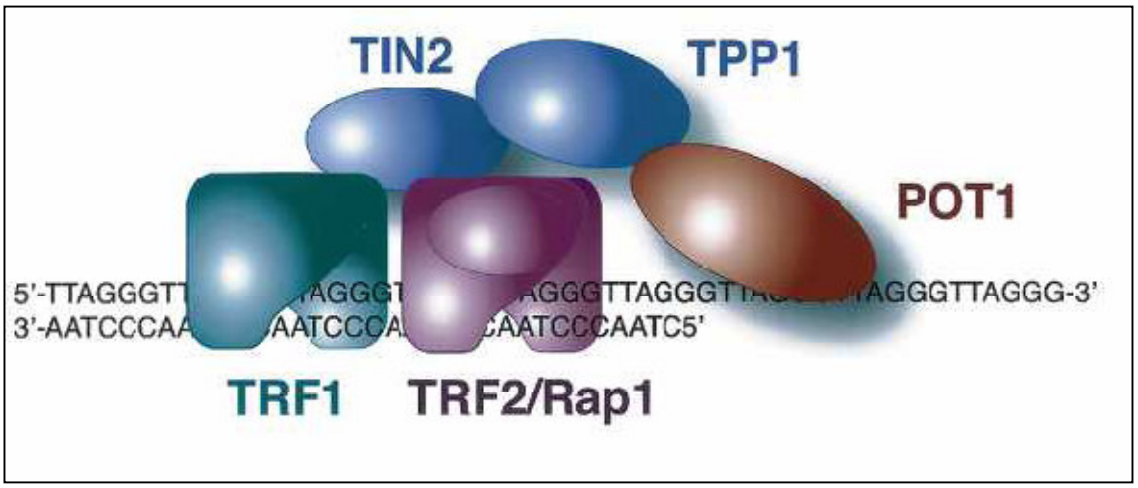

Figure 1.4. Shelterin proteins.
Schematic representation of shelterin proteins and their interaction with telomeric DNA. TRF1 and TRF2 directly bind to the TTAGGG repeats due to their Myb domain. Rap1 binds to TRF2 in a 1:1stoichiometry, and has a role in telomere length regulation and affects telomere length heterogeneity. POT1 binds to the single stranded 3´ overhang. TIN2 and TPP1 link POT1 to TRF1/TRF2. Shelterin proteins protect telomeres and hold together the lariat structure of telomeres (de Lange, 2006).

1.4 Telomere and DNA Damage Response Proteins

During the replication stage of the cell cycle, the compact structure of telomeric DNA is opened up to allow access to DNA replication machinery and therefore telomeres become subject to cellular repair machinery. In the opened up form telomeres resemble a DNA double strand break (DSB) and proteins involved in DNA damage response and repair mechanisms are then localized on telomeres (M. Matuli, 2007). However, Slijepcevic (2008), argues that the conventional model of telomeres acting as a protective mechanism, hiding telomeric DNA from DNA repair machinery constitutes a "paradox" with the finding that two of the non-homologous end joining (NHEJ) proteins, namely Ku70/80 and DNA-PKcs are physiologically present at telomeres and interact with shelterin (de Lange, 2005, Slijepcevic, 2008). Other proteins involved in DNA damage response that are found at telomeres include, Mre11, Rad50, Rad51, NBS1, ATM, WRN, PARP-2, ERCC1, XPF, BRCA1, RAD9, and PARP1 (Slijepcevic, 2008, M. Matuli, 2007, de Lange, 2005, Gitte De Boeck, 2009).

In some cases, these factors directly interact with shelterin proteins. For example, WRN helicase (protein that is mutated in Werner syndrome patients), and BLM helicase (mutated RecQ helicase protein in Bloom's syndrome) bind to TRF2 (Opresko et al., 2002). TRF2 directly interacts and recruits the MRN complex (Mre11, Rad50, NBS1) (de Lange, 2005). The MRN complex is a DNA damage sensor with multiple functions in genome integrity. Although each component of the MRN complex is found at varying concentrations at telomeric sites throughout the cell cycle, the concentration of the MRN complex is sharply increased when telomeres are de-protected, suggesting that the MRN complex recognizes

unprotected telomeres as sites of DNA breaks (de Lange, 2005, M. Matuli, 2007). One of the more recent shelterin interacting proteins discovered is hSnm1B or better known as Apollo. It has a 5´→3´ exonuclease activity and it was found to interact with TRF2 in telomere protection (Lenain et al., 2006, van Overbeek and de Lange, 2006). Table 1.1 summarizes all DNA damage response proteins that have links with telomere maintenance (Slijepcevic, 2006). Alteration in some of the DNA double strand break (DSB) repair proteins, namely Ku70/80 and DNA-PKcs have been associated with the telomere end capping function (Bailey et al., 1999). This function essentially prevents fusion between chromosomes and keeps them as separate entities. Mouse cell lines deficient in DNA-PKcs and in Ku70/80, or cells from mice genetically modified to lack these proteins have been shown to have an increased incidence of telomere end-to-end fusion, suggesting DNA-PKcs' and Ku70/80's dual role in repairing damaged DNA and also in telomeric end-capping (Bailey et al., 1999).

1.5 DNA DSB repair

Two pathways are responsible for the repair of DNA DSBs in mammalian cells. These pathways are: Non-homologous End Joining (NHEJ) and Homologous Recombination (HR). DSB is a form of DNA damage that can be caused by exogenous or endogenous agents. For example, exposure of the cell to ionising radiation (IR) can cause complex, clustered types of DSB lesions by the deposition of random energy. IR can also induce DBSs indirectly via the production of a reactive oxygen species (O'Driscoll and Jeggo, 2006). Closely packed single strand breaks can also result in the DBSs of DNA molecules. In certain recombination reactions, such as V(D)J recombination in the immunoglobulin of the immune system (i.e. the

Table 1.1 DNA damage response proteins have also been found to interact with telomeres. (Slijepcevic, 2006)

Table 1 – DNA damage response proteins involved in telomere maintenance

Protein	Cell origin	Function	Sensitivity	Telomere dysfunction			Shelterin interaction	Reference
				Length	Fusions	Other		
ATM	Human Mouse	Damage signaling	IR	Shorter	Yes	Yes	Yes	[2–4]
Ku	Mouse Human	NHEJ Shorter	IR	Shorter/ longer	Yes	ND	Yes	[5–8]
DNA-PKcs	Mouse (scid) Mouse KO	NHEJ Normal	IR	Longer	Yes	ND	Yes	[9,10]
RAD54	Mouse	HR	IR	Shorter	Yes	ND	ND	[11]
RAD51D	Mouse Human	HR	IR	Shorter	Yes	ND	Yes	[12]
NBS1	Human	Damage sensing?	IR	Shorter	No	ND	Yes	[13]
MRE11	Human	Damage sensing?	IR	ND	ND	ND	Yes	[14]
PARP-2	Human	BER	IR	Normal	No	ND	Yes	[15]
ERCC1	Human	NER	UV	ND	No	Yes	Yes	[16]
XPF	Human	NER	UV	ND	No	Yes	Yes	[16]
WRN	Human	Helicase	Topoisomerase inhibitors	Shorter	ND	ND	Yes	[17]
BLM	Human	Helicase	Topoisomerase inhibitors	Shorter	ND	ND	Yes	[17]
FANCA	Human	Damage sensing?	MMC	Shorter	Yes	Yes	ND	[18]
RAD50	Human Mouse	Damage sensing? IR	IR ND	ND Yes	ND	ND	Yes	[14,19]
BRCA1	Human Mouse	HR Shorter	IR Yes	Longer ND	Yes	ND	Yes[a]	[20–24]
Rad9	Human Mouse	Damage sensing?	IR	ND	Yes	ND	Yes	[25]
PARP-1	Human	BER	IR	Normal	Yes	ND	Yes	[26]

generation of diversity in the development of T-Cells and B-Cells), DSBs are also generated by recombination activating gene (RAG) proteins between the recombination signal sequence (RSS) and the coding sequence (Janeway, 2004, O'Driscoll and Jeggo, 2006) . Meiosis (the division of a gamete-producing cell) involves the programmed generation of a site or region specific formation of DSB through endonucleases (O'Driscoll and Jeggo, 2006). Studies have also shown that telomere shortening can activate DSB repair and propagation of apoptosis/senescence via p53 activation (Smith and de Lange, 2000). However, the variation in the occurrence of DSBs results in the activation of relevant pathways and individual factors. For example, the exogenous generation of DSBs through IR results in the activation of NHEJ and ATM signalling. On the other hand, replication fork stalling activates primarily HR and ATR signalling. The degree of DSB damage also has an effect on the activation of the relevant rejoining mechanism (O'Driscoll and Jeggo, 2006).

1.5.1 Non-homologous End Joining Pathway

The majority of DSBs in eukaryotic cells are repaired through either NHEJ or HR. Although recent findings have found a third, less characterized repair mechanism named microhomology-mediated end joining (MMEJ) as another DNA DSB repair pathway (McVey M. and Lee S.E., 2008). However, for the purpose of this thesis the two main and well characterized DNA DSB repair mechanism, namely NHEJ and HR will be described in more detail. HR takes place in late S-G2 phases, while NHEJ occurs throughout the cell cycle, but mainly in the G1 phase (O'Driscoll and Jeggo, 2005). Core proteins involved in the NHEJ process include

Ku dimers (Ku70-Ku80), DNA-PKcs, XRCC4, Ligase IV, Artemis, and recently discovered cernunnos-XLF (Buck et al 2006, Ahnesorg et al 2006). The Ku complex (Ku70/Ku80) is involved in the early detection of DNA DSBs due to its high affinity for DNA ends. The attachment of the Ku heterodimmer to the site of DSB attracts DNA-PKcs, a serine/threonine protein kinase. The regulatory Ku70/80/DNA-PKcs complex acts as a DNA damage sensor. A purified Artemis protein has shown to possess single-stranded 5' to 3'exonuclease activity. However, when Artemis protein forms a complex in the presence of DNA-PKcs, Artemis becomes phosphorylated and Artemis acquires endonucleotytic activity on 5' and 3' overhangs as well as hairpins (Ma Y. et al., 2002). Artemis provides an important nucleolytic processing activity to prepare DNA ends for re-ligation (Sekiguchi and Ferguson 2006). Once the ends of the DNA are secured, XRCC4 and Ligase IV seal the break, although another protein complex such as MRE11/RAD50/NSB1 (MRN complex) could be required for further processing of the DNA ends before re-ligation. The newly discovered member of NHEJ protein family, Cernunnos-XLF, is believed to play a role in DSB end joining alongside XRCC4 and Ligase IV. The exact role of this new protein is not yet known, but Ahnesorg et al (2006) suggested that Cernunnos-XLF may serve as a bridge between XRCC4 and Ligase IV and the other NHEJ factors to facilitate the recruitment of the other factors to the ends of DSB. Or it might be involved in the regulation of XRCC4-Ligase IV activity via the modulation of active and inactive multimeric states of XRCC4 (Sekiguchi and Ferguson 2006). Interestingly, some of the NHEJ factors are shown to be involved in telomere length maintenance.

For instance, Ku70, Ku80 and DNA-PKcs associate with telomeric DNA in several human cell types (d'Adda di Fagagna et al., 2001). Similar results were seen in mice deficient in Ku86 with increased chromosome end-to-end fusion with strong telomeric signals at point of fusion thus indicating important role of Ku86 (Ku86 is the same as Ku80) in telomere end capping in mouse (Samper et al., 2000, Espejel et al., 2002a, Espejel and Balsco 2002). Similarly, DNA-PKcs (catalytic subunit of DNA-PK) was shown to be essential in protecting mammalian telomeres (Bailey et al 2004) and that inhibition of DNA-PKcs leads to increased levels of chromatid fusions (Bailey et al., 2001, Bailey et al., 2004). Similar results were observed in DNA-PKcs deficient mice (known as SCID mice) with increased levels of telomere fusions indicative of telomere dysfunction through loss of telomere end capping (rather than telomere shortening since it has been shown that SCID mouse cells have abnormally longer telomeres (Hande et al., 1999, Samper et al 2000, Goytisolo et al 2001). The question is whether other NHEJ factors, including Artemis or Ligase 4/XRCC4, or the newly found NHEJ protein XLF, are involved in telomere maintenance. The Ligase IV deficient human fibroblast cell line with radio-sensitivity was shown to have accelerated telomere shortening in comparison to the normal cell line in a study published by Cabuy et al 2005. In the same study they showed that an Artemis-deficient human cell line (F01/240), also radio-sensitive, display accelerated telomere shortening and signs of telomere fusions (although the study was limited) (Cabuy et al., 2005)

1.5.2 Homologous Recombination (HR)

Homologous recombination is another form of the DSB repair operating mainly in late S and G2 phases of a cell cycle. HR is a preferred mechanism of simple eukaryotes such as yeast. HR is much more accurate than NHEJ since it uses a sister chromatid as a template in rejoining DSBs. HR is predominantly responsible for repairing DSBs that arise due to replication fork stalling (in the late S phase) and the HR pathway involves nucleolytic processing, strand invasion, Holliday junction formation, and branch migration (see figure 1.5).

The proteins involved in HR pathway are: RAD51, RAD52, RPA, BRCA1, BRCA2 XRCC2, XRCC3, RAD54, DNA polymerases, and DNA ligases. The HR repair follows two pathways. A RAD51-dependent pathway, which is an error free and RAD51-independent pathway, which is prone to errors in the DNA sequence (Griffin and Thacker, 2004). The RAD51-dependent pathway involves a homology search and strand invasion to allow the restoration of the original DNA sequence based on the undamaged homologous sequence (Figure 1.5).

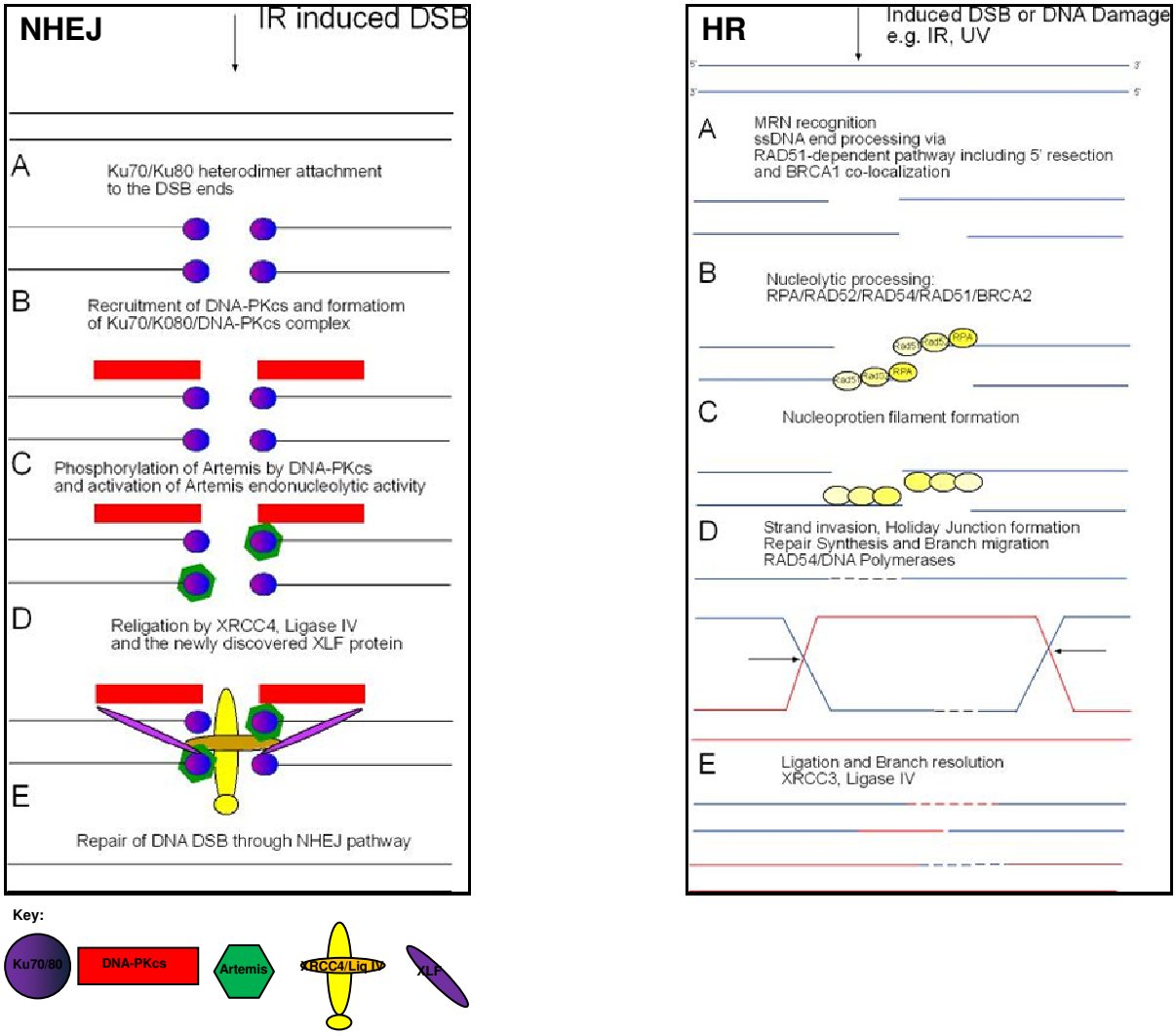

Figure 1.5 Schematic representation of NHEJ and HR.
NHEJ A: DSB is detected in a mammalian cell via sensor molecules MRN complex and ATM, which recruits Ku70/Ku80 heterodimmers that are attached to the ends of the broken DNA molecule. The doughnut shape of the Ku heterodimer is perfectly matched to its DNA double helix shape and is inserted at the ends of the broken DNA molecule. B: The dimerization of Ku70/Ku80 recruits DNA-PKcs to the ends of the broken DNA molecule, forming a Ku70/Ku80/DNA-Pkcs complex. C: One of the functions of DNA-PKcs is to phosphorylate the Artemis molecule to activate its endonucleolytic properties to "chew" any overhangs at the end of the DNA molecule, a process that is necessary for the proper re-ligation step. D: Ligation occurs in the presence of XRCC4 (known as the x-ray cross linking protein), Ligase IV protein and the newly discovered Cernunnos-XLF proteins. XLF protein may be used to bridge XRCC4 and Ligase IV proteins.
HR (see 1.5.2 for detail) (Author's own adaptation)

The RAD52 protein recognises the broken DNA ends and processes the DNA ends into a 3' single strand by nuecleolytic activities of the Mre11-Rad50-Nbs1 complex. Then the formation of a nucleoprotein filament onto the 3' single strand DNA is carried out by RAD51 by polymerization and with the aid of a single strand DNA binding protein, replication protein A (RPA) and RAD52. The RAD51 nucleoprotein filament searches for homologous duplex DNA after which the DNA strand exchange generates a joint molecule between the homologous damaged and undamaged duplex. BRCA2 helps to load RAD51 onto the ssDNA molecule, whereas BRCA1 is required as a regulatory mechanism. After branch migration and holliday junction formation, DNA synthesis takes place where DNA polymerases and accessory factors fill the gap and DNA Ligase IV, XRCC4 relegate the DSB. BRCA1 deficiency confers sensitivity to ionizing radiation as well as sensitivity to DNA cross linking agents such as mitomycin C (Powell and Kachnic 2003). Also a BRCA1 deficient human lymphoblastoid cell line shows an elevated level of chromosome end-to-end fusion that suggests a role of BRCA1 in telomere capping (Al-Wahiby and Slijepcevic 2005).

1.6 Artemis Protein Structure and Function

The Artemis gene was found to be mutated in people suffering from RS-SCID syndrome (Radio Sensitive Severe-Combined Immunodeficiency) (Moshous et al., 2001). The Artemis protein is known to be involved in DNA DSB end processing, NHEJ (see section 1.5.1). It is encoded by a gene, known as *DCLRE1C* (DNA cross-link repair 1C), located on the short arm of chromosome 10, and was described to be capable of cleaving hairpin junctions formed at

coding ends in the process of V(D)J recombination of immune B-cells and T-cells (Ma et al., 2002). Hence, people suffering from RS-SCID syndrome had their B-cells and T-cells entering an early arrest during maturation, therefore resulting in the lack of functional B and T-cells. Initially, thirteen clinical cases of patients suffering from RS-SCID due to the Artemis defect were found, with the majority of the group linked to Athabaskan speaking Native Americans of Apache or Navajo tribes (Lanying Li, 2002, Li et al., 2002). However, four new cases of RS-SCID were discovered with two novel mutations in the Artemis gene in a Japanese family (Kobayashi et al., 2003). Therefore, defects in the Artemis gene are not unique to one certain tribe of people and could be more widespread than previously thought. Here, a detailed review of the Artemis structure and function is presented, with a look at the main interaction of Artemis with DNA-PKcs and ATM.

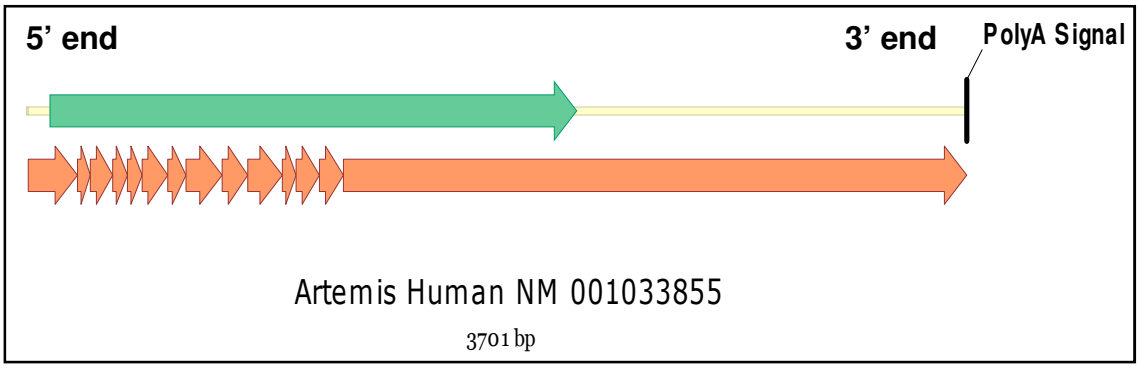

Figure 1.6. Schematic representation of Artemis mRNA.
Artemis gene is composed of 14 exons (orange arrows) with the main open reading frame (coding region) compromising of 2079 bp (green arrow). The 3' and 5' untranslated region (UTR) is in yellow (left and right of ORF respectively) with polyA tails at the 3' end. (Author's own adaptation, using VectorNTI (Invitrogen))

1.6.1 Structure of Artemis

Artemis is a protein made up of 692 amino acids (aa) with 14 exons ranging from 52bp to 1160bp (Moshous et al., 2001) (Figure 1.6). The Artemis gene was mapped to the short arm of human chromosome 10p13 (Moshous et al., 2000). The Artemis protein has three regions: 1) a metallo β-lactamase (aa 1-155), 2) β-CASP (aa 156-385), 3) C-Terminal (aa 386-692) (Poinsignon et al., 2004a). The metallo β-lactamase region of the Artemis protein shows homology to yeast PSO2 and murine SNM1 (Poinsignon et al, 2004b). This conserved homology with a catalytic activity alongside β-CASP is absolutely essential for the proper enzymatic functioning of the Artemis protein. The C terminal region of the Artemis protein contains eight Serine-glutamine(SQ)/threonine-glutamine(TQ) domains (refered to as SQ from here therein) required for phosphorylation, seven of which are conserved in humans and mice (Poinsignon et al, 2004b) (Figure 1.7). The SQ sites are where ATM, ATR, and DNA-PKcs proteins carry out phosphorylation of Artemis. Serine645 is the main site of ATM phosphorylation (highlighted in dark green, in Figure 1.7). Moshous and colleagues initially identified eight mutations in 11 families in 2001, of which two had genomic deletion that involved exons 1-4 that produced no RNA, resulting in complete null allele, one genomic deletion in exons 5-6 with K96 frameshift, and the other genomic deletion was in exon 5-8 with the deletion of K96-Q219. Other mutations involved splice donors leading to frameshift deletion in three cases, or in-frame deletion in one case (Moshous et al. 2001). Two more novel mutations in the Artemis gene were found in four Japanese cases, with one having a genomic

deletion at exon 3 and skipping exon 4 (Kobayashi et al., 2003). Two other novel mutations in the Artemis gene found in 2003 were G118V and G135E that show the absence of T-cells and B-cells (Noordzij et al., 2003). Two other mutations in Artemis were described in 2005. One form of mutation involved the substitution of H35D that is found in the Omenn syndrome, with one null and one hypomorphic mutation with the latter releasing a low level of the wild type Artemis protein (Ege et al., 2005).

```
MSSFEGQMAE YPTISIDRFD RENLRARAYF LSHCHKDHMK GLRAPTLKRR  50
LECSLKVYLY CSPVTKELLL TSPKYRFWKK RIISIEIETP TQISLVDEAS 100
GEKEEIVVTL LPAGHCPGSV MFLFQGNNGT VLYTGDFRLA QGEAARMELL 150
HSGGRVKDIQ SVYLDTTFCD PRFYQIPSRE ECLSGVLELV RSWITRSPYH 200
VVWLNCKAAY GYEYLFTNLS EELGVQVHVN KLDMFRNMPE ILHHLTTDRN 250
TQIHACRHPK AEEYFQWSKL PCGITSRNRI PLHIISIKPS TMWFGERSRK 300
TNVIVRTGES SYRACFSFHS SYSEIKDFLS YLCPVNAYPN VIPVGTTMDK 350
VVEILKPLCR SSQSTEPKYK PLGKLKRART VHRDSEEEDD YLFDDPLPIP 400
LRHKVPYPET FHPEVFSMTA VSEKQPEKLR QTPGCCRAEC MQSSRFTNFV 450
DCEESNSESE EEVGIPASLQ GDLGSVLHLQ KADGDVPQWE VFFKRNDEIT 500
DESLENFPSS TVAGGSQSPK LFSDSDGEST HISSQNSSQS THITEQGSQG 550
WDSQSDTVLL SSQERNSGDI TSLDKADYRP TIKENIPASL MEQNVICPKD 600
TYSDLKSRDK DVTIVPSTGE PTTLSSETHI PEEKSLLNLS TNADSQSSSD 650
FEVPSTPEAE LPKREHLQYL YEKLATGESI AVKKRKCSLL DT       692
```

Key:

MS	β-lactamase
VK	β-CASP
EE	C-Terminal
SQ	Serine-glutamine/threonine-glutamine
SQ	Serine 645 main site of ATM phosphorylation

Figure 1.7. Amino Acid sequence of the Artemis gene.
The three regions of the Artemis protein are highlighted alongside the 8 SQ motifs (7 red highlights and one dark green highlight) and a site of ATM phosphorylation (green highlight). Source http://www.ncbi.nlm.nih.gov/entrez/viewer.fcgi?db=protein&val=71153325. Accession Number: Q96SD1, Gene Name: DCLRE1C, OMIM: 602450.

1.6.2 Function of Artemis

The Artemis gene is known to show exonulease and endonuclease activities when in the presence of DNA-PKcs and ATP. Artemis is a DNA repair protein that is also required for V(D)J recombination during T-cell and B-cell development. In a subset of T^- B^- severe combined immune deficiency syndrome (SCID) the defect is not caused by mutation in the recombinase activating genes (RAG)1 and RAG 2, but is caused by the defective Artemis gene that encodes for a key protein responsible for V(D)J recombination and DNA double strand breaks (Kobayashi et al., 2003). This subset of T^- B^- SCID caused by the Artemis gene mutation also shows radiosensitivity and is known as RS-SCID (Moshous et al., 2001, Moshous et al., 2000). The Artemis gene is an important component of DNA DSB repair machinery, specifically in response to ionising radiation or radiomimetic drugs such as bleomycin, and is also important in genome integrity (Poinsignon et al, 2004b).

During the development of B-cells and T-cells, the immunoglobulin goes through a recombination stage where each segment of variable domain exons are assembled to form the V(D)J recombination (Janeway, 2004). In order to get each segment to join together DNA must form DSB and rejoin again, cutting out the introns. This naturally occurring DSB in a DNA molecule is repaired through the NHEJ repair pathway. The two ends of the broken DNA molecule generated by DSB are rarely compatible (Ma et al., 2002). Artemis is therefore capable of creating a hairpin opening which is one of the crucial stages of V(D)J recombination (hairpins are formed immediately after the excision of the dsDNA

molecule). Artemis, in its unphosphorylated form possesses single strand 5' to 3' exonuclease activity. However, when in the presence of DNA-PKcs and ATP it is phosphorylated and acts as endonucleases. Artemis:DNA-PKcs complex works as a hairpin opening in V(D)J recombination and overhang processing in NHEJ (Ma et al., 2004, Ma et al., 2005).

1.6.3 Artemis is Phosphorylated by DNA-PKcs

DNA-PKcs has many critical roles, ranging from protecting the ends of chromosomes from being treated as DSB by the cells, to functioning as a DNA damage sensor in the NHEJ pathway during the occurrence of DSB in a DNA molecule. DNA-PK has been found to be present at telomeres and it is involved in capping chromosomal ends and preventing them from being attacked by the NHEJ machinery by mistaking them for DSB (Burma and Chen, 2004). DNA-PKcs is also involved in signalling cell death by triggering apoptosis in response to severe DNA damage and in mounting an innate immune response to bacterial DNA and viral infection (Burma and Chen, 2004) (see table 1.2).

Ma et al (2002) reported that a 469kDa component of the DNA-PKcs phosphorylates Artemis when involved in the Ku70/Ku80 complex in response to DSB and in the NHEJ repair pathway. In a separate research reported in 2005 it was shown that endonucleatic activity of Artemis:DNA-PKcs in the presence of ATP removes 3' overhangs produced as a result of DSB and processes heterologous loops, flaps, gaps, and stem-loops generated during the religation of DSB (Ma et al., 2005). The endonucleatic activity of Artemis:DNA-PKcs is also

important in the nicking of the DNA molecule in hairpin structures generated during V(D)J recombination in formation of antigen T-cell receptors and B-cells. The arrest in hairpin nick can result in the incomplete formation of T-cells and B-cells, resulting in RS-SCID (Ma et al., 2005).

Table 1.2. Summary of DNA-PK function in mammalian cells. (Adapted from Burma and Chen, 2004).

DNA-PK component are involved in the following areas of mammalian cell			
DNA Repair (NHEJ)	**Telomeres**	**Apoptosis**	**Innate Immunity**
1. Synapsis of DNA end 2. Autophosphorylation 3. Recruitment and phosphorylation of DNA repair protein including Artemis	1. Telomere Capping 2. Telomere Length maintenance	1. Phosphorylation of p53 2. Induction of program cell death	1. Bacterial DNA: Phoshphorylation of IKK and induction of IL-6 and IL-12 2. Viral Infection: Phosphorylation of IRF3 and induction of IFN α and β

1.6.4 Artemis and ATM

ATM (ataxia telangiectasia mutated) is a serine/threonine protein kinase that is activated and recruited by DNA DSB and the MRN complex (Mre11/Rad50/Nbs1). It belongs to the group phosphoinositol-3-kinase related kinase (PIKK) family that includes (ART, DNA-PKcs, ATX/SMG1, mTOR/FRAP and TRRAP) (Shiloh, 2003). ATM resides in the nucleus of cells as inactive dimers and in the presence of DSB it autophosphorylates and becomes active. ATM then acts as a signal transducer to phosphorylate other effectors to bring about a cell cycle arrest (p53 activation, p21), DNA repair (BRCA1, NBS1), and apoptosis. ATM is a protein that is mutated in ataxia telangiectasia (AT) patients.

AT is a devastating disorder with critical clinical features such as progressive ataxia and neurodegeneration, chronic dilation of blood vessels in the skin and eye, clinical radiosensitivity, and predisposition to cancer with impaired immune response (Jeggo and Löbrich, 2005, Lobrich and Jeggo, 2005). The relation between Artemis and ATM was explained in 2004 by Riballo and colleagues. They suggested that ATM phosphorylates Artemis in response to IR induced DSBs (Riballo et al., 2004). Artemis is recruited to sites of DSBs to process the broken ends before religation by ligase IV. However, damage sensor proteins such as MRN complex, 53BP1, and γH2AX are also phosphorylated by ATM and recruited to the site of DBS. γH2AX is phosphorylated within minutes of DBS recognition by ATM and eventually other effectors are phosphorylated and this brings about cell cycle arrest. Once the cell cycle is arrested, the NHEJ components are involved and repair 90 percent of the DSB induced by IR (Jeggo and Löbrich, 2005). The remaining 10 percent of unrepaired DSB induced by IR is repaired in an ATM dependent manner through NHEJ(Riballo et al., 2004). In other words, evidence suggests that the two processes of ATM activation and NHEJ recruitment to sites of DSB occur independently for a subset of DNA DSB repair. According to Jeggo and Löbrich, (2005) "…Artemis represents a novel ATM-substrate required for the processing of a fraction of DNA ends prior to rejoining." This shows that Artemis is a downstream effector of ATM-dependent signalling, uniquely affecting ATM's role in DSB repair (Riballo et al., 2004). But the situation is reversed when comes to V(D)J recombination, where DNA-PK is indispensable and ATM is dispensable during hairpin opening by Artemis. Both

DNA-PK and ATM are required for Artemis function in DSB repair (Riballo et al., 2004). The presence of γH2AX and 53BP1 at the site of DSB may serve as a "scaffold" for proper functioning of Artemis and Mre11 and Nbs1 may also be required for efficient Artemis phosphorylation (Riballo et al., 2004) (see table 1.3 for summary of Artemis function).

1.6.5 Artemis and Telomeres

The involvement of DNA-PKcs, Ku70, and Ku86, (components of DNA-PK) in telomeric end capping from studies using fluorescence in-situ hybridization (FISH) probes detecting telomeres, published in a paper by Bailey et al in 1999, showed that telomere shortening was not the cause of telomeric fusion in cells mutated in the above proteins. Instead telomere fusion was suggested to be due to the loss of telomere end-capping function and this was proven by the presence of telomeric DNA signals at points of telomeric fusion (Bailey et al., 1999). Knocking out the XRCC4 gene (another NHEJ protein) in mice contributed to elevated telomeric chromosomal end to end fusion (Bailey, 2004a). Rooney and colleagues in 2003 showed that Artemis deficient mouse embryonic stem (ES) cell lines have a higher degree of chromosomal instability in comparison to control cells. Interestingly, they found increased incidence of telomeric fusions (Rooney et al., 2003) pointing to the possibility that defective Artemis may affect telomere function. In 2006, two labs reported that a new protein that interacts with TRF2 has close homology to the Artemis and named it Apollo (Lenain et al., 2006, van Overbeek and de Lange, 2006). Apollo, also known as hSNM1B, has found to act upstream of ATM in response to IR, by phosphorylating ATM and

hence playing a critical role in the maintenance of genome integrity (Demuth et al., 2008). Apollo defective cells exhibited increased levels of telomeric fusions thus clearly indicating the role of this close homolog of Artemis is directly involved in telomere maintenance.

To date, 19 DNA damage response proteins have been found to be involved in telomere maintenance, either through affecting telomere length or telomere capping function, with three of these DNA damage response proteins involved in the NHEJ processes of DNA repair (DNA-PKcs, Ku70/80, ERCC1) (Slijepcevic, 2006, Gitte De Boeck, 2009).

Given that Artemis defective mouse cells show elevated levels of telomeric fusions and that its close homolog, Apollo, is directly involved in telomere maintenance (interacts with TRF2 and affects telomere capping function) it seems reasonable to examine whether Artemis defect in human cells will have any effects on telomere maintenance.

Table 1.3 Summary of Artemis function in mammalian cells

Artemis protein is involved in the following areas:			
DNA Repair (NHEJ)	**V(D)J recombination**	**ATM**	**Telomere length**
1. Overhang processing of DNA DSB (5'-3-exonuclease activity) 2. Endonuclease activity on 5' and 3' overhangs and hairpins in the presence of DNA-PKcs 3. If mutated, cells exhibit radiation sensitivity.	1. In creating hairpin opening 2. Overhang processing in the presence of DNA-PKcs (through endonuclease activity) 3. Mutation of Artemis leads to SCID syndrome with radio-sensitivity	1. Repair of subset of DNA DSBs (around 10%) requires action of both ATM and Artemis	1. Defective Artemis causes accelerated telomere shortening in primary fibroblast cells

1.6.6 Aim and outline of PhD

The aim of this PhD project is to search for evidence of chromosomal abnormalities in Artemis defective human cells that reflect telomere dysfunction. This can be achieved through; a) cytological analysis using both a classical Giemsa staining method and FISH with a telomere specific probe, and b) through analysis of telomere function using a recently developed immunocytochemistry based protocol.

Moreover, we are proposing to assess the relationship between DNA-PKcs and Artemis in telomere maintenance by inhibiting of DNA-PKcs in Artemis defective human cell lines. Finally, we aim to examine further the Artemis:DNA-PKcs relationship from the perspective of telomere maintenance in DNA-PKcs deficient human glioblastoma cell lines.

Chapter 2 : Materials and Methods

2.1 Cell lines and tissue culture methodology

2.1.1 Primary Human Fibroblasts

Two primary human fibroblast cell lines that were defective in the Artemis protein were derived from two different patients suffering from Radiosensitive-Severe Combined Immunodeficiency syndrome (RS-SCID) and provided to us by Dr. P.A. Jeggo, University of Sussex, Brighton, UK (see Table 2.1). The two Artemis defective cell lines CJ179 and F01-240 have genomic deletions within Artemis gene with CJ179 producing no Artemis transcript (Riballo et al., 2004).

A normal primary fibroblast cell line was purchased from the National Institute of General Medical Sciences (NIGMS) Coriell Institute for Medical Research in the United States (Table 2.1).

2.1.2 Human Glioblastoma cell lines

Human glioblastoma cell lines were kindly provided by Dr. Chris Parris from Brunel Institute of Cancer Genetics and Pharmacogenomics. MO59K and MO59J (Table 2.1) were both derived from the same tumor with MO59J exhibiting hypersensitivity to ionising radiation and a lack of functional DNA-Protein Kinase catalytic subunit (DNA-PKcs). MO59K exhibited normal DNA-PKcs and was not radiosensitive. Both cell lines were near pentaploid and had multiple copies of chromosome 8 (The *PRKDC* gene that codes for DNA-PKcs is located on this chromosome) (Anderson et al, 2001).

2.1.3 Mouse Lymphoma cell lines

Mouse lymphoma LY-R (radio-resistant) and LY-S (radio-sensitive) cells (Table 2.1) were used as a reference for cytological testing of DNA-PKcs inhibitory drug (IC86621, sigma) and telomeric measurements using FLOW-FISH techniques.

2.1.4 Tissue Culture

All cell lines were kept frozen in liquid nitrogen. When required vials of frozen cells were thawed and set up in either a 25cm^2 flask or 75cm^2 flask with filter head (Nunc) to avoid fungus contamination. All primary human fibroblast cell lines were cultured in Dulbecco's modified Eagle medium (D-MEM) (Gibco/invitrogen) supplemented with 10% fetal calf serum (Gibco/invitrogen) at 37℃ with 10% CO_2, and incubated in a HeraCell 150 (Heraeus, Germany) incubator. A HeraSafe safety cabinet class II (Heraeus, Germany) hood was used at all times. All primary fibroblast cell lines were subcultured 1:3 by gentle trypsinization with trypsin-EDTA (Gibco/invitrogen) for five minutes at least every three to four days at 80 percent confluence. Prior to trypsinization the cells were washed with 3ml of D-PBS (Gibco/invitrogen). After trypsinization the cells were spun down in a centrifuge (Megafuge 1.0, Heraeus) at 1200rpm for five minutes. All solutions were brought to room temperature prior to trypsinising using a waterbath (Techne) with a monitor (Tempette Junior TE-8J) to keep the temperature at a constant 37ºC. The waterbath was constantly cleaned and disinfected alongside the incubator and the hood to avoid spreading any fungus or bacterial infection. Supernatants were removed and the cell pellets were

Table 2.1 Summary of cell lines

Cell Line	Cell type	Syndrome/Defect protein	Estimated Population doubling (PD)	Sensitivity	Cellular Sensitivity	References
F01-240	Human/Fibroblast	RS-SCID/Artemis	4	Ionising radiation	Ionising radiation	Riballo et al 2004
CJ179	Human/Fibroblast	RS-SCID/Artemis	+10	Ionising radiation	Ionising radiation	Riballo et al 2004
GM08399	Human/Fibroblast	None/Normal	5	Normal	Normal	http://locus.umdnj.edu/nigms/
LY-R	Mouse/Lymphoma	None/Normal		Normal	Normal	
LY-S	Mouse/Lymphoma	SCID/Not known		Ionising radiation	Ionising radiation	
MO59K	Human/ Glioblastoma	Glioblastoma multiform/Normal	4	Normal	Normal	Anderson et al 2001
MO59J	Human/ Glioblastoma	Glioblastoma multiform /DNA-PKcs	4	Ionising radiation	Ionising radiation	Anderson et al 2001

re-suspended by gentle flicking in the fresh medium. One ml of suspended cells was then put in a new flask with the fresh medium. Human glioma-derived MO59K and MO59J cell lines were cultured in DMEM (Gibco/invitrogen) with 10% FCS (Gibco/invitrogen) at 37ºC with 5 percent CO_2 incubated as above. Cells were sub-cultured 1:3 as mentioned above.

Mouse lymphoma LY-R and LY-S cell lines were grown in suspension under standard tissue culture conditions as mentioned above using RPMI 1640 medium (Gibco/invitrogen) and 10 % fetal calf serum at 37ºC in the atmosphere of 10 % CO_2. Cells were sub-cultured at the ratio of 1:10 every two or three days, preferably before the medium colour changed to yellow.

2.1.5 Cryopreservation of cells

Cells were preserved in liquid nitrogen to avoid aging and contamination. After checking cells for contamination, cells were trypsinized as described above. Cell suspension was mixed with 1ml of freezing medium containing 90 % fetal calf serum (Gibco/invitrogen) and 10 % DMSO (dimethylsulfoxide, Sigma). The cell suspension was aliquoted into cryogenic vials for storage in liquid nitrogen. Prior to storage in liquid nitrogen the vials were kept in a Nalge nunc cooler for 24 hours. This plastic holder was filled with Isopropyl alcohol (IPA). The specific heat of the coolant in the base insulates the container and gives a cooling rate of ~1º/min in the cryotube. Finally the ampoules were transferred into liquid nitrogen for long-term storage.

Thawing of Cryopreserved cells

The medium was aliquoted and warmed inside the incubator before the ampoule was taken out of the liquid nitrogen. The cryopreserved cells were handled with great care. The ampoules were thawed for two to three minutes and the content immediately put into the pre-warmed medium. Cells were transferred into appropriate flasks. After 24 hours the medium in flasks was changed to wash away any residual DMSO.

2.1.6 Mycoplasma Screening of Cell Culture

Mycoplasma is a form of bacteria which lacks a cell wall. It is therefore unaffected by many common antibiotics. It is important to regularly check cell lines for any signs of possible mycoplasma contamination. A quick way of testing for mycoplasma contamination involves a PCR-based method. Two rounds of PCR using nested primers were used routinely in our laboratory to detect any contaminant cell lines (Table 2.2 for detail of primer sequences). DNA was extracted from a sample cell line using a Wizard DNA extraction kit (Promega). The following 20µl reaction mixtures were made using mycoplasma primers and purified DNA from cell cultures:

First round of PCR:

- 1µl of 150ng of DNA
- 1µl of Forward GPO1 primer (at 4µM)
- 1µl of Reverse MGSO primer (at 4µM)
- 17µl of ReddyMix Master Mix (Ab genes)

- Total 20µl

Second round of PCR:

- 1µl of product from first round of PCR
- 1µl of Forward GPO2 primer (at 4µM)
- 1µl of Reverse MGSO primer (at 4µM)
- 17µl of ReddyMix Master Mix (Ab genes)
- Total 20µl

Both PCR amplification cycles were done at:

95℃ hot start for 30 seconds one cycle; 95℃ for 30 seconds with 55℃ annealing temperature for 30 seconds, and 72℃ extension for one minute for 35 cycles.

Both PCR products were run on 1.5 percent agarose gel containing ethidium bromide (See RT-PCR section for detail on how to make the gel, chapter 2.5.4). A strong positive sample gave two bands; one at 720bp from the first PCR and one at 145bp from the second PCR. A weak positive sample gave one band only at 145bp on the second PCR. Image below (Figure 2.1) shows a mycoplasma screening performed on several cell lines with no positive sign of mycoplasma contamination.

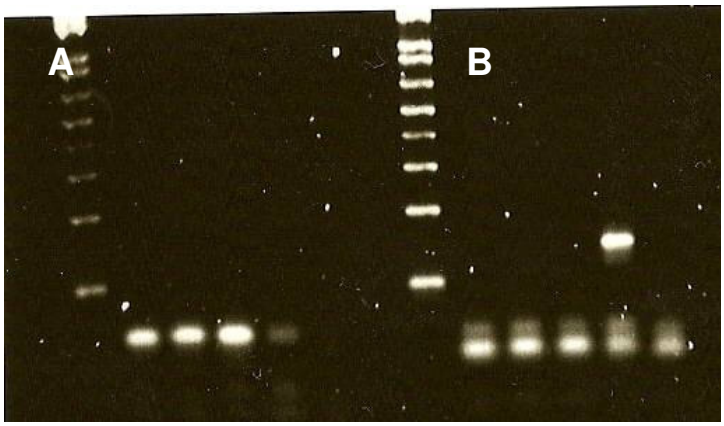

Figure 2.1. Mycoplasma PCR screening.
A| First round of PCR. lane 1: F01-240, lane2: CJ179, lane 3: GM08399, lane 4: positive control, lane 5: negative control. **B**| only one positive band on lane 4.

Table 2.2. Mycoplasma screening primer sequence

Primer	**Orientation**	**Sequence**
Mycoplasma GPO1	Forward	5´-ACTCCTACGGGAGGCAGCAGTA-3´
Mycoplasma GPO2	Forward	5´-CTTAAAGCAATTGACGGGAACCCG -3´
Mycoplasma MGSO	Reverse	5´-TGCACCATCTGTCACTCTGTTAACCTC-3´

2.1.7 Conversion of passage number into population doubling

Population doubling (PD) is a two-fold increase in the total number of cells in a culture. However, during tissue culturing passage numbers were recorded that reflected the number of times a cell culture had been trypsinized and split with a constant dilution factor (i.e. 1:3, 1:4, or 1:10) depending on cell type and cell

growth rate. This kept all cells in the logarithmic growth phase. In order to convert the passage number into PD one of two formulas was used:

Formula 1:

2^n = dilution factor [1], where n = PD

Taking log of [1] and rearrange it

PD = Log dilution factor / Log 2 x passage number

Formula 2:

PD = (Log N_1/Log 2) – (Log N_1/Log 2)

Where; N_0 is the total number of cells at the beginning of cell culture

N_1 is the total number of cells at the end of cell culture period

2.1.8 Irradiation of cells

A higher activity Cobalt-60 source was used to irradiate cells with ionising radiation. Cells were grown up to 80-90 percent confluent level either in non-filtered tissue culture flask (Nunc, Fisher) for metaphase preparation, or on poly-prep slides (Sigma) for assays that required use of antibodies (see 2.3.1). Datasheets were used to calculate dosages of radiation measured in Gray (Gy) per minute (See appendix 1). In our studies cells were only subjected to low doses of radiation i.e. 0.1 Gy, 0.5 Gy and 1.0 Gy, with a maximum dose of 3.0Gy that was tested once only.

2.2 Cytogenetic Analysis

2.2.1 Metaphase Preparation using fibroblast cell lines

A high mitotic index is important in scoring a large number of metaphases in a short time and it is also important to get high quality metaphase spreads. Twenty four hours after irradiation (i.e. ~ one cell cycle), the semi-confluent flask (80-90 percent) was treated with colcemid (10µg/ml) (Sigma-aldrich). Colcemid was used to arrest cells in metaphase by inhibiting spindle formation. Initially cells were treated for four hours with colcemid (10µg/ml) prior to trypsinization and harvesting. This method gave a low mitotic index when using primary fibroblast cell lines and it was time-consuming if a large number of metaphases were needed for the analysis. The following changes were implemented to yield a higher mitotic index:

1. Colcemid time was increased from four hours to seven hours of treatment. This ensured that most cells reached M-phase of cell cycle, therefore increasing the mitotic index.

2. A mock flask was used without adding colcemid as a control to check the number of dividing cells. This method gave us a rough idea of when to stop the colcemid's action.

3. During harvesting, culture supernatant were retained to collect mitotic cells in suspension and spun down in a centrifuge at 1000rpm for five minutes and

before each spin a fresh fixative solution was added. This ensured that metaphases were not lost.

4. Greater care was taken in handling the cells in the culture. For instance, cells were subcultured when reaching 60-70 percent confluence rather than 80-90 percent as in previous experiments. This ensured that cells were kept healthy and in the exponential growth phase.

After roughly seven hours of treatment with colcemid, cells were washed in PBS, trypsinized, and spun down at 1000rpm for five minutes. Cells were then treated with 10ml of hypotonic buffer (75mM of KCl) for 15 minutes in a 37ºC waterbath. Fixation was followed using methanol-glacial acidic acid (3:1) as fixative. The process of fixation was carried out two times and each time a 1ml of fresh fixative was added dropwise, followed by the addition of 2ml of extra fixative. The cells were left at room temperature for 10 minutes and 30 minutes respectively. Finally, the cell pellets were re-suspended in fresh fixative and 15µl of cell suspension was dropped onto pre-cleaned slides. The fresh fixative ensured that cells were spread over the surface of slide. Once the slides were dried they were checked under a phase contrast microscope.

Treatment of microscope slides with Methanol/HCl

Microscope slides were washed in a combination of 70 percent (v/v) methanol and 3 percent (v/v) of concentrated HCl for about 24 hours and rinsed in four liters of ddH_2O before spreading. Slides were stored in the fridge suspended in

dH_2O. However, prior to spreading, the slides were kept at room temperature for few minutes since cold slides did not produce high quality spreads.

2.2.2 Metaphase preparation of other cell lines

Preparation of metaphases from other cell lines (i.e.Human glioblastoma and mouse LY-R and LY-S) were performed as described above (2.2.1) but with maximum colcemid (10µg/ml) (Sigma-aldrich) incubation of four hours only. These cell lines grow at faster rate than human primary fibroblasts and therefore did not require the changes described above (2.2.1). The remaining protocol was the same as described above.

2.2.3 Giemsa Staining

Slides were stained with 8 percent (v/v) giemsa (Sigma-Aldrich) for five minutes in 50ml of ddH_20. Giemsa stain was filtered with standard filter paper (3MM Watman paper) for purity. After staining, slides were rinsed quickly with ddH20 and left to air dry while covered with paper to prevent dust settling onto the slide. Slides were mounted with DPX mountant (BDH laboratories), covered with cover slips, and left overnight to dry. DPX is a neutral solution of Polystyrene Plasticizer in Xylene. By applying this solution the coverslips were permanently attached onto the slides. A clean dust free and evenly stained slide with high mitotic index was selected for analysis using conventional microscopy (Zeiss Axioplan2) equipped with CCD camera and MetaSystem software.

2.2.4 Telomeric-Fluorescence in situ hybridization (Telo-FISH)

Twenty µl of cells were spread on a pre-cleaned slide with fresh fixative (3:1 methanol to acetic acid glacial) and then subjected to a previously published protocol for telomere analysis (Al-Wahiby and Slijepcevic 2005). There were four stages in the preparation of the Telo-FISH slides.

Solution and slide preparation

All solutions were made fresh on the day of experiments. Four percent (v/v) of formaldehyde (Sigma-Aldrich) was made using a mixture containing four ml of formaldehyde and 96ml of distilled H_2O. Five hundred µl of pepsin stock (Sigma) (10 percent pepsin in water) was mixed in 50ml of acidified ddH2O (pH2). The acidified water was made by adding 500µl of concentrated HCl (BDH laboratories). The pepsin was kept in a waterbath set at 37℃ throughout the day (pepsin needs to be defrosted first and used immediately). Final solution preparation involved 70 percent formamide (Fisher Scientific UK) that was made by mixing 70ml of formamide with 10ml of 20 X sodium chloride sodium citric acid (20X SSC) and 20 ml of ddH_2O.

Slides with metaphase cells were aged overnight at 55℃. Alternatively, slides were aged at room temperature for three to four days before an overnight incubation at 55ºC.

Pre-hybridization Washes

Slides were washed for 15 minutes with phosphate buffer saline (PBS) on the shaker set at mark two (200rpm/minute). Fixation was done in 4 percent

formaldehyde for two minutes and washed again with fresh PBS three times, five minutes each time. Slides were incubated in pepsin at 37℃ in a waterbath for 10 minutes. Finally a round of fixation was completed with 4 percent formaldehyde for two minutes. Slides were then dehydrated in an ethanol series starting with 70%, 90%, and 100% concentration for five minutes each. Slides were then left to air dry on a slide rack at room temperature.

Denaturing and hybridization

Slides were denatured for two to three minutes at 70-75℃ using a heater block with digital display and hybridized with 15µl of synthetic peptide nucleic acid (PNA) telomeric oligonucleotides $(CCCTAA)_3$ (Applied Biosystems), labeled with cyanine-3 (Cy-3), and left in the dark for two hours in a damp container. Post hybridization washes involved washing twice with a 70 percent (v/v) formamide for 15 minutes in coupling jars, plus three times with PBS for five minutes each. Slides were then dehydrated in ethanol (starting with 70%, 90%, and 100% respectively) for five minutes each. Fifteen µl of Vecta-shield, an anti-fade DAPI mounting medium (Vector Laboratories), was added to each slide and then they were mounted with cover slips and sealed with clear nail varnish. The metaphase cells were analyzed using the computerized Axioskop 2 Zeiss fluorescence microscope equipped with a CCD camera and MetaSystems software.

2.3 Immunofluorescence and Telo-FISH

2.3.1 Immunofluorescence Telomere dysfunction Induced Foci (IF-TIF) assay

The TIF assay described here is based on the combination of antibody detection and hybridization with synthetic telomeric PNA. The original TIF technique was first described in 2003 by Takai *et al*, in which co-localization between two antibodies were analyzed. One antibody binds to a DNA damage response protein such as 53BP1 and the second antibody binds to a telomere repeat binding protein (TRF1). A co-localization between the two antibodies was then detected and the site of co-localization represents DNA damage at a telomere and it is called TIF. However, in our experiments a modified version of TIF is described based on immunofluorescence and FISH techniques hence we termed it IF-TIF (see chapter 4 for more detail)

This technique was developed after seven weeks of trial experiments testing different reagents and hybridization methods to find the optimal condition with the least amount of fluorescence background.

Cells were grown in tissue culture flasks two days prior to experiments and after cells reached 80-90 % confluence, they were trypsinized and 1ml of cell suspension (containing roughly 50,000 cells) were added onto poly-prep slides (Sigma) and placed inside a petri dish (to minimize infection). Cells were left to grow for 24 hours at 37ºC in the atmosphere of 10% CO_2. If irradiating the cells was necessary, five mls of pre-warmed medium was added into petri dishes before transferring the cells to the irradiation room. All of the procedure was done

at room temperature unless stated otherwise. After cells were irradiated with the required dose, slides were incubated for between 30 minutes and 24h at 37ºC before further processing. After that slides were rinsed in PBS and fixed in 4 percent formaldehyde for 15 minutes. Cells were then permeabilized in 0.2 percent of Triton-X in dH_2O at +4.0ºC for 10 minutes followed by blocking with 0.5 percent BSA (Bovine Serum Albumin) in PBS for 30 minutes and covered with parafilm. One hundred µl of γH2AX antibody (Upstate) solution was added (dilution of 1:500 with 0.5 percent BSA) for one hour in dark, damp conditions after which slides were washed with TBST for three minutes twice on a shaker. Then, 100µl FITC secondary anti-goat antibody was added (diluted 1:400 with 0.5% BSA) for one hour in dark, damp conditions then washed with TBST for five minutes, three times in a dark coplin jar and on an orbital shaker. Cells were fixed again with 4 percent formaldehyde for 20 minutes with no shaking in a dark place and this second fixation prevents bleaching of the fluorescence signals. At this point the slides can be analysed for the presence of γH2AX signals if necessary or the protocol can be continued to detect telomeres.

For telomere detection slides were dehydrated with an ethanol series (70%, 90% and 100% concentration) for five minutes each and then air dried. After this, slides were hybridized for two to three minutes at 70° C with PNA telomeric oligonucleotides $(CCCTAA)_3$, labeled with Cy-3 (Applied Biosystems), and left for two hours in dark and damp conditions. Post hybridization washes were performed using 70% formamide for 10 minutes, twice, and then finally washed with TBST for 10 more minutes before adding 15µl Vecta-shield anti-fade DAPI

mounting medium (Vector Laboratories). The slides were analysed using the computerized Axioskop 2 Zeiss fluorescence microscope equipped with a CCD camera and MetaSystems software.

2.3.2 Immunofluorescence/Immunohistochemistry

This protocol is performed to visualize various protein localizations in-vitro in various cell lines. Cells are grown on poly-prep slides (sigma) for 24 hours before fixation in 4% formaldehyde in PBS for 15 minutes. Then cells are permeabilized in 0.2 percent Triton-X 100 (Sigma) for 10 minutes at 4℃. Cells are then blocked with 0.5 percent BSA (Bovine Serum Albumin) in PBS for 30 minutes and covered in parafilm in humid containers. Primary antibody is added at the relevant concentration (see Table 2.5 for summary of antibodies that were used in this research), for one hour in humid containers covered with parafilm. Slides were washed with three times for two minutes each in PBS. Secondary antibody was added at relevant concentrations for one hour in a dark and humid container. Finally slides were washed in PBS for five minutes three times and dehydrated with serial ethanol as previously mentioned, and DAPI vectashield was added and cover slides are sealed with nail varnish.

2.4 Telomere length measurement using fluorescence activated cell sorting (FACS)

2.4.1 Flow-FISH

Telomere length measurement *in-vitro* can be done using various methods and protocols. One such high throughput method is based on flow-cytometry and it utilizes a fluorescence tag hybridized to the telomeric repetitive sequence of

$(CCCTAA)_3$. The method is named Flow-FISH and a modified version described by Cabuy et al (2004) is used here.

Cells were grown as described and $5x10^5$ cells were collected in suspension, washed in PBS once, and spun down at 1,500 rpm for five minutes. Supernatant was discarded carefully and the cells were re-suspended in the remaining PBS solution. Cells were then hybridized using a hybridization mixture containing five hundred µl of hybridization mixture of 70 percent formamide, 20mM Tris-HCl pH 7.0, 1 percent BSA made in PBS, and 0.3µg/ml of Fluorescein isothiocyanate (FITC) conjugated peptide nucleic acid (PNA) probe $(CCCTAA)_3$. The hybridization mixture was heated at 80°C to denature the DNA for 10 minutes. Samples without the PNA telomeric probe were used as negative controls. The samples were then left in the dark at room temperature for two hours. Post-hybridization washes mixtures contained 70 percent formamide, 10mM Tris-HCl, 0.1 percent BSA in PBS and 0.1 percent Tween 20. This would ensure that excess and unbound probe is washed away thus reducing the background fluorescence. After each wash samples were centrifuged at 3,000 rpm for five minutes to collect cells and the supernatants were discarded. Second washes were done again twice using a 500µl solution containing PBS, 0.1 percent BSA and 0.1 percent Tween-20 and cells were centrifuged at 2000rpm for five minutes. A second incubation was done with propidium iodide (PI) (Sigma) to quantitatively assess the DNA content of cells. PI is a widely used fluorescence dye that binds directly to DNA by intercalating between the bases. PI also binds to RNA so it is therefore important to digest all RNA in the sample by treating it

with RNase A (Invitrogen). The second incubation solution contained PBS, 0.1 percent BSA, 10µg/ml of RNase A, and 0.1µg/ml of PI. The samples were incubated in the dark for 45 minutes to one hour at 4°C. The samples were kept on ice all the time prior to the measurement with the FACS machine.

FACSCoulter EPICS XL (Becton Dickinson) was calibrated using flow-check fluorospheres (Beckman Coulter) to check laser alignment on all four channels. Flow-check was conducted before each measurement. The software was calibrated to measure the FITC telomeric signal on the FL1 channel, and the PI signal on FL3 channel. Cells were electronically gated for the G0/G1 phase of cell cycles form the FL3 histogram window. The Telomeric fluorescence intensity (TFI) of cells in the G0/G1 stage was recorded. TFI from the negative control cells was also measured and subtracted from the main sample reading to remove the background reading. TFI readings from a minimum of 5,000 cells and a maximum of 20,000 cells were recorded and TFI units were converted into base pairs using the formula $y = 4.13x + 2.56$ ($R^2 = 1$) (McIlrath et al., 2001). The accuracy of this formula was tested using LY-R and LY-S mouse cell lines.

2.5 Reverse Transcription Polymerase Chain Reaction (RT-PCR)

2.5.1 RNA extraction using TRIZOL reagent

Trizol (Invitrogen) is a ready to use mono-phase solution of phenol and guanidine isothiocyanate that maintains the integrity of RNA while disrupting cells and dissolving cell components during homogenization or the lysis step.

Cell homogenization:

Total RNA is extracted using an Invitrogen Trizol reagent from primary fibroblast cell lines growing in a 60mm petri dish. Cells were washed at 80 to 90% confluence twice with 10ml of cold PBS. Two ml of the Trizol reagent is added and left for at least two minutes at room temperature to the cell sample. The lysate is gently retropipetted two to three times and used immediately or stored – at -80℃ for long-term storage.

Phase separation:

The homogenized samples were incubated for five minutes at room temperature. Two hundred µl of molecular biology grade chloroform (Sigma) was added per 1ml of Trizol. Samples were shaked vigorously for 15 seconds at arm's length to avoid any possible eye contact followed by incubating samples for 2-3 minutes at room temperature, then centrifuged at 12,000 g or (13,000 rpm) for 30 minutes at 2-8℃ (preferably 4℃) in a temperature controlled ultra mini centrifuge. The chloroform causes the trizol to separate into a colorless aqueous phase and an organic phase (containing phenol and chloroform). RNA remains exclusively in an upper aqueous phase. DNA and protein can be extracted from the organic phase by further precipitation.

RNA precipitation, wash, and re-dissolving:

The aqueous phase was transferred into a separate Eppendorf tube taking care not to mix any of the red phenol with the colourless aqueous phase. A total of

750µl of molecular biology grade isopropyl alcohol (Sigma) per ml of trizol was added to the aqueous phase and mixed gently. The sample was incubated at room temperature for 10-15 minutes and centrifuged at 12,000 g (13,000 rpm) for 20 minutes at 2-8℃ (preferably 4℃). The addition of isopropyl alcohol precipitates RNA and forms a visible mass at the bottom of the Eppendorf tube after the centrifugation. The RNA pellet should be gently removed by tipping off the isopropyl alcohol (making sure RNA is still at the bottom of the Eppendorf tube) followed by washing with 1ml of 75 percent ethanol per ml of initial trizol reagent used in the homogenization step. It is recommended to dissolve 75ml of pure ethanol with 25ml of nuclease-free water (Dharmacon) or a diethyl pyrocarbonate (DEPC) treated nuclease free water. Samples should be mixed by vortexing for about 10 seconds and centrifuged at 7,500g (8,000rpm) for five minutes at 2-8℃ (preferably 4℃). The ethanol should be carefully removed as the RNA pellet may detach at this stage. The sample should be left to air dry for about 10-15 minutes at room temperature. It is important not to let the pellet dry completely as this will reduce the solubility. Partly dissolved RNA samples have $A_{260/280nm}$ ratio <1.6. The RNA pellet should be re-dissolve in 20µl of nuclease free water and retropipetted several times. The sample should be left on ice for at least one hour. RNA must be stored at -80℃.

The absorbance of RNA is read using a spectrophotometer (Eppendorf) absorbance reader at 260nm wavelength using a cuvette (Invitrogen) diluted 100X (i.e. 1µl of total RNA plus 99µl of nuclease free water) with nuclease free water (Table 2.3). The absorbance reader is blanked against 100µl of nuclease

free water. The table below represents the readings from the total RNA extraction from one of the experiments.

Table 2.3 Sample readings from total RNA extraction.

Sample name	$A_{260/280nm}$ ratio	RNA concentration (ng/µl)	RNA concentration (µg/µl)
GM08399 (WT)	1.64	2632.7	2.6327
F01-240 (Art)	1.62	1365.2	1.3652
CJ179 (Art)	1.64	1080.1	1.0801

2.5.2 Reverse Transcription

Deoxyribonuclease I, amplification grade treatment

Four µg of total RNA is treated with DNase I, amp grade (Invitrogen) and RNase-Out (Invitrogen) to remove any gDNA (genomic) and inhibit RNase enzymes respectively. Following reagents were added in a 15µl of 4µg of total RNA:

- 2µl of DNase I, amp grade, 1U/µl
- 0.5µl of RNase Out
- 2µl of 10x reaction Buffer
- Nuclease free water to 20µl

The sample should be left at room temperature for 30minutes to one hour. DNase I reaction should be stopped by adding 2µl of 25mM EDTA solution to the reaction mixture followed by heating for 10 minutes at 65°C. The RNA sample is now ready for reverse transcription. The sample can be stored at -80°C for future

use. Five µl of DNase I treated total RNA is used in the reverse transcription step, giving 1µg of total RNA.

First Strand cDNA Synthesis with SuperScript III (Invitrogen)

The first strand cDNA synthesis was done using Invitrogen superscript III recommended protocol. Superscript III can be used on total RNA with Oligo(dT), random primers (Invitrogen), or a gene-specific primer.

The following reaction reagents were added in a 200µl eppendurf tube:

- 5µl of 4µg DNase I treated total RNA
- 1µl of gene specific reverse primer (diluted 1:200 from the original stock in nuclease free water)
- 1µl of 10mM dNTP mix (10mM each of dATP, dGTP, dTTP, dCTP at neutral pH) (Invitrogen)
- Nuclease free water to 12µl

The tube was incubated at 65℃ for five minutes and quickly chilled on ice for at least one minute. This step opens up the 3D configuration of RNA and allows the primer(s) to bind along the RNA molecule. The content is collected and the following mixture is added:

- 4µl of 5x First Strand Buffer
- 2µl of 0.1M DTT (Dithiothreitol)
- 0.5µl of RNase Out
- 1µl of (40U/µl) of Superscript III

The tube was mixed gently and centrifuged briefly to collect the content. The sample was heated at 55℃ for 50 minutes for a gene specific primer, or 50℃ for 50 minutes for random primers, or Oligo(dT) primers followed by 15 minutes at 70℃ to inactivate the reaction. The first strand of cDNA is now ready for amplification by PCR.

2.5.3 Polymerase Chain Reaction (PCR)

One to 5 µl of cDNA can be used for amplification using ReddyMix PCR Master Mix (ABgene) containing 15mM $MgCl_2$. A 20µl reaction is made using the following reagents:

- 1-5µl of cDNA
- 1µl of forward primer of gene of interest (10pmol)
- 1µl of reverse primer of gene of interest (10pmol)
- 17µl of ReddyMix Master Mix (ABgene)

The sample was gently mixed and briefly centrifuged to collect it. The tube was placed into a thermal cycle PCR machine configured with the following program:

	Temperature	**Time**	**No. of Cycles**
Initial Denaturation	95℃	5 minutes	1cycle
Denaturation	95℃	15 seconds	30-40 cycles
Annealing	55℃	45 seconds	
Final Extension	72℃	5 minutes	1 cycle

A PCR optimization must be performed to find the correct annealing temperature for each primer set to reduce primer dimer and unspecific primer binding.

2.5.4 Agarose gel electrophoresis

To visualize the PCR product, a 1.5 percent agarose gel made with 1X Tris-borate EDTA buffer solution (Sigma) was prepared. One µl of 10mg/ml of ethidium bromide is added per 100ml of molten agarose gel before pouring the gel into an agarose gel electrophoresis tank. Once the agarose gel is set, 300ml of 1xTBE (tris-borate EDTA) buffer was added and each PCR sample loaded into appropriate wells in the gel. A suitable molecular weight ladder was used to accurately size the PCR product. The gel was run at 70V for at least one hour or until the PCR product is run three quarters of the way into the gel. The PCR product can now be visualized using an Alphaimager under U.V. light. A single band should be seen in a positive lane, and no band should be seen in a negative control lane. The size of the PCR product must match the expected product size.

2.5.5 Primer Design

The primers are designed using Applied Biosystems (AB) ABI Prism primer express version 2.0. Primer parameters are set as follows:

- Primer Tm (melting temperature): min (57℃) – max (63℃), optimum (60℃)
- Primer length: min (18bp) – max (22) bp, optimum (20)

- Primer GC% content: min (45%) – max (55%)

- Amplicon product size: min (150bp) – max (200bp)

The FASTA sequence of mRNA of interest was downloaded from National Centre for Biotechnology Information (NCBI) and loaded into the primer express software. The chosen primer pair sequences were then BLASTED in NCBI website to check for specificity of each primer.

The sequence of all primer sets are detailed below:

Table 2.4 Human primer sequences for RT-PCR and real-time PCR

Gene Name	**Orientation**	**Sequence**
GAPDH (house keeping gene)	Forward	5´-GAAGGTGAAGGTCGGAGT-3´
GAPDH (house keeping gene)	Reverse	5´-GAAGATGGTGATGGGATTTC-3´
PRKCD (DNA-PKcs)	Forward	5´-CCGGACGGACCTACTACGACT-3´
PRKDC (DNA-PKcs)	Reverse	5´-AGAACGACCTGGGCATCCT-3´
DCLRE1C (Artemis)	Forward	5´-ATCTCCATAGACCGCTTCGAT-3´
DCLRE1C (Artemis)	Reverse	5´-AGCTGCACTCCAACCTTCTTT-3´

2.6 Real-Time quantitative Reverse Transcription PCR (Real-Time qRT-PCR)

A two step RT-PCR can be performed using SYBR Green I dye (Applied Biosystems) to detect in “real time” direct measurements of PCR products with an ABI prism 7900HT Sequence detection system (Applied Biosystems). SYBR

Green I dye is attached directly to the double stranded DNA and the release of fluorescence is measured and recorded by the real time machine.

Reverse transcription was performed as described above and once cDNA is made, 1µl of cDNA was added to the SYBR Green PCR master mix as follows:

- 12.5µl of SYBR Green master mix (2x concentration)
- 1µl of forward and reverse primer
- 1µl of cDNA
- nuclease free water to 25µl

The above reaction dilutes the original stock of 2x concentration of SYBR Green to 1x concentration reaction mix. The reaction mix was then added to a MicroAmp optical 96-well reaction plate (Applied Biosystems) in triplicate. The reaction plate was sealed with an ABI-prism optical adhesive cover (Applied Biosystems), briefly centrifuged for 30 seconds to collect the sample, and run in the real time machine.

The programs used for real time PCR were:

	Temperature	**Time**	**No. of Cycles**
Hot Start	95℃	5 minutes	1 cycle
Denaturation	95℃	15 seconds	30-40 cycles
Annealing	60℃	45 seconds	

Dissociation curve analysis was performed immediately after the PCR run to check and verify results. The dissociation curve allows the check for primer dimer and non-specific amplification that may affect the quality of the data. Dissociation was always performed at the end of the PCR reaction. The PCR amplicons were dissociated at 95°C and allowed to slowly re-anneal. The change in fluorescence was plotted against the temperature. The change in fluorescence is due to a dye or probe interacting with the double-stranded DNA. Consequently, the quantitative PCR product can be run on an agarose gel to check for a clean single band at the estimated band size.

2.6.1 Optimizing primer concentration

Each set of primers must be optimized individually to determine the minimum primer concentrations that gives the lowest threshold cycle (C_t) and maximum ΔR_n while minimizing non-specific amplification.

Primer optimization studies:

Four different concentrations of forward and reverse primers were tested to find the optimized primer concentration. Figure 2.2 shows a primer concentration optimization test performed on human primary fibroblast (GM08399, F01-240, and CJ179) with the following concentrations of primers: 10pmol, 5pmol, 2.5pmol, and 1pmol.

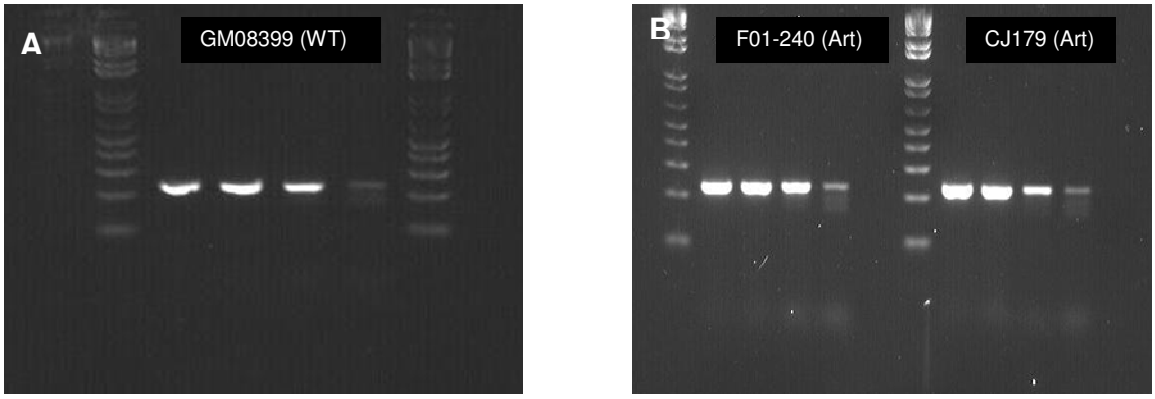

Figure 2.2 Sample gel electrophoresis
A| Expression of GAPDH in the GM08399 control cell line. Lanes 1 and 6 are markers. Lane 2: 1pmol, Lane 3: 2.5pmol, Lane 4: 5pmol, Lane 5: 10pmol. B| Expression of GAPDH in the F01-240 cell line (left) and the CJ179 cell line (right) at different concentrations of forward and reserve primers. Lanes 1 and 6 are markers. Lane 2, 7:1pmol, Lane 3, 8:2.5pmol, Lane 4, 9:5pmol, Lane 5, 10:10pmol.

DNA-PKcs annealing temperature optimization

Annealing temperature optimization was done to find the optimum temperature that would give the highest PCR product yield without the formation of secondary products or primer dimer formation.

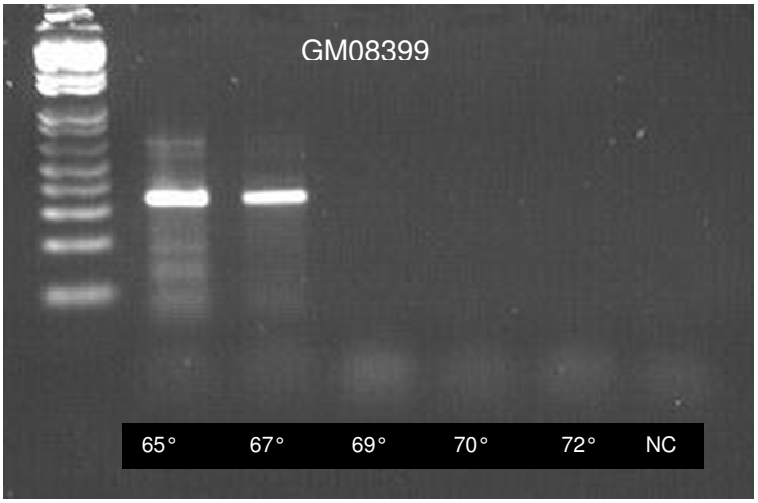

Figure 2.3 Optimizing primer annealing temperature
PCR image of PRKDC gene (DNA-PKcs), showing different annealing temperatures of DNA-PKcs in the GM08399 cell line.

From the above experiment (Figure 2.3) the optimum annealing temperature of primers designed to amplify the *PRKDC* gene (DNA-PKcs) was 67°C.

Real time RT-PCR optimization

After the PCR primer optimization was completed, the next step was to test the primer concentration using real-time RT-PCR. Figure 2.4 represents the amplification curve from real-time PCR showing the effect of the primer concentration on the efficiency of amplification.

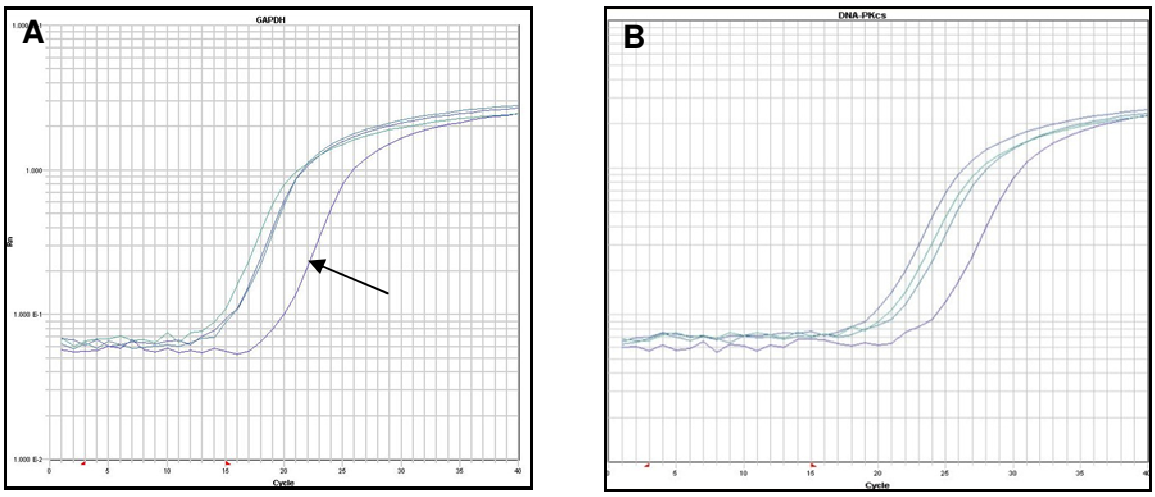

Figure 2.4 Real time PCR amplification curve.
A| Amplification curve for *GAPDH* primers at various concentrations. 10pmol of primer has reduced the amplification efficiency of GAPDH (arrow). **B**| Amplification curve for PRKDC gene (DNA-PKcs) primers at various primer concentrations. In both cases the control GM08399 cell line was used.

best set of primers that would only amplify the product of interest with no or a minimal amount of primer-dimer formation. Often primers anneal to their own 3' end or with 3' end of the other primer and this is usually visible as a low weight molecular band in gel electrophoresis. Primer dimer normally interferes and

often competes with the DNA fragment of interest and hence may distort the final PCR product. In real-time PCR technology, formation of primer dimers can distort the final fluorescence reading and must be removed completely from the reaction. Figure 2.5 show examples of reactions with and without primer dimer formation.

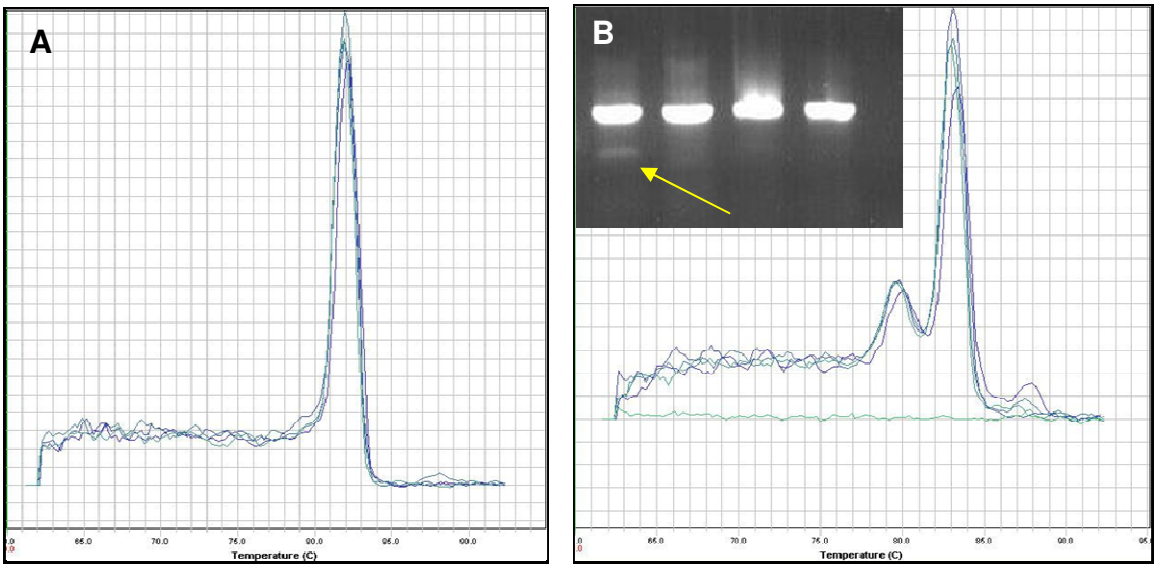

Figure 2.5 Dissociation curve
A| *GAPDH* showing a clean PCR product amplified under real time conditions. There are no signs of primer dimmer formation or secondary products.
B| DNA-PKcs primer with primer dimer formation. The extra peak on the left is a sign that extra product has been made (confirmed on gel electrophoresis yellow arrow). Therefore this specific DNA-PKcs primer set was not optimum and not used for analysis

2.7 Western blot

Western blot is a technique used to specifically detect and quantify protein from a tissue or cell samples. It uses gel electrophoresis to separate proteins according to size and mobility. Proteins are then transferred to a Polyvinylidene Fluoride (PVDF) membrane in a wet blot condition and the primary antibody detects and

binds to the specific target. Chemiluminescent dye is used to detect the Horseradish peroxidase (HRP) conjugated secondary antibody that is bound to the specific primary antibody and the protein of interest is detected on an X-ray film.

2.7.1 Protein Sample Preparation

Cells were grown to 80-90 percent confluence and the plate was rinsed six times with cold PBS. All the excess liquid was removed and 900µl of a 5x sample buffer (SB) containing 10 percent (v/v) sodium dodecyl sulfate (SDS), 250mM Tris pH 8.0, 50 percent (v/v) glycerol and 0.01 percent (w/v) bromophenol blue plus 50µl of protease Inhibitor and 50µl of beta-mercaptoethanol (BME) were added for at least one minute onto the plate. Cells were then scraped off using a cell scraper. Samples were collected into an Eppendorf tube and were stored at -20℃ for long-term storage. The sample was thawed and mechanically sheared ten times using a 1ml syringe and a 23g needle. The samples were kept on ice at this stage at all times to prevent protein denaturing. The samples were then spun at 13,000rpm for five minutes and the supernatant was aliquoted and transferred to a clean Eppendorf tube and stored at -20℃. It is recommended to avoid repeated thawing and freezing of the protein sample as this reduces the quality of the protein band and can denature the proteins.

2.7.2 Protein Quantification

Each protein in the sample was quantified using a RC DC-protein assay (Bio-rad). This assay was used since it was compatible with reagents in the sample

buffer and had a mainly high concentration of SDS and a strong reducing agent such as beta-mercaptoethanol. The assay was performed according to manufacturer's recommended protocol. In short, a serial dilution of 0.2mg/ml – 1.6mg/ml of protein standard was made using bovine serum albumin (BSA) diluted in sample buffer. This was used to construct a standard curve where all unknown sample protein concentration was measured against the standard curve.

One hundred and twenty five µl of reagent I was added to 25µl of each protein standard and protein sample vortexed and left for one minute. One hundred and twenty five µl of reagent II was added to the sample tube vortexed briefly and centrifuged at 15,000xg (13,000rpm) for five minutes at room temperature. The supernatant was discarded by tipping it onto a dry paper tissue. 127µ of reagent A', made earlier by 5µl of DC reagent S to 250µl of DC reagent A, was added to the tube and left for five minutes after a brief vortexing. It normally takes longer than five minutes for all the proteins to dissolve completely, as some surface membrane proteins are insoluble and difficult to dissolve. With a regular vortexing for 15 minutes all proteins were dissolved. At this point 1ml of DC reagent B was added to the tube, vortexed, and left for 15 minutes to incubate at room temperature. After 15 minutes absorbance was read at 750nm wavelength using a spectrophotometer (Eppendorf). The absorbance of protein standard was recorded first and a standard curve of protein concentration in mg/ml against absorbance was constructed (Figure 2.6). Absorbance of each protein sample

was read using the spectrophotometer and the concentration of each protein sample was calculated from the standard curve.

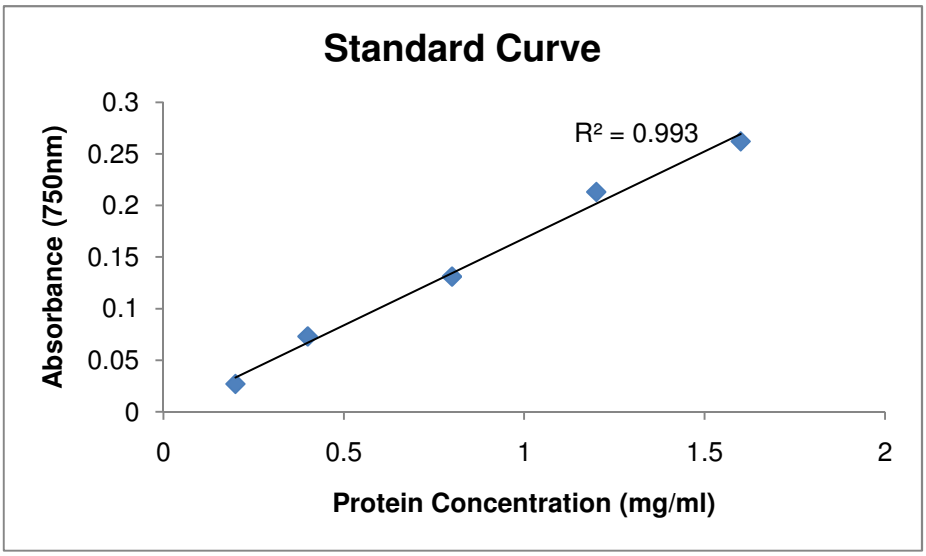

Figure 2.6. Standard curve used in protein quantification analysis.

2.7.3 Protein Gel Electrophoresis

An equal concentration of 50µg/50µl of each protein sample was diluted down in a sample buffer from its original concentration. Forty µl of the above protein sample was mixed with 20µl of the sample buffer, 1.5µl of protease inhibitor, and 1.0µl of beta-mercaptoethanol. The lid of the eppendurf tube was pierced and the protein sample was heated up to 95℃ for five minutes to denature the globular structure of the proteins.

Thirty µl of the prepared samples and 10µl of a high molecular weight protein marker (Invitrogen) was added to each well of a ready-made 4 percent precast gel (Bio-Rad). The lower the molecular weight of a protein of interest, the higher

the percentage of gel that is required. For example, a 10% gel will be sufficient for the separation of protein of 250KDalton (kDa) or less. In our experiments where heavy proteins such as DNA-PKcs (molecular weight of 460kDa) were involved, a 4 percent gel was used. The gel was bought ready-made or was made using the following ingredients:

-4.9ml distilled water (DW)

-6.0ml 30 percent acrylamide mix (protogel EC890)

-3.8ml 1.5M Tris pH 8.8 (36.3g Tris/200ml)

-150µl 10 percent SDS

-150µl 10 percent ammonium persulphate (APS) freshly made

-10µl TEMED

The above formula will give a 12 percent gel that is poured into the gel tank plate. The gel tank plate was set up following the manufacturer's protocol. The above gel was loaded immediately onto the gel plate, topped with water for even distribution, and left for 30 minutes to set. The stacking gel was then made with the following reagents:

-2.7ml DW

-670µl 30 percent Acrylamide mix

-500µl 1M Tris pH 6.8 (24.2g Tris/200ml)

-40µl 10 percent SDS

-40µl 10 percent APS

-6µl TEMED

The stacking gel was poured onto the gel (the excess water was blotted off first) and left to set for at least 15 minutes with a separation comb in place. Eventually the comb was removed and 30µl of prepared protein sample was loaded carefully onto each well. The protein marker was normally loaded on the first and last wells. The interior and exterior of the tank was filled with 1x running buffer made with 3.0g (w/v) of tris base, 14.4g (w/v) of glycine, 1g of SDS, distilled water to 1 liter. The samples were initially run at 100V until proteins were evenly located in the gel and the power was switched to 150V for approximately 45 minutes. The samples were checked regularly to prevent running off of the protein samples.

2.7.4 Blotting and transfer

Once proteins were separated in the gel based on their size and mobility (heavier proteins move slower and hence were at the top of the gel, whereas smaller proteins move faster and were found near the bottom of the gel), proteins were transferred onto a blotting paper. Polyvinylidine fluoride (PVDF) is a non-reactive membrane that has a non-specific affinity to amino acids. PVDF was activated by soaking in 100 percent methanol for 10 seconds. A sandwich of filter pad, 3mm filter paper, activated PVDF membrane, gel, 3mm filter paper, and filter pad was assembled according to the manufacturer's protocol (Bio-Rad). A small magnetic stirrer was placed in the tank, topped with 1x transfer buffer made with 11.25g (w/v) of glycine, 2.42g (w/v) of tris base, 200ml (v/v) of methanol and distilled water to 1 liter. The blotter was placed inside the tank and the tank was run at 100V for at least 90 minutes on a magnetic stirrer to create an even distribution

of the electrolysis. An ice pack was also placed inside the tank to prevent overheating of the buffer solution.

2.7.5 Blocking and antibody incubation

Once the transfer of protein from gel onto the PVDF membrane was complete (always check that protein markers were transferred onto the membrane) the proteins must be blocked with 5% blocking reagent containing 5g (w/v) of semi-skimmed milk (Marvel) in 100ml of Tris buffer saline-Tween (TBST) made with 16g (w/v) of NaCl, 0.2g (w/v) KCl, 3g (w/v) of Tris base, 0.1 percent (v/v) Tween-20 added to 800ml of distilled water adjusted pH to 7.6, and distilled water added to 1 liter. The membrane was left in 30ml of blocking solution for about one hour on a shaker at RT. The milk mixture blocks the unspecific binding of an antibody with the membrane. After one hour of blocking, the membrane was rinsed with TSBT and the primary antibody was added. The primary antibody was diluted down according to the manufacturer's recommendation and was further optimized by the user. Table 2.5 below shows all antibodies used in our experiment with optimized dilution ranges.

Primary antibody was diluted in a one in five dilution of 5 % blocking buffer in 1x TBST and added onto the membrane overnight on a shaker set at medium pace (200rpm/minute) at 4℃. The following day the membrane was washed twice with 1x TBST for 15 minutes each and incubated with a secondary antibody diluted in one in five dilution of 5 % blocking buffer on a shaker at RT for a minimum of one hour.

2.7.6 Protein detection with chemiluminescence

After one hour incubation with a secondary antibody the membrane was washed twice in 1x TBST for 15 minutes. Meanwhile ECL plus (Enhanced chemiluminescence) kit (GE Healthcare) was taken out of the fridge and left at RT to warm up. The amount of ECL required for detection was based on the size of the membrane and was recommended by the manufacturer to be of a final volume of 0.125m/cm^2 of membrane. The manufacturer's protocol was consulted for the exact mixture of chemical A and chemical B. As a rule of thumb, 2ml of reagent A was mixed with 50µl of reagent B. That is 1 part of reagent A mixed with 40 parts of reagent B. The ECL mixture was added onto the membrane and covered with saran wrap for five minutes in a dark room. The excess of the ECL was tipped off onto a paper towel, wrapped in the membrane facing down onto a piece of clean Saran wrap and placed in an x-ray cassette.

Table 2.5 Summary of primary and secondary antibodies used in western blot.

Antibody	**Manufacturer**	**Source**	**Clonality**	**Dilution (µl)**	
DNA-PKcs	Neomarker (Ab-4)	Mouse	Monoclonal	1:500	primary
Artemis	Santa Cruz (sc-23099)	Goat	Polyclonal	1:100	primary
Artemis	Abcam (ab3834)	Goat	Polyclonal	1:500	primary
Beta-actin	Abcam (ab8224)	Mouse	Monoclonal	1.25:1000	primary
GAPDH	Abcam (ab8245)	Mouse	Monoclonal	1:5000	primary
Anti-goat	Abcam	Rabbit	HRP-conjugated	1:2000	secondary
Anti-mouse	Abcam	Rabbit	HRP-conjugated	1:5000	secondary

Unexposed ECL plus hyperfilm (GE healthcare) was put on top of the membrane and the cassette closed and left for exposure for five minutes. The x-ray films were developed either manually in developer first (Kodak) and fixer (Kodak), or using an automatic machine (Xograph). The exposure time was assessed accordingly depending on the size of the exposed bands. If the protein bands were faint and could not be visualized then a second film was exposed for a longer period. The ECL chemiluminescence was active for at least one hour.

2.8 Ribonucleic Acid interference (RNAi)

2.8.1 Short interfering RNA (siRNA)

Since the discovery of RNAi in 1998 by Fire and Mello using *C. Elegans* (Fire et al., 1998), a whole range of small RNA molecules have been identified including microRNA (miRNA), small interfering RNA (siRNA), and Piwi-interacting RNA (piRNA) (Ghildiyal and Zamore, 2009) (for latest review). Each class of these RNAs differ in their modes of target regulation, their biogeneses, and in the biological pathways they regulate. RNAi was described by Fire and Mello to be a form of post-transcriptional gene silencing, whereby a dsRNA induces the degradation of homologous endogenous transcript, either reducing or totally inactivating the mRNA transcript of a specific gene (Fire et al., 1998).

In essence, a dsRNA is subjected into a cell with the aid of either a modified transfection medium in a passive manner (Dharmacon Accell delivery medium), or by lipofectamine coating or electroporation (in an active insertion). Depending on the mode of entry into a cell, dsRNAs are cleaved into short interfering RNA

(siRNA) duplexes by dicers that are part of the RNase III family of ds-RNA specific endonucleases (Nature Review online Animation, 2004. RNAi). Duplexes of siRNA then form a ribonucleoprotein complex known as RNAi silencing complex or RISC. RISC mediates the unwinding of siRNA duplexes, creating single stranded siRNA. These single stranded siRNA coupled with RISC then bind to target mRNA in a sequence specific manner and cleave the sites of mRNA binding. The cleaved mRNA section is recognised by the cell as aberrant and hence is destroyed. By destroying sections of mRNA of interest, translation is therefore prevented and hence the expression of the gene from which the mRNA was transcribed is silenced (Nature Review online Animation, 2004 RNAi http://www.nature.com/focus/rnai/animations/index.html).

This method of post-transcriptional gene silencing is transient and the expression of the specific mRNA will revert back to normal in human cells within 7 to 10 days post transfection.

2.8.2 Effective controls for RNAi Experiment

The selection of the proper controls in any RNAi experiment with an analysis of loss of function (LOF) of a target gene is key to the reliability, effectiveness, and efficacy of the specific RNAi experiment (Huppi et al., 2005). There are several criteria that should be met for an acceptable LOF analysis through RNAi experiment for publication that editors of *Nature Cell Biology* suggested in 2003. In short these criteria are as follows:

1. Mismatched or scrambled RNA (Also known as non-targeting siRNA)

2. Basic controls: Reduction in the expression level must be measured at the mRNA and protein levels, as well as the functional read outs whenever possible.

3. Quantitative control: A titration of siRNA is recommended to detect the lowest minimal concentration of siRNA for the required effect.

4. Multiplicity control: To be confident in the RNAi data is to demonstrate that the desired effect can be achieved with two or more siRNAs targeted to different sites in the message under study (Editorial, Nature Cell Biology 2003).

2.8.3 Experimental Procedure

2.8.3.1 Re-suspension of siRNA

The siRNA oligonucleotides (Accell smartpool) were purchased from Dharmacon (Thermo Scientific) and were re-suspended according to the manufacturer's recommended protocol. All siRNA oligonucleotides were delivered in a dry powder form and re-suspended in a siRNA re-suspension buffer provided by the manufacturer (Table 2.6).

All siRNAs were briefly centrifuged in a tube to collect the siRNA pellet at the bottom. According to the amount of siRNA, all the siRNA stock was diluted to a final concentration of 100µM/µl in 5x siRNA re-suspension buffer (Dharmacon), containing 20mMKCl, 6mM HEPES-pH 7.5, and 0.2 mM $MgCl_2$, diluted down to a

Table 2.6 Summary of controls in RNA Inhibition experiments

Control Type	Function	Products used
Positive Control	Optimizes and monitors efficiency of siRNA delivery into cells	Accell GAPD siRNA
Negative Control	Distinguishes sequence specific silencing from non-specific effects	Accell Non-targeting siRNA
Transfection Control	Determines optimal delivery condition	Accell Green Non-targeting siRNA
Untreated Control	Determines baseline cell viability phenotype and target gene level	Cells cultured without any siRNA treatment
Multiplicity Control	More than one siRNA is targeted to different sites of mRNA	Accell siRNA pool (with four siRNAs)

1x siRNA buffer with RNase free water (Dharmacon). Fifty µl of 1x siRNA buffer was added to 5nmol siRNA tube to give a final concentration of 100µm/µl. The solution was resuspended with a pipette three to five times to avoid introducing any bubbles. The solution was left on an orbital shaker set at 200rpm/minute for 30 minutes at RT. Then the solution was briefly centrifuged and the quality and concentration of siRNA was verified using an ultra violet (UV) spectrophotometer (Eppendorf) at 260nm. Table 2.7 summarizes the purity, quality, and total concentration of all siRNAs used in our experiments.

2.8.3.2 Accell siRNA delivery

The delivery of Accell siRNAs was unique in a sense that no transfection reagent was necessary for the uptake of the siRNAs into the cell. The modified Accell siRNA protocol works with the Accell delivery medium that was provided by the

company (Dharmacon). Due to its unique passive delivery method, a higher concentration of siRNAs was needed compared to conventional siRNA, with minimal disruption of the expression profile. Little or no delivery optimization was needed.

The schematic below (Figure 2.7) represents the exact experimental procedure used in all siRNA experiments.

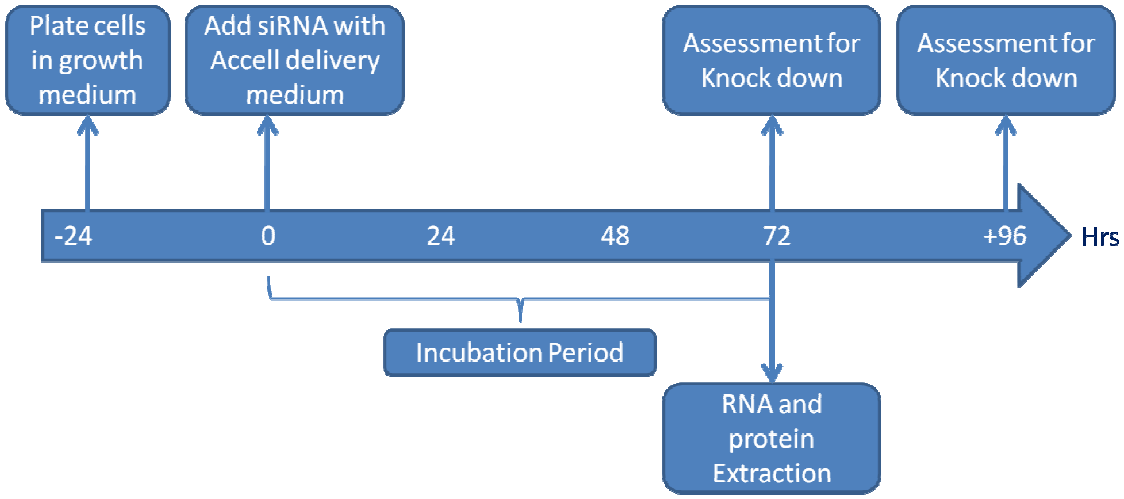

Figure 2.7. Work-flow and plate set up diagram of RNAi experiments

All siRNA experiments were performed using a 24-well plate (Nunc) with duplicates for each time point. For example, two wells were extracted for the assessment at 72, 96 hours, etc., post incubation. Cells were trypsinized and plated at a density of $0.045x10^6$ cells/1/2ml (roughly at 40 percent confluency) for all wells 24 hours prior to incubation at 37℃ with 10 % CO_2. All steps were done in a laminar flow cell culture hood using sterile techniques.

The stock solution of 100µM siRNAs was diluted down to 1µM with an Accell delivery medium (Dharmacon) the day prior to the incubation period.

Table 2.7. Summary of Accell short interfering RNA used in RNA inhibition experiments.

siRNA	Company/ Type	Stock Quantity	Working Quantity Concentration	Working Volume of 1x re-suspension buffer	Recommended Concentration	A260/280 (>2.0 is pure)
GAPDH (Housekeeping gene)	Dharmacon/Accell smart Pool	5nM	100µM	50µL	1µM	2.10
Non-Targeting (Scrambled)		5nM	100µM	50µL	1µM	2.20
Green Non-Targeting (FITC conjugated		5nM	100µM	50µL	1µM	N/A
PRKDC (DNA-PKcs)		50nM	100µM	500µl	1µM	2.17
DCLRE1C (Artemis)		50nM	100µM	500µl	1µM	2.09

A 2ml of Accell delivery medium containing 1µM final concentration of siRNA was added to each well after the removal of the growth medium. The cells were then left to incubate with the Accell delivery medium for at least 72 hours before the medium was replaced with standard growth medium (DMEM with 10%FCS). The mRNA and protein levels were assessed post each incubation. Proteins were extracted using a sample buffer and the total RNA was extracted using a Trizol reagent.

2.9 Statistical Analysis

Basic statistical analysis such as descriptive measurements and graphical display were done using Microsoft Excel 2007 software. In cases where comparative analysis between means were required, more advanced statistical software such as Minitab version 13 was used. All t-tests were done at 95 percent significance with α set at 0.05. In some cases SPSS version 13 software package was used.

Chapter 3 :

Analysis of chromosomal aberrations in Artemis defective human cell lines

3.1 Introduction

Telomeres are specialized structures found at the end of most eukaryotic and all of mammalian chromosomes. The combined action of telomeric DNA, telomere associated proteins, and telomerase, facilitate the protection, degradation, and in pathological cases fusion of mammalian chromosomal ends (de Lange, 2006). The discovery of telomeres by Muller and McClintock based on their cytological experiments, showed that broken chromosome ends, induced by ionizing radiation (IR), fuse together in contrast to natural chromosomes ends (telomeres) which remain intact (Muller 1938, McClintock 1941). Today it is well understood that IR causes double strand breaks (DSBs) in cellular DNA. These DSBs are largely responsible for generating chromosomal aberrations (CAs), including what Muller and McClintock referred to as “broken chromosome ends”, whereas telomeres are thought to act as protectors against CAs (de Lange, 2006). Studies have also shown that critically short telomeres behave as DSBs and this in turn activates the DNA damage response pathway and propagation of apoptosis/senescence via p53 activation (Smith and de Lange, 2000). It is likely that telomere shortening alters telomere structure leading to telomere deprotection or chromosome un-capping, a process in which the T-loop structure (see Chapter 1) collapses and the end of chromosome becomes, in effect, a DNA DSB. Therefore, the currently accepted view is that telomeres hide natural chromosomal DNA ends from cellular processes that recognize and repair DSBs.

One of the objectives of this thesis is to examine further the relationship between telomere maintenance and processes involved in DSB repair. As explained earlier (Chapter 1), mammalian cells use two mechanisms for DSB repair: HR and NHEJ.

Previous studies have shown that two NHEJ proteins, Ku and DNA-PKcs, if dysfunctional, will cause telomere deprotection or chromosome un-capping which manifest as the presence of high numbers of chromosome end-to-end fusions or telomeric fusions in affected cells (de Lange, 2006). Follow up studies have conclusively demonstrated that both proteins are actually present at telomeres thus establishing that telomere maintenance and NHEJ are inter-related processes. It is therefore of interest to examine whether other NHEJ proteins affect telomere maintenance.

In this chapter a detailed analysis of spontaneous and radiation induced CAs in primary fibroblast cell lines from two RS-SCID patients have been carried out. RS SCID is a human syndrome cause by defective Artemis, one of the proteins involved in NHEJ.

3.2 Results

3.2.1 Analysis of CAs induced by IR using classical cytological methods

Artemis defective human cell lines show elevated frequencies of radiation induced CAs, in particular chromosome breaks (Darroudi et al., 2007). We used primary fibroblast cell lines from two RS-SCID patients (F01-240 and CJ179) in which defects with Artemis transcript have been well characterized (Riballo et al., 2004) (see section 2.1.1) and a normal human primary fibroblast cell line (GM08399) to check whether IR induced CAs show previously published pattern (Darroudi et al., 2007). All three cell lines were subjected to 0.5Gy and 1.0Gy of gamma rays. We used the classical Giemsa staining method to detect CAs and recorded chromosome breaks, dicentric and ring chromosomes. Complex CAs were also noted. Two independent experiments were performed and in each experiment at least 100

metaphase cells were analyzed totalling 200 in some groups (see table 3.1) (except in CJ179 and GM08399 where 65 and 72 metaphase spreads were recorded respectively at the dose of 0.5Gy). In total, 1,396 metaphase cells were analysed. A summary of cell numbers analyzed and distribution of individual CAs are given in Table 3.1. The same results accompanied by the statistical analysis are presented in a graphical format in Figure 3.1. Examples of CAs observed are given in Figure 3.2.

The frequencies of spontaneously occurring CAs were similar in all three cell lines (Table 3.1and Figure. 3.1). When cells were subjected to IR exposure, the two Artemis defective cell lines showed ~3.5 fold increase in frequencies of IR induced chromosome breaks at the dose of 1.0 Gy compared to the normal cell line. At the dose of 0.5 Gy only one cell line (CJ179) showed significantly higher level of chromosome breaks relative to the control line. The difference between the two Artemis defective lines at the dose of 0.5 Gy can be attributed to different mutations that may cause quantitatively different effects at low doses. A similar situation with different Artemis defective cell lines was noted by (Musio et al., 2005). However, our results show a slight difference in comparison with those of Darroudi et al. (2007) when analyzing frequencies of dicentric and ring chromosomes. We observed a small but significant increase in frequencies of dicentric and ring chromosomes at the dose of 1.0 Gy in Artemis defective cell lines relative to the control line. In contrast, Darroudi et al., (2007) found no difference in frequencies of either IR induced dicentric/ring chromosomes nor other IR induced exchange CAs such as translocations between Artemis defective and control cell lines.

Table 3.1 Classical cytological analysis of CA.
Results from the two sets of experiments based on the classical cytological (giemsa staining) method of analyzing CAs. (Numbers in brackets refer to event per cell.)

Cell line	Metaphase cells analysed	Chromosome breaks	Ring chromosomes	Dicentric chromosomes	Complex CAs
CJ179 (Artemis defective)					
Control	201	13 (0.065)	5 (0.025)	1 (0.005)	6 (0.030)
0.5 Gy	65	19 (0.290)	1 (0.015)	3 (0.046)	4 (0.060)
1 Gy	188	65 (0.350)	22 (0.117)	14 (0.074)	4 (0.021)
F01-240 (Artemis defective)					
Control	184	9 (0.049)	4 (0.022)	0 (0.000)	6 (0.033)
0.5 Gy	191	19 (0.099)	16 (0.084)	5 (0.026)	5 (0.026)
1 Gy	126	36 (0.286)	12 (0.095)	2 (0.016)	8 (0.063)
GM08399 (normal control cell line)					
Control	211	12 (0.057)	9 (0.043)	2 (0.009)	4 (0.019)
0.5 Gy	72	8 (0.111)	4 (0.060)	0 (0.000)	2 (0.030)
1 Gy	100	10 (0.100)	5 (0.050)	1 (0.010)	4 (0.040)

We attribute the difference between our results and results of Darroudi et al. (2007) to either a different quality of IR used in two studies or the fact that the numbers of dicentric and ring chromosomes observed are relatively low and different statistical methods used in two studies may give different results.

Taken together our results show that Artemis defective human cell lines have higher levels of IR induced chromosome breaks, compared to the control cell line. This finding confirms the published results in particular those of Darroudi et al. (2007) and are also similar to that of Musio et al., (2005). However, we also observed increase

in IR induced dicentric/ring chromosomes in Artemis defective cells in contrast to Darroudi et al. (2007).

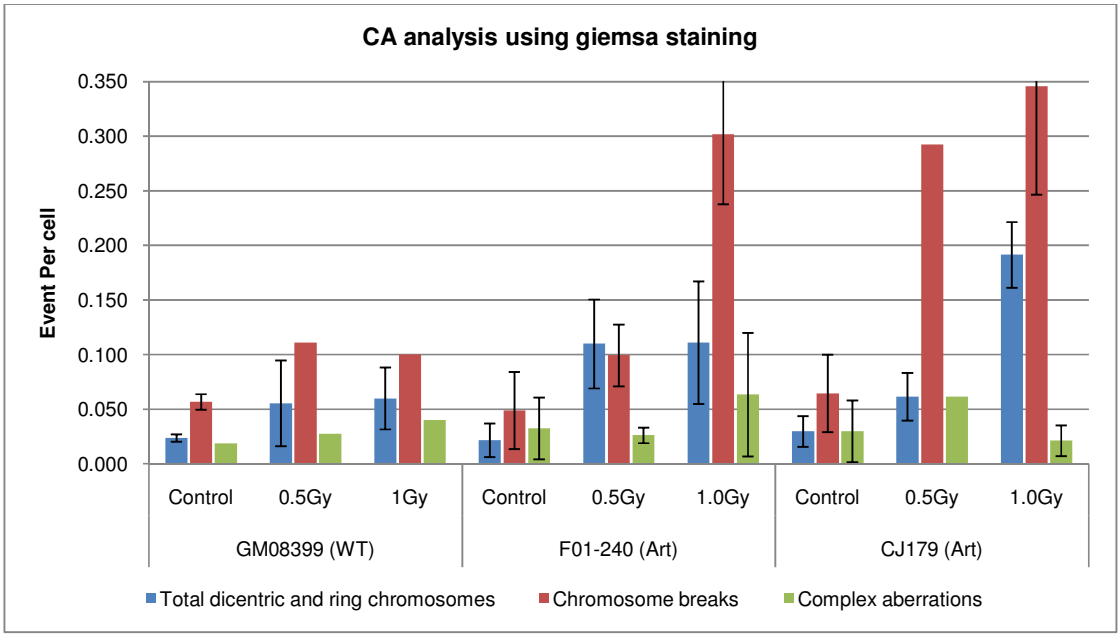

Figure 3.1 CAs induced by IR in Artemis defective and control cell lines. Based on the two sets of independent experiments. Error bars indicate SD.

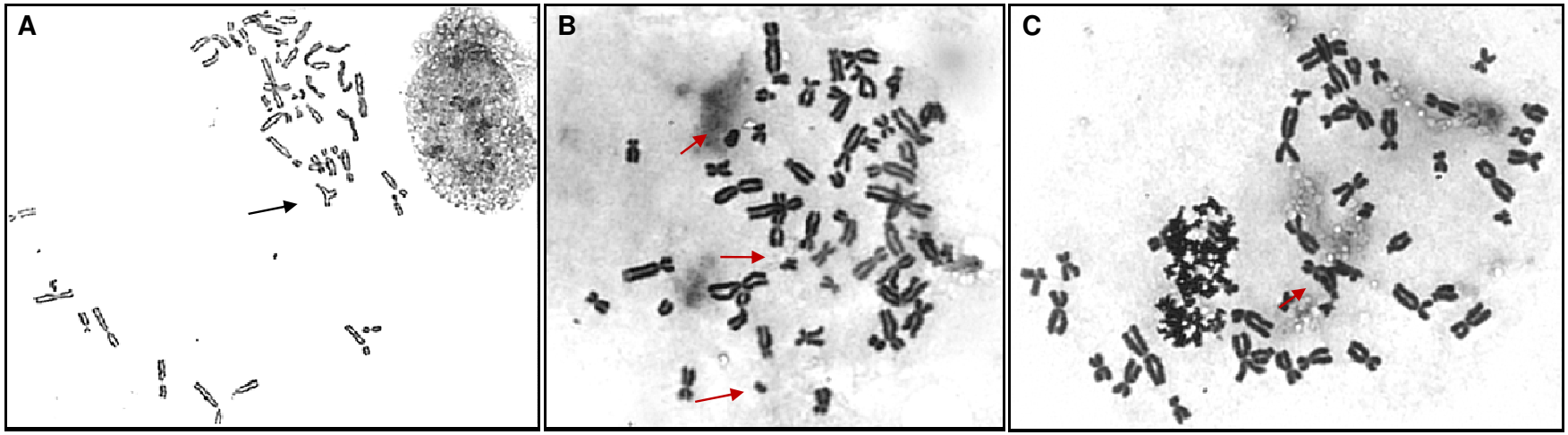

Figure 3.2 Examples of radiation induced CAs in Artemis defective cell line.
CJ179 cell line were exposed to 1.0Gy of gamma radiation. **A**| A complex structural aberration – Triradial. **B**| Chromosome and chromatid breaks and a small ring chromosome. **C**| Dicentric chromosome.

3.2.2 Analysis of CAs involving telomeres by FISH

Having established that the two Artemis defective cell lines show elevated frequencies of IR induced CAs we wanted to find out whether the same cell lines show any evidence of telomere dysfunction at the cytological level. The easiest way to test for this possibility is to apply the FISH method that detects telomeric sequences using a highly efficient telomeric peptide nucleic acid (PNA) probe (see Chapter 2). We will refer to this method as Telo-FISH in the rest of the text.

The clearest evidence of telomere dysfunction at the cytological level is the presence of end-to-end chromosome fusions or associations in affected cells. The analysis of spontaneous CAs in Artemis defective cell lines by classical cytological methods (Table 3.1 and Figure 3.1) did not reveal any evidence of telomeric fusions which manifest as end-to-end chromosome fusions which are in effect dicentric chromosomes lacking chromosome fragments. However, classical cytological staining methods would miss more subtle telomere defects such as single chromatid fusions/associations or fusions involving acrocentric chromosomes.

Furthermore, elevated levels of telomeric fusions were observed by Rooney et al. (2003), in Artemis deficient mouse embryonic stem (ES) cells after extensive FISH analysis. For those reasons we resorted to the Telo-FISH methodology to find out whether Artemis defective human cell lines show any evidence of telomere dysfunction at the cytological level.

3.2.2.1 Spontaneous chromosome fusions in Artemis defective lines

We started by analyzing spontaneous chromosome fusions by Telo-FISH (Table 3.2). We classified chromosome fusions into two categories: Type 1 and Type 2 (Figure 3.3). Type 1 chromosome fusions are true telomeric fusions and they represent a clear

sign of telomere dysfunction (see Figure 3.3). Type 2 chromosome fusions largely represent IR induced exchange CAs such as dicentrics and translocations (see Figure 3.3). Therefore, Type 2 fusion does not constitute CAs caused by telomere dysfunction.

The total number of chromosome fusions, chromosome breaks, and missing chromatid signals (MCS) were recorded. In four separate experiments a total of 478 metaphase cells were analysed (Table 3.2). Spontaneous chromosome or chromatid breaks can occur at a very low frequency in primary fibroblast cells (see section 3.2.1). These can arise endogenously as a result of failed V(D)J recombination processes in formation of immune cells and in meiosis during cross over and DNA replication (Riballo et al., 2004). We observed no significant differences between the frequency of spontaneous chromosome breaks and fragments in any of the three cell lines, therefore confirming our findings from the previous section (3.2.1) and published data (Darroudi et al., 2007).

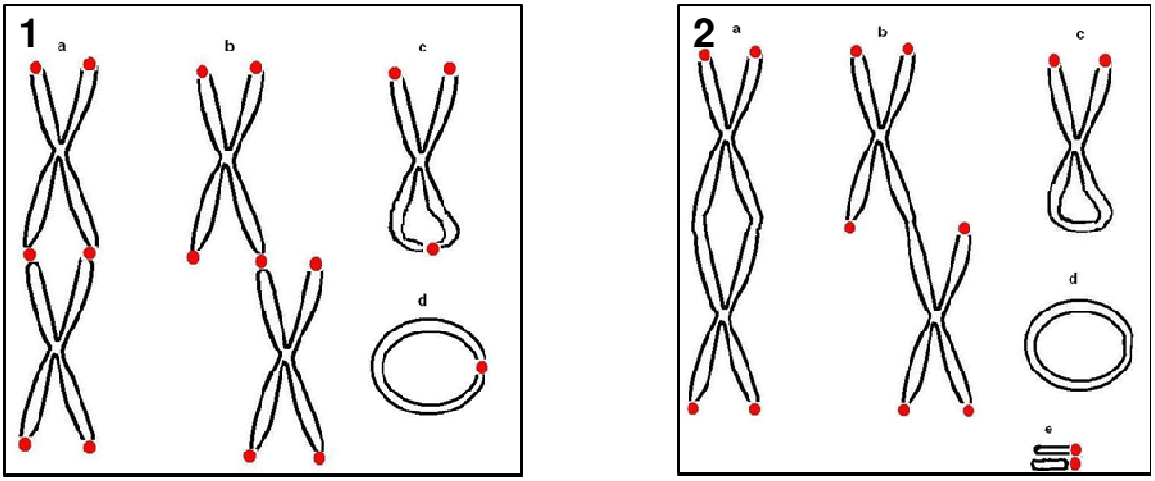

Figure 3.3 Schematic representation of Type 1 and Type 2 chromosome fusions.
1| Type 1 chromosome fusion occurs when telomeres fuse or associate together (a| chromosome type, b| chromatid type, c| sister chromatid union, d| ring chromosome). Type 1 fusion is easily recognized by the presence of telomeric signal (red) at fusion points. 2| Type 2 chromsome fusion occurs without the presence of telomeres at fusion points. (a & b| chromosome and chromatid type, c| sister chromatid union, d| ring chromosome, e| acentric/chromosome fragment. Type 2 chromsome fusion included IR induced CAs.

Table 3.2 Spontaneous chromosome fusions in Artemis defective cell lines. (Numbers in bracket indicate event per cell.)

Cell Line	Metaphase cells analysed	Chromosome /Chromatic Breaks	Telomere (Type 1)	Fusions	Missing chromatid signals
CJ179 (Art)	193	3 (0.016)	13 (0.067)		181 (0.94)
F01-240 (Art)	174	7 (0.040)	14 (0.080)		202 (1.17)
GM08399 (WT)	111	3 (0.027)	2 (0.018)		201 (1.8)

The total number of Type 1 telomeric fusions, however, was significantly higher in the two Artemis defective lines compared to a normal control line ($p<0.001$) (Table 3.2, Figure 3.4) Both Artemis defective lines, on average, were four times more likely to have Type 1 fusions indicative of dysfunctional telomeres than the normal control cell line. Most Type 1 fusions observed were of chromatid type. We have not observed any Type 2 chromosome fusion. Therefore, our results show low levels of spontaneous Type 1 chromosome fusions in Artemis defective human cell lines (Table 3.2, Figure 3.4). We found no significant differences in the observed number of MCS between cell lines.

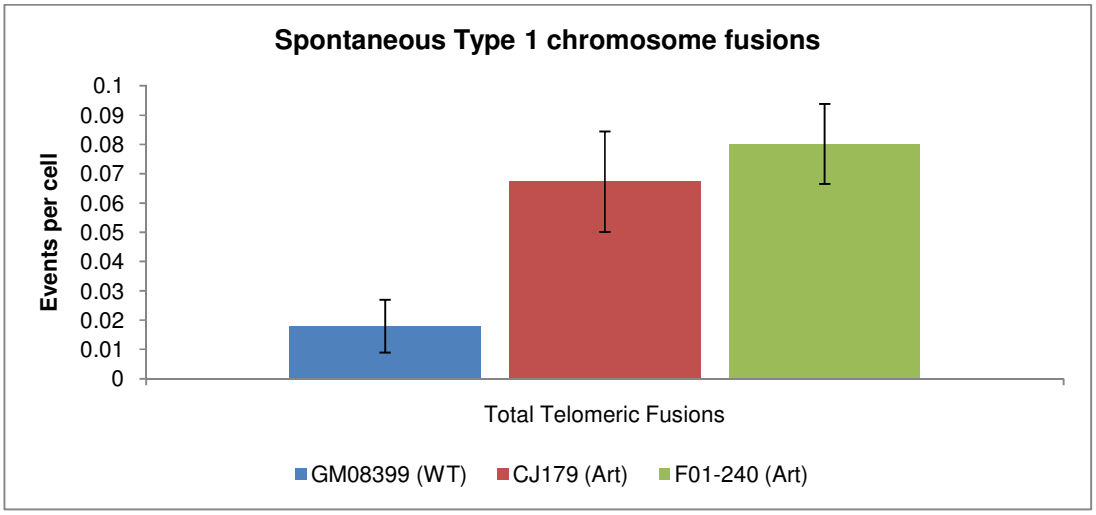

Figure 3.4: Spontaneous Type 1 chromosome fusions in Artemis defective cell lines. Error bars represents SD.

3.2.2.2 Radiation induced telomere dysfunction in Artemis defective lines

We next examined whether the frequency of Type 1 chromosome fusions is elevated following exposure of Artemis deficient cell lines to IR. We performed three independent experiments using does of 0.5Gy and 1.0Gy gamma rays.

Table 3.5 (Appendix I) represents the summary of all three experiments. Both Type 1 and Type 2 chromosome fusions were recorded (Table 3.3, Figure 3.5). In total, 1,168 metaphases were analysed (Table 3.3). It is important to note that Type 2 fusion represents IR induced dicentric and ring chromosomes. The frequencies of Type 2 fusions should, therefore, match frequencies of dicentric and ring chromosomes observed after the classical cytological analysis presented in Table 3.1, Figure 3.1. As expected this was roughly the case. For example, the CJ179 showed 0.14 Type 2 fusions per cell at the dose of 1.0 Gy almost whereas we observed 0.19 dicentrics/cell using the Giemsa staining (Table 3.1, Figure 3.1). Given that Type 2 fusions are not relevant for telomere function as they are caused by DSBs occurring at interstitial chromosome locations they have not been considered in further analysis.

Interestingly, the level of Type 1 fusions, which represent genuine telomeric fusions and therefore signify a telomere associated defect, were significantly higher in both Artemis defective lines than in the control line ($p < 0.001$) at the dose of 1.0 Gy (Table 3.3). However, only the CJ179 cell line showed statistically significant difference in Type 1 fusions relative to the control line at both doses (0.5 and 1.0 Gy). Relative insensitivity of the F01-240 cell line to Type 1 fusions at 0.5 Gy can be attributed to different mutations that cause quantitatively different effects as discussed earlier. Therefore, our results suggest that IR induced CAs that affect telomeres in Artemis defective cell lines are slightly, but significantly, elevated in comparison to their

counterparts in the control cell line. This further indicates the presence of a mild telomere dysfunction phenotype as a result of Artemis deficiency in human cells.

Telo-FISH have also confirmed that the two Artemis defective cell lines showed higher frequencies of IR induced chromosome breaks compared to the normal control cell line, and the difference was significant ($p < 0.001$) (Figure 3.5). This was similar to our data from classical cytogenetic studies (Table 3.1, Figure 3.1) and results published by(Darroudi et al., 2007).

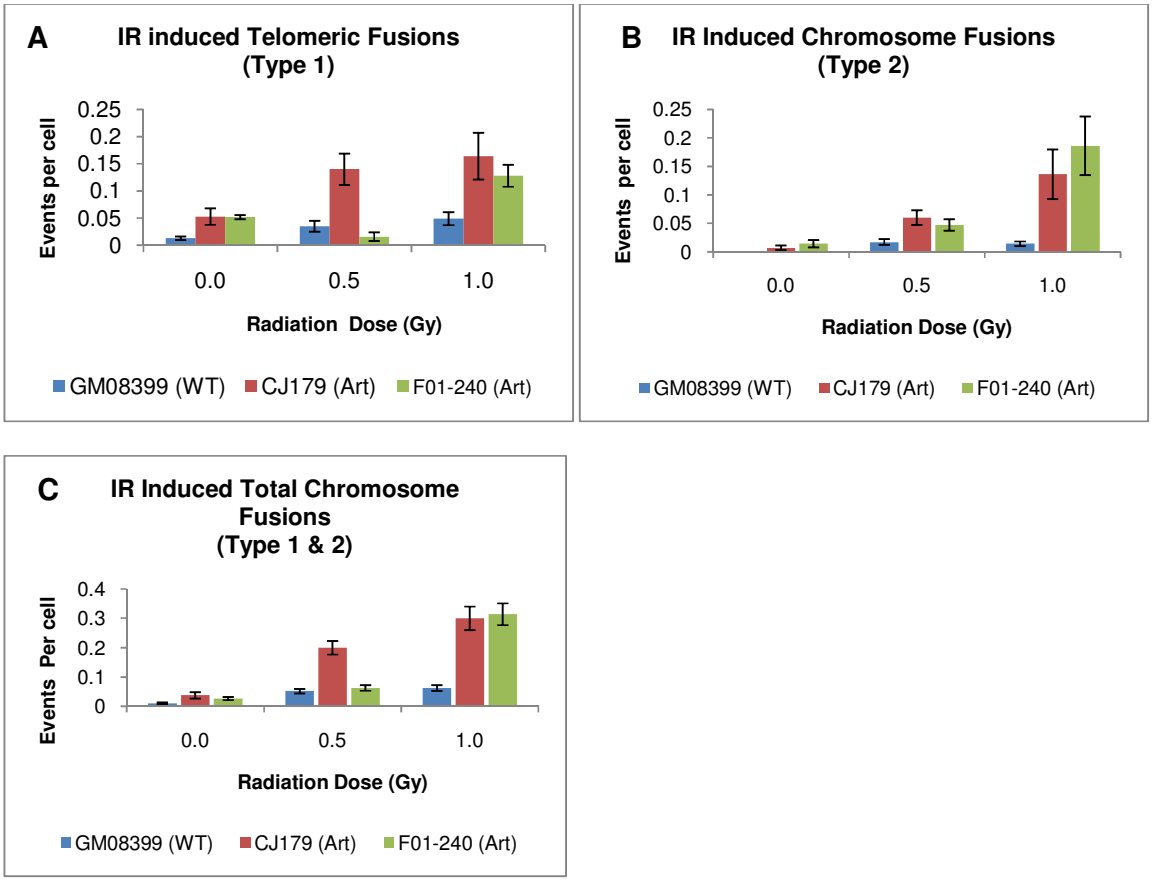

Figure 3.5. Graphical representation of IR induced chromosome fusions.
A| Type 1 chromosome fusions **B**| Type 2 chromosome fusions **C**| Type 1 and Type 2 chromosome fusions. The error bars indicates SD.

Table 3.3. Summary of IR induced CAs.
Missing chromatid signals (MCS) from each metaphase cells were also noted. (Numbers in bracket indicate events per cell.)

Cell Line	Radiation Dose (Gy)	Metaphase cells analysed	Chromosome/Chromatid Breaks	Type 1 & 2 chromosome fusions	Type 1 chromosome fusions	MCS
CJ179 (Art)	0	131	11 (0.084)	5 (0.038)	4 (0.031)	(1.473)
	0.5	100	14 (0.140)	20 (0.200)	14 (0.140)	(1.700)
	1.0	110	42 (0.382)	33 (0.300)	18 (0.164)	(1.345)
F01-240 (Art)	0	151	14 (0.093)	4 (0.027)	2 (0.013)	(0.331)
	0.5	128	28 (0.219)	8 (0.063)	2 (0.016)	(0.891)
	1.0	102	43 (0.422)	32 (0.314)	13 (0.128)	(0.941)
GM08399 (WT)	0	187	2 (0.011)	2 (0.011)	2 (0.011)	(1.219)
	0.5	115	5 (0.043)	6 (0.052)	4 (0.035)	(0.983)
	1.0	144	14 (0.097)	9 (0.063)	7 (0.049)	(1.194)

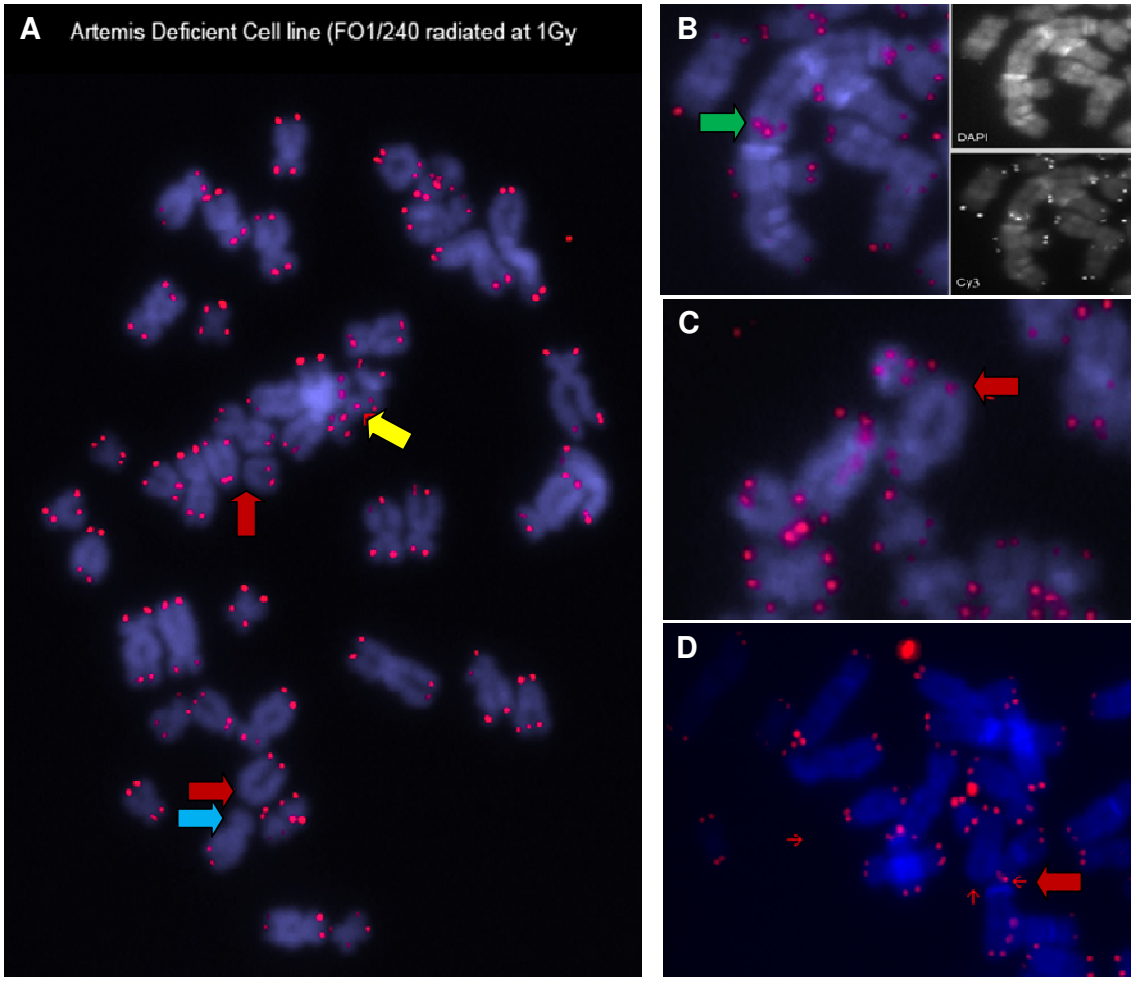

Figure 3.6 Examples of chromosome abnormalities observed after Telo-FISH.
A| A metaphase spread from an Artemis defective cell line (F01-240) with multiple chromosome breaks (red arrow), a chromatid type 1 telomeric fusion (yellow arrow), and a sister chromatid union without a telomeric signal (blue arrow). **B**| Chromosome type dicentric type 1 telomeric fusion (green arrow). Please note the fusion of telomeres in the middle of the Dicentric chromosome (inner pictures). **C**| Appearance of sister chromatid union as Type 1 fusion (red arrow). **D**| Another example of a chromosome type Dicentric with telomeric fusion (Type 1) (red arrow).

3.3 Discussion

The first evidence of chromosomal abnormalities in Artemis defective cells that result from telomere dysfunction was presented by Rooney et al. (2003). Their analysis of mouse ES cells that lack functional Artemis revealed significantly higher levels of telomeric fusions in comparison to the control cell line.

In contrast, two published studies that used Artemis defective human cell lines (Darroudi et al. 2007, Musio et al. 2005) reported no evidence of either spontaneous or IR induced CAs resulting from telomere dysfunction. However, these studies were not designed to specifically probe for telomere dysfunction in Artemis defective cell lines. Telomere dysfunction at the cytological level can be conclusively identified only by Telo-FISH as shown by Rooney et al. (2003). None of the above mentioned studies using Artemis defective human cell lines employed the Telo-FISH method.

The aim of our study was, therefore, to employ the Telo-FISH method with the purpose of identifying subtle chromosome abnormalities resulting from telomere dysfunction in Artemis defective cell lines that cannot be detected by classical cytological methods. In line with Rooney et al. (2003) our results revealed a slight but significant increase in both spontaneous and IR induced telomeric fusions in Artemis defective cell lines relative to the control cell line. It is important to stress that most of telomeric fusions observed were of chromatid type.

Previous studies have shown that two more NHEJ proteins, namely Ku and DNA-PKcs, affect telomere function. For example, Ku and DNA-PKcs defective mouse cells show high levels of telomeric fusions (Bailey et al,. 1999). In many instances multiple telomeric fusions were present in a single cell (Bailey et al,. 1999 and 2004). In contrast, frequencies of telomeric fusions in Artemis defective mouse cells were much lower than in Ku or DNA-PKcs defective cells as reported by Rooney et al. (2003). For example, Rooney et al. (2003) found 8 spontaneous telomeric fusions in 130 analyzed mouse ES cells (0.06/ cell). This is remarkably similar to our results. We found, on average, 0.05 spontaneous telomeric fusion/cell in two Artemis defective human cell lines. In contrast, the levels of spontaneous telomere fusions in

Ku or DNA-PKcs defective cells were > 10 times higher (Bailey et al., 1999). This suggests that the effect of dysfunctional Artemis on telomeres in mammalian cells is much milder in comparison with Ku or DNA-PKcs defects. In that sense, the Artemis effect on telomeres is more similar to another DSB repair protein, namely RAD54. Mice defective in this protein show slightly but significantly elevated levels of telomeric fusions in comparison with cells from control mice (Jaco et al., 2003).

It is interesting that we have also found increased incidence of IR induced telomeric fusions in Artemis defective cell lines (Table 3.3 and Figure 3.5). This finding suggests that IR can destabilize further telomeres in Artemis defective cells and probably convert them into DSBs which then can interact with other destabilized telomeres or DSBs located at interstitial chromosome locations to produce either true telomeric fusions (end-to-end chromosome fusions) or exchange CAs such as translocations. Our Telo-FISH method was not able to distinguish between the above two types of events. A method called CO-FISH (chromosome orientation FISH) can make distinction between end-to-end chromsome fusions and exchange CAs such as translocations that involve telomeres. Using this method Bailey et al. (2004) demonstrated two types of CAs involving telomeres in mouse DNA-PKcs defective cells: end-to-end chromosome fusions and translocations. Observed end-to-end chromosome fusions were mostly of chromatid type as in our case. Therefore, our results reveal a potential similarity between Artemis and DNA-PKcs effects on telomeres, namely elevated levels of chromatid type telomeric fusions following exposure of cells to IR.

An obvious question to ask is how exactly Artemis causes telomere dysfunction in mammalian cells. There are two potential scenarios here. It is well documented that

DNA-PKcs and Artemis functionally interact during the NHEJ process. Artemis is one of the DNA-PKcs phosphorylation targets (Ma et al., 2004, Ma et al., 2005). Given that DNA-PKcs associate with telomeres through associations with the shelterin complex (Hsu et al., 1999 & 2000, Song et al., 2000, d'Adda di Fagagna et al., 2001) it is possible that dysfunctional Artemis may affect this association. The consequence would be the induction of alterations in molecular structure of telomeres and subsequent telomere deprotection or chromosome un-capping.

Alternatively, Artemis could affect telomere maintenance true interactions with a protein called Apollo. This protein, which is a close homologue of Artemis, directly interacts with TRF2 (Lenain et al., 2006, van Overbeek and de Lange, 2006). Furthermore, the Apollo defect in human cells leads to increase in telomeric fusions (Lenain et al., 2006). Apollo is also involved in DNA damage response. For example. Apollo defective mouse cells show sensitivity to IR suggesting a deficiency in DNA damage response (van Overbeek and de Lange, 2006). Given a close homology between Artemis and Apollo they may functionally interact during cellular DNA damage response and these interactions may have effects on telomere maintenance. In this sense it is of interest to examine biochemical associations between Artemis and shelterin. Unfortunately, examination of these interactions was beyond the scope of this thesis.

In conclusion, we have shown that Artemis defect in human cell lines causes a mild telomere dysfunction phenotype detectable at the cytological level. The nature of telomere dysfunction phenotype appears to be similar to that observed in DNA-PKcs defective cells as exemplified by the presence IR induced chromatid telomeric

fusions in both cell types. However, mechanisms by which dysfunctional Artemis affects telomeres remain unclear.

Chapter 4 : Analysis of telomere function in Artemis defective cell lines using TIF assay

4.1 Introduction

In the previous chapter we have shown that Artemis defective human cell lines show mild telomere dysfunction which manifests as the presence of higher frequencies of Type 1 chromosome fusions in comparison with the control normal cell line. This finding is significant as it implies that Artemis, which is essentially a NHEJ protein, may directly or indirectly, affect telomere function. The role of Artemis in telomere function was not unanticipated. A study employing mouse ES cells lacking functional Artemis reported elevated frequencies of telomeric fusions (Rooney et al., 2003). Similarly, one of the Artemis defective cell lines (F01-240) used in this study was shown earlier to have accelerated telomere shortening (Cabuy et al., 2005). Accelerated telomere shortening is usually associated with the subsequent loss of telomere function (Cabuy et al., 2005). Furthermore, a protein called Apollo, which is a close relative of Artemis, has recently been shown to affect telomere maintenance. Cells lacking Apollo show elevated frequencies of telomeric fusions (Lenain et al., 2006). Apollo itself was found to be associated with TRF2, a telomeric protein which constitutes a part of the shelterin complex (Lenain et al., 2006, van Overbeek and de Lange, 2006)

It is of interest to examine this mild telomere dysfunction phenotype in Artemis defective cells in more detail. A relatively quick way of analyzing telomere function in human cells is through the use of a recently developed method called Telomere dysfunction Induced Foci (TIF) (Takai et al., 2003). When telomeres become dysfunctional they are no longer able to provide chromosome “capping” function, most likely as a result of the collapse of the T-loop structure. This, in turn, exposes natural chromosomal ends, normally hidden by the T-loop structure, as ordinary

DSBs and leads to activation of DNA damage response (d'Adda di Fagagna et al., 2003, Takai et al., 2003). Therefore, the TIF protocol must rely on the combination of markers that simultaneously detect a) DNA damage including DNA DSBs and b) telomeres. A common marker of DNA damage in mammalian cells is the phosphorylated form of histone γH2AX (Jeggo & Lobrich, 2005). Another suitable marker is 53BP1 (Takai et al., 2003). Antibodies against both proteins have been used in the original TIF protocol with equal success (Takai et al., 2003, van Overbeek & de Lange 2006, Dimitrova & de Lange, 2006). In the original TIF protocol telomeres have been detected using antibody against TRF2 (Takai et al., 2003). When two antibodies (first antibody: marker of DNA damage; second antibody telomere marker) are combined simultaneously they should be labelled with different fluorochromes so that the actual site of a DSB at a telomere can be recognized as an overlap between two colours.

Our aim in this chapter is to describe a) development of a modified TIF protocol and b) analysis of telomere function by this protocol in Artemis defective cell lines. In our modified protocol a marker for detecting telomeres is no longer an antibody but rather a highly sensitive telomeric PNA probe (Landsdorp, 1996). Therefore, our modified protocol is based on a combination of immunocytochemistry and FISH and it is an example of an increasingly used set of protocols referred to as immuno-FISH. The key reason for replacing telomeric antibody with a probe is sensitivity. The assumed resolution of PNA FISH is ~200 base pairs (Landsdorp, 1996, Poon and Landsdorp 2001). This length of DNA is far beyond antibody detection. The advantage of a modified TIF is that it can detect telomeres more reliably than an antibody against telomeric proteins which could miss very short telomeres.

4.2 Results

4.2.1 Setting up a modified TIF assay protocol

The original TIF method described by Takai et al., (2003) was sensitive enough but had a serious disadvantage. It relied on detecting telomeres using an antibody against a telomeric protein. Currently, there are no commercially available antibodies against telomeric proteins that can be used reliably to detect telomeres on cytological preparations. Takai et al (2003) used their own high quality antibody which is not commercially available. Furthermore, use of antibodies to detect short DNA sequences such as telomeres is questionable as the shortest telomeres would be undetectable. For these two reasons we decided that in our modified TIF protocol the telomeric antibody will be replaced by the telomeric PNA probe which can reliable detect very short telomeric DNA sequences (i.e. 200 b.p.). Detection of DNA damage remains unchanged and it relies on an antibody against γH2AX. Therefore, our modified protocol is an example of immuno-FISH.

The biggest problem in immuno-FISH is to establish conditions which will allow preservation of antigens following a harsh treatment of cells by FISH protocols which effectively destroy proteins and preclude their subsequent detection. The usual procedure is to a) detect desired antigens by an appropriate primary antibody, b) apply additional fixative treatment designed to protect bound antibody against the subsequent FISH related treatment, c) perform FISH and d) detect the primary antibody by an appropriate fluorochrome attached secondary antibody (Herbig et al., 2004). We have spent almost seven weeks setting up the modified TIF protocol. Table 4.1 summarizes all the experiments carried out with the outcome from each experiment until a reliable protocol was established.

A similar protocol was published by Herbig et al (2004). However, we needed to modify this protocol to suit fibroblast cell lines. We also received invaluable practical advice from Dr. Julio Masabanda, a research fellow from Division of Biosciences at Brunel University. All experiments listed in Table 4.1 have been performed on the normal primary fibroblast cell line (GM08399).

Table 4.1. Establishment of TIF assay protocol.
All experiments were performed on normal human primary fibroblasts (GM08399) grown on poly-prep slides (See Chapter 2 for methodology). In each experiment duplicate slides were incubated, one as a control slide and one exposed to Bleomycine to induce DNA-damage.

Experiment No:	Aim	Method used	Change(s) to the method	Outcome
Experiment 1	To test the new antibody (γH2AX)	Immunohistochemistry	N/A	Positive
Experiment 2	Simultaneous FISH and immunocytochemistry	PNA was added after antibody addition and hybridized for two minutes	PBS was used to wash after each part	No visible γH2AX signal. Clearly visible telomeric PNA signal
Experiment 3	FISH before addition of γH2AX antibody.	Hybridize with PNA for two minutes, wash with PBS and add γH2AX	PNA followed by γH2AX. Extra fixation.	Negative – No γH2AX or telomeric signal.
Experiment 4	Complete Immunohistochemistry followed by FISH	Immunohistochemistry and then Hybridization with PNA (Telo-FISH protocol)	Extra fixation with 4% formaldehyde after hybridization	Negative – weak signals from both γH2AX and Telomeric PNA
Experiment 5	Modified Experiment 4 protocol4.	Immunohistochemistry and then Hybridization with PNA (Telo-FISH protocol)	Increase concentration of Triton-X from 0.1percent to 0.2%.	PNA signal positive; γH2AX signal weak
Experiment 6	Modified experiment 5 protocol	Immunohistochemistry and then Hybridization with PNA (Telo-FISH protocol)	Washing with TBST instead of PBS	Positive γH2AX signal; positive telomeric PNA signal. Protocol suitable for further experiments

Previous studies have established that normal untreated human cells have a) approximately 0.5-1 γH2AX positive spot per nuclei and b) a large majority of all telomeres detectable by PNA FISH (Riballo et al., 2004, Jeggo & Lobrich, 2005). Therefore, the main criteria required from the modified TIF protocol to pass as

acceptable for our purpose were: a) that the frequency and quality of γH2AX positive foci before and after FISH are the same and b) that the frequency of detected telomeres after immuno-FISH matches that of FISH only. Examples of images produced using the modified TIF protocol are given in Figure 4.1. In the rest of the text we will refer to the modified TIF protocol as immuno-FISH TIF (IF TIF).

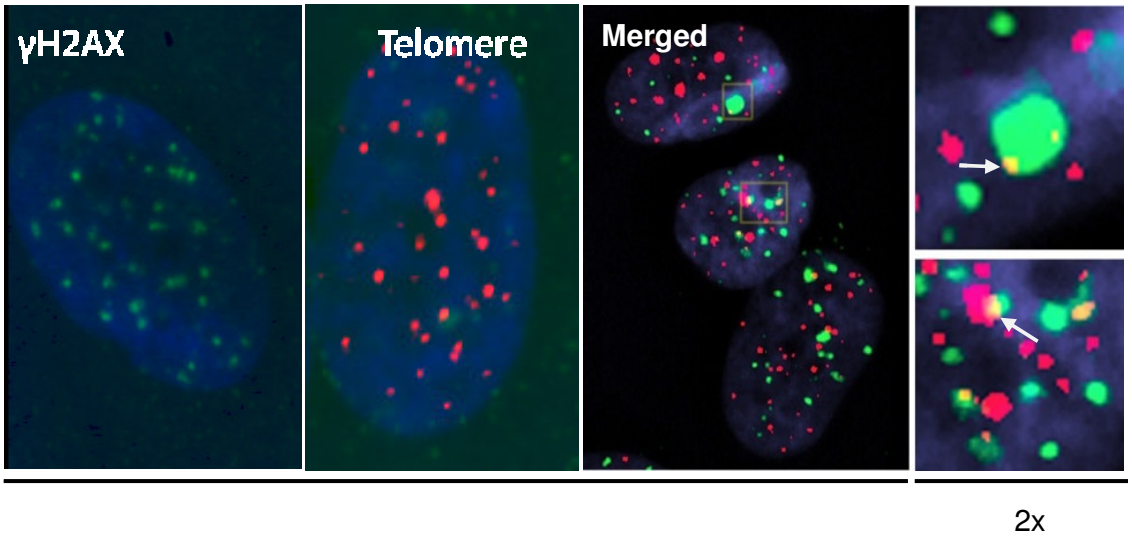

Figure 4.1 Examples of images generated by IF TIF.
Cells were incubated with primary γH2AX antibody (Upstate) and hybridyzed with synthetic Peptide Nucleic Acid (PNA) telomeric sequence $(CCCTAA)_3$ conjugated with a cy-3 fluorescence label (middle image) (Applied Biosystems). Co-localization of the γH2AX foci and telomeres represent a TIF. Please note that only complete overlaps between two colours have been scored as TIFs.

4.2.2 Study of telomere dysfunction in Artemis defective human cell lines using IF TIF protocol

The normal fibroblast cell line, GM08399, has consistently shown approximately 0.52 γH2AX positive spot per cell and a large majority of telomeres detected after IF TIF. The work in Prof. P. Jeggo's laboratory (University of Sussex) has confirmed that IF TIF reliably detects dysfunctional telomeres in different cell lines (Slijepcevic P., personal communication). Therefore, we were satisfied that the IF TIF protocol is suitable for testing telomere function in Artemis defective cell lines.

4.2.2.1 Analysis of telomere function in untreated cells

We started by analyzing telomere function in untreated (non-irradiated) Artemis defective cell lines relative to the control cell line. Given that telomeres shorten in proliferating primary human fibroblasts (Hayflick, 1960, de Lange et al., 1990, Harley et al., 1990, Huffman et al., 2000) and that this shortening can affect telomere function (Harrington and Robinson, 2002, Campisi, 2005, Shay and Wright, 2005) we decided to analyze cells relatively early in their proliferative history ("younger" cells) as well as cells which are relatively late in their proliferative history ("older" cells). We estimated replicative history of cells as described in Chapter 2 and this is expressed as population doubling (PD) number. The Artemis defective cell lines (obtained from the laboratory of Prof. Jeggo) have already undergone a significant number of PDs. We therefore decided to use cells with PD value below 16 (range 12-18) as "younger" cells and cells with PD value in the range of 19-37 (indicated as PD +32 therein) as "older" cells. It is important to note that the "older" cells have not shown significant signs of cell cycle arrest as a result of cell senescence which occurs in fibroblasts typically after 45-50 PDs (Allsopp et al 1995, Kipling et al 1999).

Results of our analysis are shown in Figure 4.2. It is clear that frequencies of γH2AX positive foci were similar in all cell lines and were in line with published studies. For example, Artemis defective and normal "younger" cells had similar frequencies of γH2AX positive foci (Figure 4.2 A) and this is in line with published data (Riballo et al., 2004). However, γH2AX positive foci increased in both Artemis defective and normal "older" cells relative to "younger" cells (Figure 4.2 B). This finding is in line with results observed in the same Artemis defective cell lines in other laboratories (Prof. Jeggo, personal communication). Interestingly, the difference in frequencies of

γH2AX positive foci between Artemis defective and normal "older" cells was statistically significant suggesting that a higher proportion of spontaneous DSBs remain unrepaired in Artemis defective cells than in normal cells. This could indicate that older Artemis defective cells are less efficient in repairing the endogenous DNA DSBs than the normal control cells of the same age.

The results of IF TIF analysis show no difference between Artemis defective and normal "younger" cells (Figure 4.2 C). Therefore, the observed mild spontaneous telomere dysfunction in Artemis defective cells, which manifests itself as an elevated level of Type 1 fusions (see Chapter 3) cannot be linked to results of IF TIF analysis. However, it is important to note that the average PD of cells used in experiments described in chapter 3 was PD24 (range 19 – 32). Therefore, it is possible that the observed mild spontaneous telomere dysfunction (Chapter 3) only occurs in "older" cells. In line with this possibility our IF TIF results in "older" cells revealed a significantly higher frequency of TIFs in Artemis defective cells relative to normal cells. Based on these results it seems reasonable to argue that telomere dysfunction in Artemis defective cells increases with PD number. When Artemis defective cells are relatively "young" (low PDs) they show functional telomeres (Figure 4.2 C and E). However, when Artemis defective cells become "older" (PD 32+) but not senescent yet, they show a small but significant increase in TIF frequency relative to normal cells of similar age ($p<0.001$) (Figure 4.2 D and F).

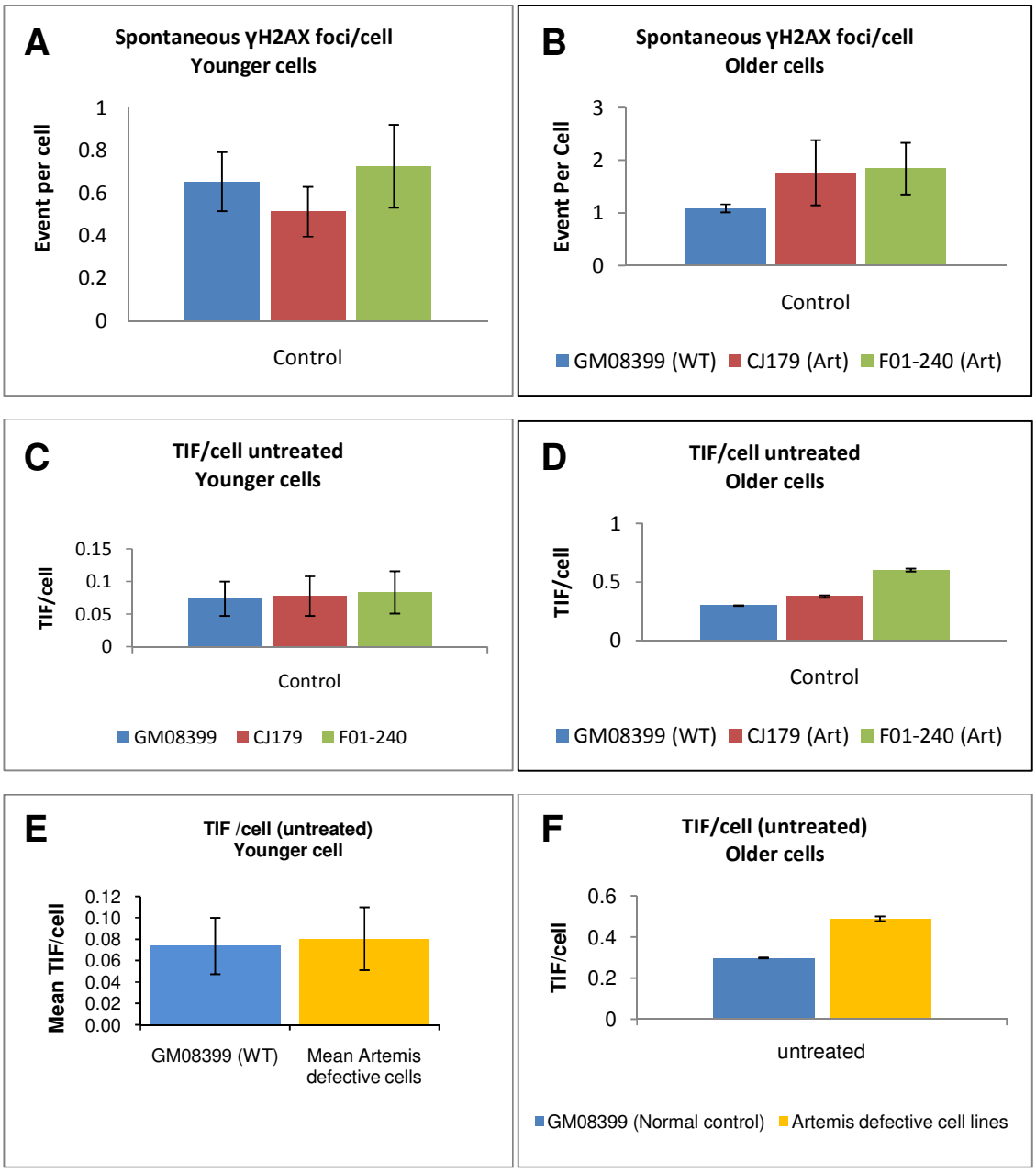

Figure 4.2 Frequencies of γH2AX positive foci and TIFs in untreated "Younger" and "Older" cells.
A| Average γH2AX foci/cell in untreated (non-irradiated) "Younger" cells (PD<16, range 12-18). B| Average γH2AX foci/cell in untreated (non-irradiated) "Older" cells (PD>32, range 19-37). C| Average TIF/cell in untreated "Younger cells). D| Average TIF/cell in untreated "Older cells". The error bars are SEM.

4.2.2.2. Analysis of telomere function following exposure to low doses of IR

Given that we observed an increase in Type 1 telomeric fusions in Artemis defective cells relative to control cells after exposure to IR (Chapter 3), we next examine

whether IF TIF will show any difference between Artemis defective and normal cells after exposure to IR. IF TIF can also be used to monitor repair kinetics of both total DSBs and DSBs occurring within telomeric sequences or TIFs. We decided to expose both "younger" and "older" cells to 1.0 Gy gamma rays and follow levels of γH2AX positive foci, as well as TIFs immediately after irradiation, 5 h and 24 h after irradiation. The numbers of performed experiments and analyzed cells are shown in Table 4.2 and Table 4.4 (Appendix I). Figures 4.3 and 4.4 show actual results expressed as frequencies of events per cells, as well as repair kinetics of both γH2AX foci and TIFs.

Table 4.2. Summary of TIF experiments
Five independent IF TIF experiments were carried out including a pilot experiment (non-induced). In all experiments three time points were selected for analysis of γH2AX and TIF foci except experiments 4 and 5, where four time points were used. In each experiment at least 200 cell nuclei were captured and the number of γH2AX and TIFs were captured and recorded.

Name of Experiment	Irradiation dose (Gy)	Repair Time (in Hour)	Cell lines and PD	Number of cells scored/cell line
Experiment 1 (Pilot test)	No	N/A	CJ179 (PD19), F01-240 (PD19), GM08399 (PD27)	200 cells/point
Experiment 2	0.1, 0.5, 1.0	0.05, 5, 24	CJ179 (PD21, PD30), F01-240 (PD12. PD18), GM08399 (PD27, PD37)	200 cells/point
Experiment 3	0.1, 0.5, 1.0	0.05, 5, 24	CJ179 (PD22), F01-240 (PD14), GM08399 (PD27)	200 cells/point
Experiment 4	0.1, 0.5, 1.0	0.05, 5, 24, 48	CJ179 (PD24), F01-240 (PD15), GM08399 (PD32)	200 cells/point
Experiment 5	0.1, 0.5,1.0	0.05, 5, 24, 48	CJ179 (PD24),	200 cells/point

Artemis defective and normal "younger" cells showed expected kinetics of DSB repair. For example, Figure 4.3 shows that "younger" Artemis defective cells had a higher proportion of unrepaired DSBs 24 h after IR relative to normal "younger" cells. This finding is in line with published studies (Riballo et al., 2004, Wang et al., 2005,

Krempler et al., 2007). However, the IF TIF results were slightly different in that only one “younger” Artemis defective cell line (CJ179) have shown elevated levels of TIFs at all time points after IR relative to the “younger” control line (Fig. 4.4A). The other “younger” Artemis defective cell line (F01-240) exhibited results was very similar to those observed in the “younger” normal control line. Therefore, these results are inconclusive; we cannot say with certainty whether Artemis defective “younger” cells show elevated level of IR induced TIFs relative to control cells.

Interestingly, “older” Artemis defective cells behaved differently from the “younger” Artemis defective cells as shown in Figure 4.4B. It is important to note that frequencies of γH2AX foci immediately after irradiation were lower in “older” than “younger” cells (Figures 4.3 A and Figures 4.3 C). This difference can be attributed to differences in irradiation protocols used. We first irradiated “older” cells and used the protocol designed in our laboratory as follows. Cells seeded on poly-prep slides were irradiated, transported to a cell culture incubator immediately after IR exposure and kept there only briefly (5-10 min) before applying IF TIF protocol. When we completed these experiments we met Prof. Jeggo and her PhD student and compared results of γH2AX frequencies from their laboratory employing the same cell lines. Kinetic results were similar (i.e. γH2AX frequencies at 5 and 24 h post IR) (see figure 4.5). However, their protocol generated higher frequencies of γH2AX positive foci immediately after IR for the reason that they incubated cells in the standard tissue culture conditions for at least 30 min after exposure to IR and then proceeded with immunocytochemistry. This technique would allow maximum number of γH2AX foci to appear.

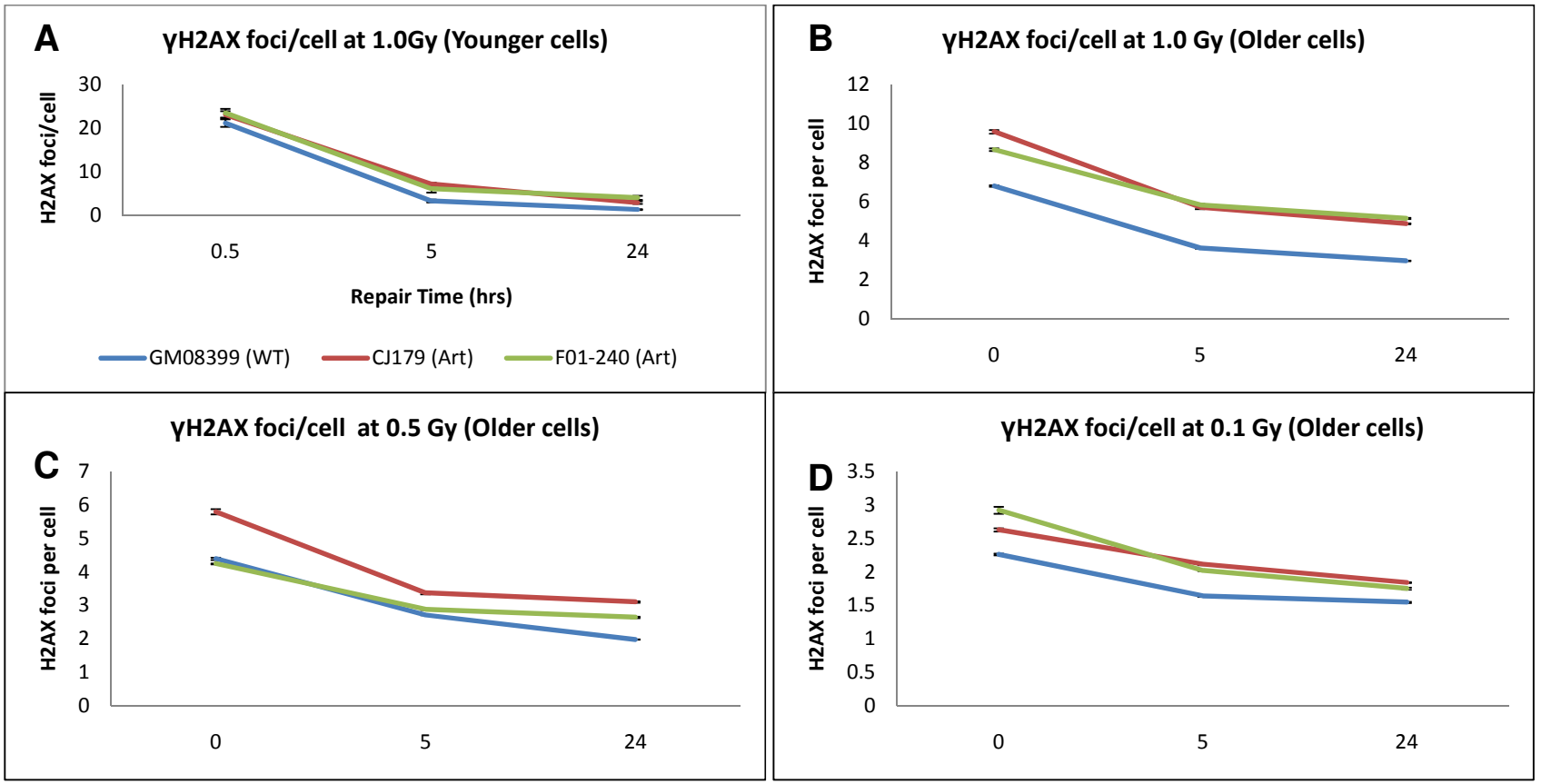

Figure 4.3 Summary of γH2AX results.
A| Average γH2AX foci frequency per cell after 0.05 (i.e. 30 minutes), 5, and 24 hours post irradiation at 0.1 Gy, 0.5 Gy, and 1.0Gy gamma radiation in two Artemis defective (CJ179 in red line, F01-240 in green line) and a normal control (GM08399 in blue line). **B**| Average γH2AX foci frequency per cell in induced Artemis defective and control cell lines with IR at 0 (i.e. 5 minutes), 5 and 24hrs. Error bars represent SEM for figure B-D and SD for figure A. 200 nuclei were scored for each point in three-four independent experiments.

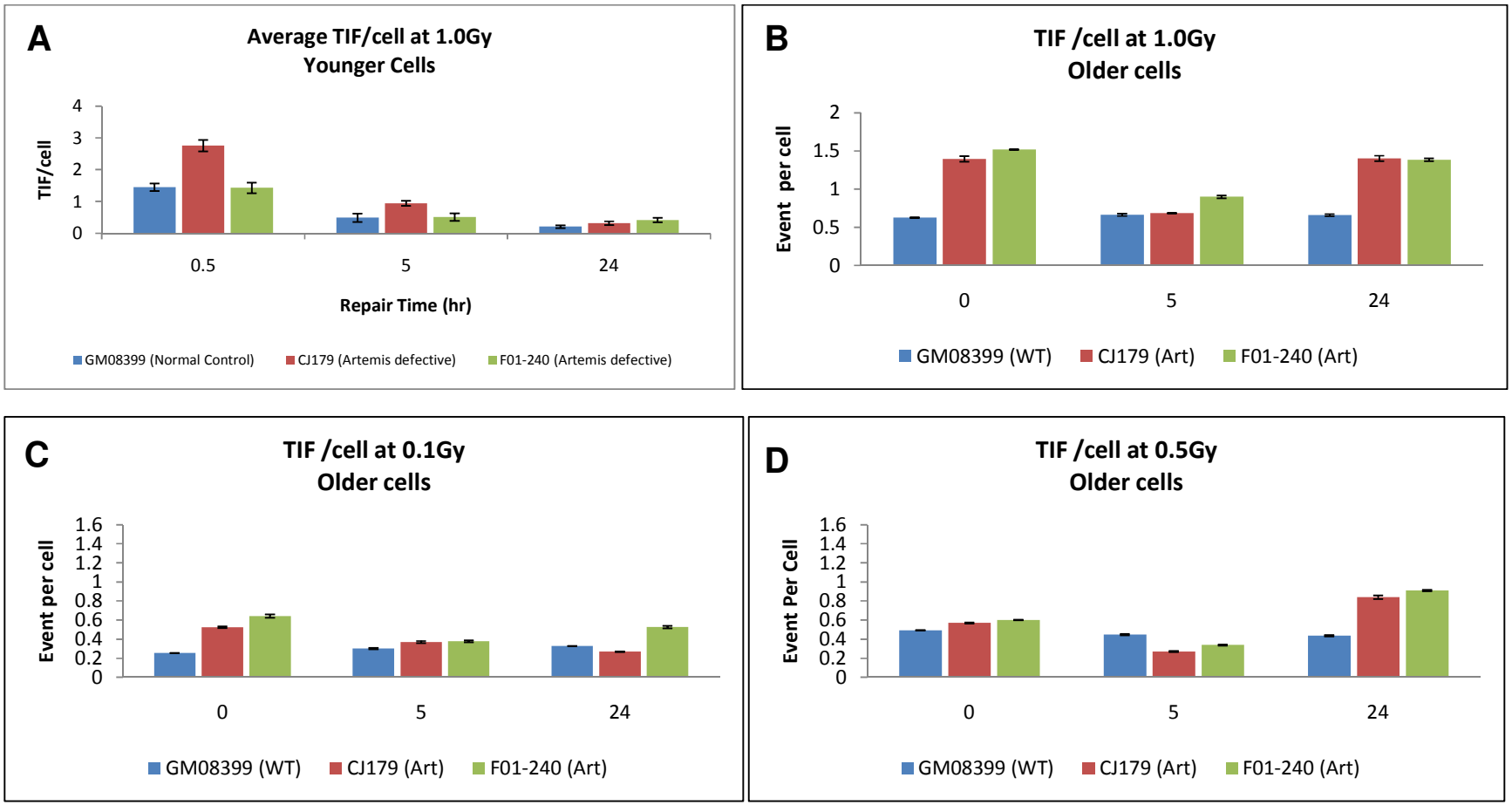

Figure 4.4 Summary of TIF results.
A| Average number of TIF per cell in irradiated cell lines after 0.05 (i.e. 30 minutes), 5, and 24 hours post irradiation. **B**| Average TIF frequency per cell in non-irradiated cell lines. Error bars represents SEM. Two hundred nuclei were scored for each point in three-four independent experiments. Blue bar represents GM08399 (WT), red bar CJ179 (Art), and green bar F01-240 (Art).

Therefore, short time incubation after IR exposure (5-10 min) in our protocol did not allow “expression” of all γH2AX positive foci and resulted in the observed lower frequencies of γH2AX immediately after IR in “older” cells than in “younger” cells. When performing experiments on “younger” cells (chronologically later in our study) we decided to adopt Prof. Jeggo’s protocol and incubate cells at least 30 min at 37°C following IR. Please note that no difference in γH2AX frequencies were observed at time points 5 and 24 h after IR in either “younger” or “older” cells between our protocol and the protocol used in Prof. Jeggo laboratory. Results of γH2AX kinetics obtained for “younger” cells were in line with published results from Jeggo’s laboratory (Evans et al., 2006) i.e. similar levels of DSBs in Artemis and normal “younger” cells immediately after IR and higher level of unrepaired DSBs in Artemis defective cells 24h post IR (Evans et., 2006, Krempler et al., 2007).

Most importantly, normal and Artemis defective “older” cells showed the same level of TIFs immediately after IR and 24 h after IR suggesting that no repair of DNA damage has taken place within the telomeric sequences within this time frame (Figure 4.4 B). It is interesting that Artemis defective cells have shown a dip in TIF frequencies 5 h after IR. These results argue that repair kinetics of TIFs in “older” cells is impaired relative to “younger” cells. To verify this observation further we exposed “older” cells to two more low doses of IR: 0.1 and 0.5 Gy and observed expected (i.e. a clear difference between repair kinetics in the two wArtemis defective cell lines and the normal control) frequencies of γH2AX foci (Fig 4.3. C and D) but persistence of TIFs in all cell lines (Figure 4.4 C and D).

However, the level of TIFs in Artemis defective “older” cells at 24hrs was clearly much higher than in normal cells. For example, at the dose of 1.0 Gy normal “older”

cells had approximately 0.6 TIFs/cell (Figure 4.4 A). Two Artemis defective cell lines had 1.4 and 1.5 TIFs/cell respectively. When the level of spontaneous TIFs (0.3 in normal and 0.5 in Artemis defective “older” cells is deducted from the above values the difference in the frequency of IR induced TIFs is approximately three-fold higher in Artemis defective “older” cells than in their normal counterparts.

Figure 4.6A shows the percentage of unrepaired TIFs in all three “older” cell lines 24h after irradiation at all three doses relative to total percentage of DSBs (as detected by γH2AX staining) induced by IR. Figure 6.6A shows the 22% of γH2AX were located within telomeres in normal cells at all doses. In Artemis defective cells the frequency of IR induced DSBs located at telomeres were approximately 10% higher i.e. approximately 32%. The difference, however, is not statistically significant ($P<0.052$).

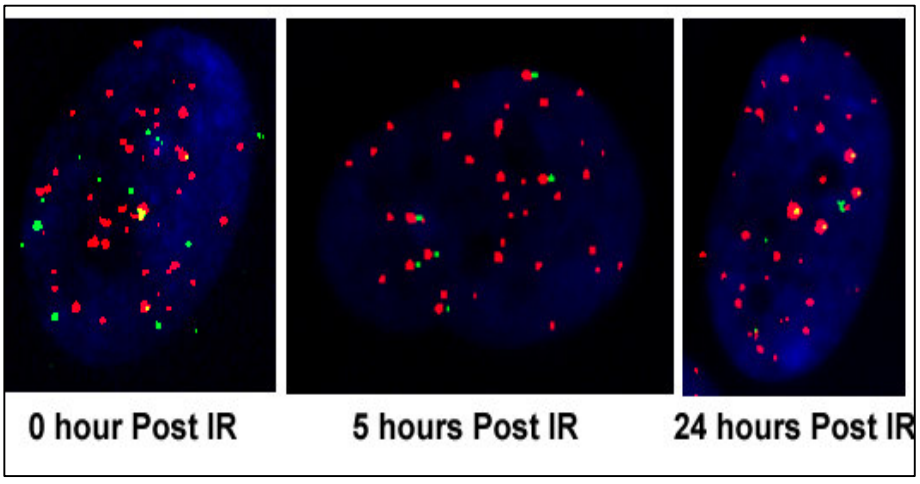

Figure 4.5 Repair kinetics 24 hrs post irradiation.
An example of an Artemis defective line (F01-240) at three time points after 0.5Gy of irradiation. The reduction in frequency of γH2AX foci was clearly evident. But note the levels of persistent TIFs 24hrs post IR.

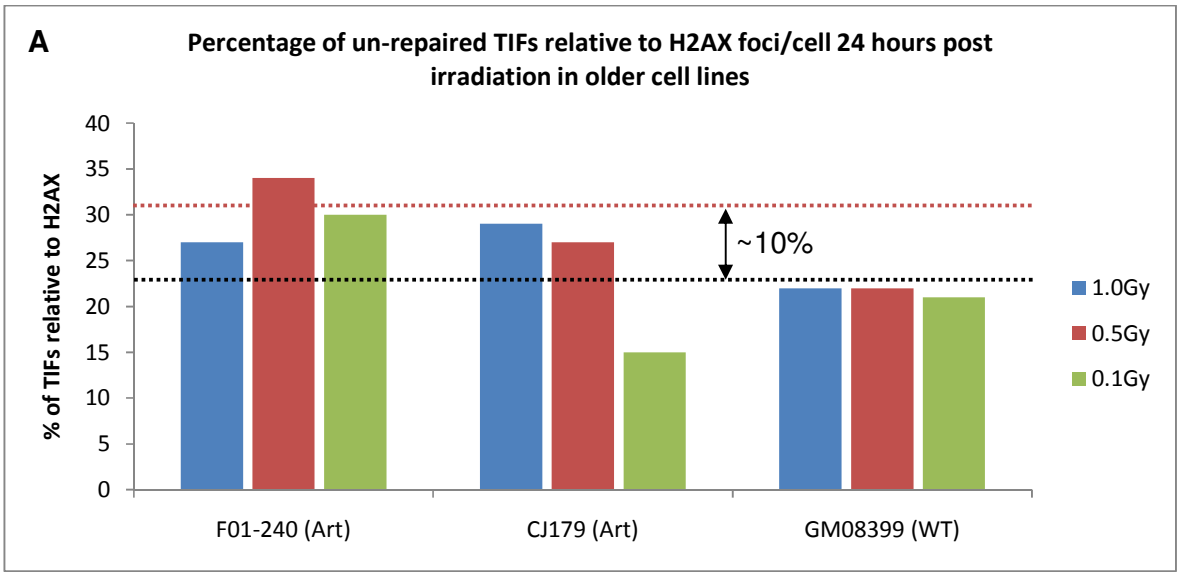

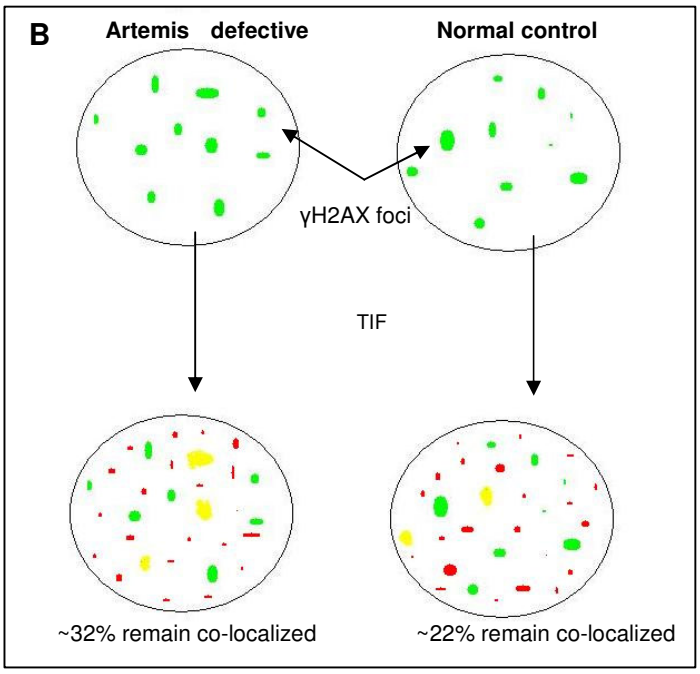

Figure 4.6 Relative frequency of unrepaired TIFs 24hrs post irradiation in Artemis defective cell lines.
A| Each bar represents the percentage of unrepaired TIFs in both Artemis defective cell lines (left and middle) and the normal control line (right) induced at three doses of IR; 0.1Gy (green bars), 0.5Gy (red bars), and 1.0Gy (blue bars). **B**| The maximum number of induced unrepaired TIFs induced in control lines accounts for ~22 percent of the overall DSBs (yellow foci in B and black dotted line in A). This represents the baseline threshold frequency of expected un-repaired TIFs. The two Artemis defective cell lines have a higher percentage of un-repaired TIFs well above the 22 percent baseline threshold by about 10 percent on average ~32 percent remained co-localized as TIFs (red dotted line on A).

4.3 Discussion

In this chapter we presented two novel findings. First, “older” cells, irrespective whether they are Artemis defective or normal, cannot efficiently repair DNA damage at telomeres as shown by the presence of equal levels of TIFs immediately after IR and 24 h after IR (Figure 4.4). Second, the level of IR induced DNA damage at telomeres, as observed by scoring TIFs, was significantly higher in Artemis defective “older” cells than in their normal counterparts.

4.3.1 Repair of DNA damage at telomeres

A number of studies have reported differences in sensitivity to DNA damaging agents between telomeric sequences and the rest of the genome. Alvarez et al. (1993) reported that IR induced CAs tend to localize within interstitial telomeric sequences in Chinese hamster chromosomes significantly more frequently than expected based on the size of these sequences within the Chinese hamster genome. Follow up studies confirmed this finding and, in addition, demonstrated that interstitial telomeric sequences in Chinese hamster chromosomes are frequent sites of spontaneous chromosome breakage (Balajee et al. 1994; Slijepcevic et al. 1996). These studies suggested that interstitial telomeric sequences (a) may behave as chromosome fragile sites and (b) repair of DSBs within these sequences may be less efficient than in an average genomic DNA sequence.

It has recently been demonstrated conclusively that mammalian telomeric sequences indeed behave as fragile sites. Sfeir et al. (2009) reported that telomeric sequences pose a significant challenge to DNA replication machinery causing replication-dependent abnormalities very similar to aphidicolin-induced fragile sites. Indeed, direct exposure of wild type mouse cells to aphidicolin resulted in a

significant fragility at telomeres which became even more elevated after conditional deletion of TRF1 (Sfeir et al. 2009). Our observation of persistent DNA damage at telomeres is certainly in line with the notion that telomeres behave as fragile sites. It would appear that the presence of a DSB within telomeric sequences would cause a problem for repair mechanisms leading to the persistence of TIFs for at least 24 h following their induction. It is of interest to examine for how long DSBs within telomeres remain unrepaired. To answer this question we did perform one experiment in which we followed the fate of TIFs for 48 h after irradiation but we did not have time to repeat this experiment. Preliminary data suggest that TIFs persist on “older” cell lines for up to 48hrs post IR and we observed a difference between one Artemis defective (F01-240) and normal control cell lines. Although this experiment must be repeated and statistically verified.

Apart from our results there are no other published studies examining directly DSB repair within telomeric sequences. However, Kruk et al. (1995) examined repair of UV induced DNA damage at telomeres. They found that UV induced damage at telomeres was repaired less efficiently than in active genes but more efficiently that in other non-coding DNA sequences. More importantly for us Kruk et al. (1995) found that DNA repair efficiency in cells from older donors was lower than in cells from younger donors. This is similar to our observation that TIFs persist at telomeres up to 24 h after IR only in “older” non-senescent cells (PD > 32). In contrast, “younger” cells repair IR induced damage at telomeres efficiently.

4.3.2 IR induced TIFs are elevated in Artemis defective cells

In Chapter 3 we described elevated frequencies of spontaneous and IR induced telomeric fusions in Artemis defective cell lines and characterized this as a mild

telomere dysfunction phenotype. From results presented in this chapter it is clear that this telomere dysfunction phenotype is present only in cells that underwent a significant number of PDs (32+) but are not senescent yet. Although IR induced TIFs persist in both Artemis defective and normal “older” cells the level of TIFs is significantly higher in Artemis defective cells as shown in Figure 4.4. From published studies it is known that IR induced DSBs are not repaired uniformly by the same set of NHEJ proteins. For example, ~90% of IR induced DSBs are repaired relatively quickly and require Ku, DNA-PKcs and LIG-4/XRCC4 (Riballo et al. 2004). The remaining fractions of 10% DSBs are repaired by the combined action of ATM (ataxia telangiectasia mutated) and Artemis (Riballo et al. 2004). Since Artemis has a single strand specific endonuclease activity it is reasonable to assume that this fraction of 10% DSBs could have single stranded tails. It is also important to stress that Artemis is only active in its phosphorylated form and that DNA-PKcs provides this phosphorylation.

It is not clear as to why defective Artemis causes telomere dysfunction only in “older” cells. Given the fact that Artemis is involved in the repair of a subset of 10% DSBs, together with ATM (Riballo 2004), it is possible that the biochemical environment of an “older” cell creates difficulties for Artemis specific repair processes. Interestingly, a recent study revealed that the subset of 10 % DSBs repaired by ATM and Artemis are DSBs occurring within heterochromatic regions of the genome (Goodarzi et al. 2008). Telomeres are typical heterochromatic parts of the genome (Garcia-Cao et al, 2004, Gonzalo and Blasco, 2005). It is possible that Artemis and ATM are required specifically for repair of DSBs occurring within telomeric sequences. If this is true than we can argue that when Artemis is defective, as in the case of two cell

lines used in this study, DSBs at telomeres cannot be repaired efficiently resulting in the observed increased frequencies of TIFs in Artemis defective cells relative to control cells (Figure 4.4).

In this context it is also important to understand the role of ATM at telomeres. ATM defective cells show increased fragility at telomeres as exemplified by the presence of extrachromosomal telomeric fragments in affected cells and accelerated telomere shortening (Hande et al., 2001). Given that telomere shortening is a physiological mechanism occurring in all primary proliferating human cells (Harley et al 1990, Allspopp et al 1995) one may expect that a phenotype similar to ATM defective cells could occur when perfectly normal cells undergo a substantial number of PDs on their way to become senescent as a result of telomere shortening. This possibility is in line with our observation that normal “older” cells show persistent TIFs 24 h after exposure to IR in contrast to normal “younger” cells.

In conclusion, we have demonstrated in this chapter that (a) DNA damage occurring within the telomeric DNA is difficult to repair or irreparable in older cells and that (b) Artemis defective “older” cells show higher proportion of DNA damage at telomeres than their normal counterparts.

Chapter 5 :
Effects of DNA-PKcs inhibition on telomeres in Artemis defective cell lines

5.1 Introduction

Results presented so far indicate that defective Artemis causes a mild telomere dysfunction phenotype. This phenotype manifests in two forms. First, Artemis defective cells show elevated frequencies of telomeric fusions. Second, Artemis defective cells that underwent a significant numbers of PDs (32+) but are not senescent yet show elevated frequencies of IR induced TIFs in comparison to normal control cells that underwent similar numbers of PDs. However, the mechanism(s) by which Artemis affects telomere maintenance are not clear. Artemis is a component of the NHEJ machinery and it is required for the repair of only a ~10% subset of DSBs most likely in an ATM dependent manner (Lobrich and Jeggo, 2005, Lobrich and Jeggo, 2007, Riballo et al., 2004). In terms of molecular properties Artemis is a single-strand specific endonuclease that is regulated by another NHEJ component, DNA-PKcs, which actively targets Artemis by phosphorylation (Ma et al., 2002, Ma et al., 2005). Phosphorylated Artemis processes DSBs by removing 5' and 3' overhangs to make ends ready for ligase IV/XLF-Cernunnos mediated ligation (Buck et al., 2006, Lieber, 2008).

It is interesting that DNA-PKcs plays an active role in telomere maintenance. DNA-PKcs forms, through interaction with shelterin, a protective 'cap' at telomeres the function of which is to prevent formation of end-to-end chromosome fusions (Bailey, 2004, Bailey et al., 2004). Even a partial deficiency of DNA-PKcs causes telomere dysfunction phenotype (Peng et al., 2002, Zhang et al., 2007). There are no published data that examine combined effect of defective Artemis and defective DNA-PKcs on telomere maintenance. Examination of this double defective phenotype may shed some light on the mechanisms by which Artemis affects

telomere maintenance. In this chapter we set out to inhibit DNA-PKcs in Artemis defective cell lines and therefore create a cellular environment with a double NHEJ deficiency. We used a well characterized and highly specific inhibitor of DNA-PKcs, IC86621 (Bailey et al., 2004). We verified the levels of DNA-PKcs through western blot analysis and assessed effects of the double deficiency on telomeres by IF TIF.

5.2 Results

There are five different synthetically produced inhibitors of DNA-PKcs that have shown to reduce levels of DNA-PKcs activity. Two such inhibitors, NU7026 (2-(Morpholin-4-yl)-benzo[h]chromen-4-one) and IC86621 (1-(2-Hydroxy-4-morpholin-4-yl-phenyl)ethanone), have been shown to generate telomere dysfunction phenotypes in mammalian cells by directly affecting DNA-PKcs (Williams et al., 2009, Zhang et al., 2007). In our study we used IC86621 (Sigma-Aldrich, Inc.).

In order to demonstrate that IC86621 can generate telomere dysfunction phenotype in a mammalian cell environment we first used a pair of mouse lymphoma cell lines L5178Y (LY-R) and L5178Y-S (LY-S). These cell lines are easy to maintain *in vitro*. Furthermore, mouse cells have large telomeres, a possibility which allows fast identification of any potential telomere dysfunction phenotype. Our intention was to show that IC86621 can cause telomere dysfunction phenotype in mouse cells before examining effects of DNA-PKcs inhibition (DNA-PKcsi) on telomeres in Artemis defective cell lines.

5.2.1 Inhibition of DNA-PKcs in mouse cell lines

Despite the fact that human and mouse telomeres have many common features, such as conserved telomeric repeat sequences, similar shelterin proteins, and similar telomeric structure (de Lange, 2006) , there are two observable differences

between human and mouse telomeres. On average, human telomeres range in length from 10kb-15kb, whereas the telomere length in *Mus musculus*, ranges from 40kb-80kb (Blasco et al., 1997, de Lange, 2006). Telomerase, the enzyme that regulates telomere length (Greider and Blackburn, 1985), is found to be expressed at high levels in human germline cells, but at low levels in somatic cells, with the exception of activated leukocytes and tissue stem cells (Masutomi et al., 2003, Newbold, 1997). In murine cells however, levels of telomerase activity are higher in somatic tissues relative to human counterparts (de Lange, 2006).

LY-R and LY-S have been well characterized in terms of DNA damage response capacities and telomere maintenance. LY-R cells show normal sensitivity to IR and have telomeres typical of mouse cells i.e. 40-50 kb (McIlrath et al, 2001, Wong and Slijepcevic, 2004). In contrast LY-S cells show IR sensitivity and have much shorter telomeres which are in the region of ~ 7 kb (McIlrath et al. 2001, Wong and Slijepcevic, 2004). The mechanism(s) of increased IR sensitivity in LY-S cells are not known. It has been suggested that this radiosensitivity is due to a deficiency in the DSB repair machinery (Wlodek and Hittelman, 1987). However, DNA-PKcs and all known components of NHEJ pathway known at the time (Ku70/80) were functional in both cell lines (Jaworska et al., 2001, McIlrath et al., 2001). The only component of NHEJ not examined in these cell lines is a recently discovered protein XLF/Cernunnos.

We exposed LY-R and and LY-S cells to IC86621 for 24 h and analyzed cytologically visible CAs using Telo-FISH (Table 5.1).

Table 5.1 Summary of two DNA-PKcsi experiments using mouse lymphoma LY-R and LY-S cell lines.
Cell lines were incubated with 20μM of IC86621 for 24 hours. Levels of Robertsonian fusion (RB), Type 1 telomeric fusion, and chromosome breaks were recorded. Numbers represent event/cell.

Cell Line	*Metaphases Scored*	*Rb fusion*	*Telomeric Fusion*	*Breaks/Fragments*
LY-R cell line		Events per cell		
Control	**213**	**0.037**	**0.075**	**0.056**
Treated	**201**	**0.088**	**0.279**	**0.277**
LY-S cell line				
Control	**189**	**0.159**	**0.126**	**0.14**
Treated	**200**	**0.249**	**0.410**	**0.212**

LY-S cells showed elevated levels of spontaneous RB fusion, possibly as a result of shorter telomeres and higher levels of missing telomeric signals (McIlrath et al., 2001). We observed a four-fold increase in spontaneous levels of RB fusion, a 1.7-fold increase in Type 1 telomere fusion, and a 2.5-fold increase in levels of chromosome breaks in LY-S relative to LY-R cells (Table 5.1 and Figure 5.1). The elevated levels of endogenous chromosome breaks observed in the LY-S cell line probably reflect lack of functional DSB repair machinery in these cells.

DNA-PKcsi caused significant increase in all types of CAs analyzed in both cell lines (Table 5.1 and Figure 5.1). A 3-fold increase in Type 1 chromosome fusions in both LY-R and LY-S treated cell lines is indicative of telomere dysfunction resulting from DNA-PKcsi (Bailey et al., 2004). Therefore, these results demonstrate that DNA-PKcsi with 20μM of the IC86621 causes telomere dysfunction phenotype observable at the cytological level in both LY-S and LY-R cell lines. Examples of CAs observed are shown in Figure 5.2.

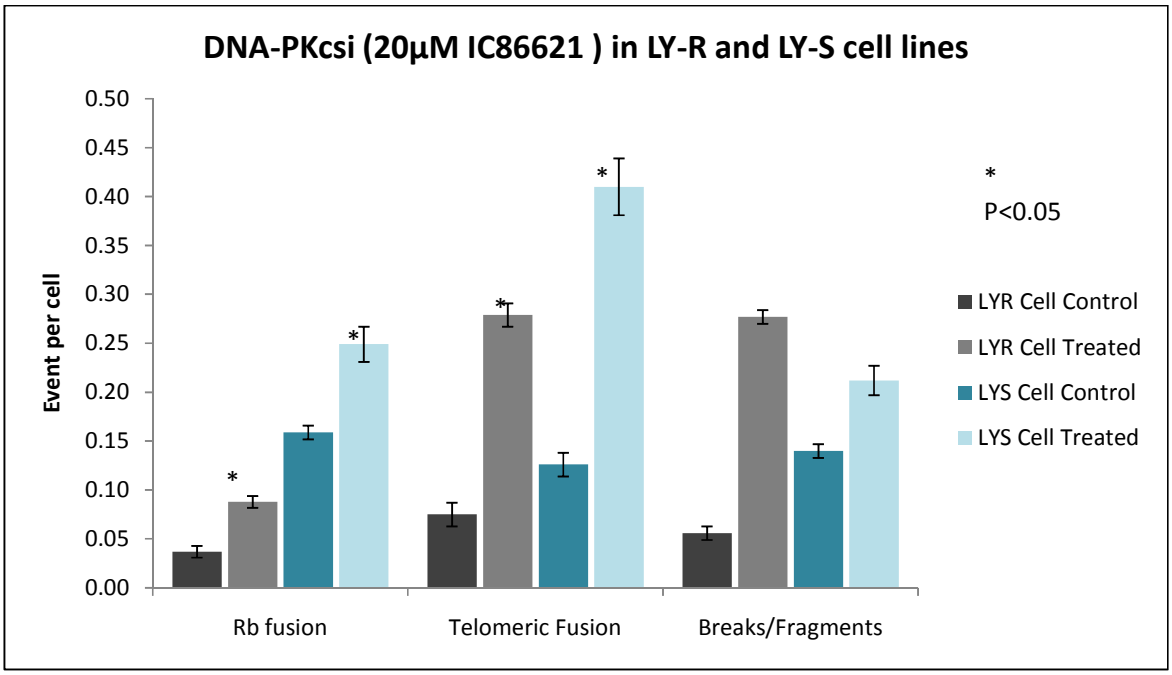

Figure 5.1 CAs frequenceis in LY-R and LY-S cells after Telo-FISH.
Error Bars indicate SEM. Asterisk (*) indicates statistically significant differences between treated and untreated cells.

5.2.1.2 DNA-PKcsi causes telomere shortening

As mentioned above, LY-R and LY-S cells have varying telomere lengths (McIlrath et al., 2001). The radioresistant LY-R cell line has an average telomere length of 48kb and the radiosensitive LY-S cell line has telomere length of 7kb as measured using quantitative FISH (Q-FISH) (Alexander, 1961, McIlrath et al., 2001). Q-FISH measurements have been confirmed with the use of fluorescence activated cell sorting (FACS) based method to measure telomere length known as Flow-FISH (Cabuy et al., 2004). The Flow-FISH technique is a fast and reliable method for analyzing telomere length dynamics through the measurement of the average telomere length in a given cell population. We measured the average telomere length in LY-R and LY-S cell lines using Flow-FISH before and after DNA-PKcsi (Figures 5.3 and 5.4). A total of six separate experiments were performed and the percentage

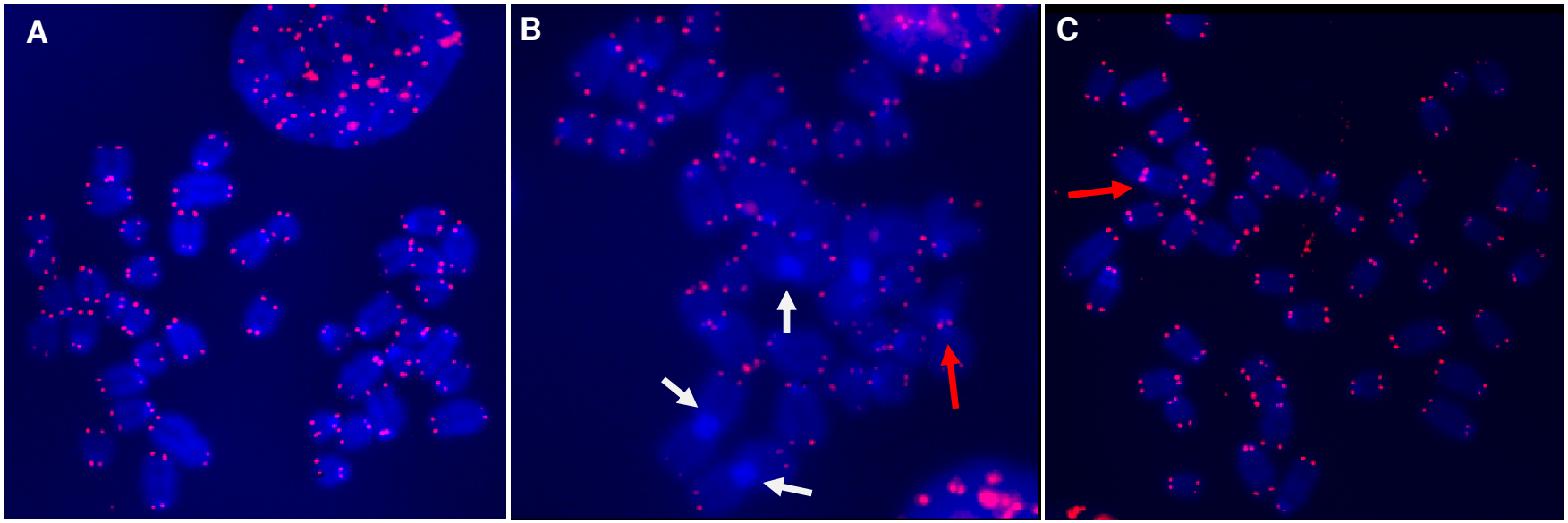

Figure 5.2 **.** Examples of CAs observed in LY-R and LY-S cells.
Metaphase spreads were probed with the telomeric probe (red) and stained with DAPI (Blue). **A|** Untreated LY-R cell with no sign of telomeric fusion. **B|** A Robertsonian fusion (white arrow) and Telomeric fusion (red arrow) in a treated LY-S cell. **C|** Telomeric fusion (red arrow) in a treated LY-R cell.

differences in telomere length between treated and untreated cell lines were calculated.

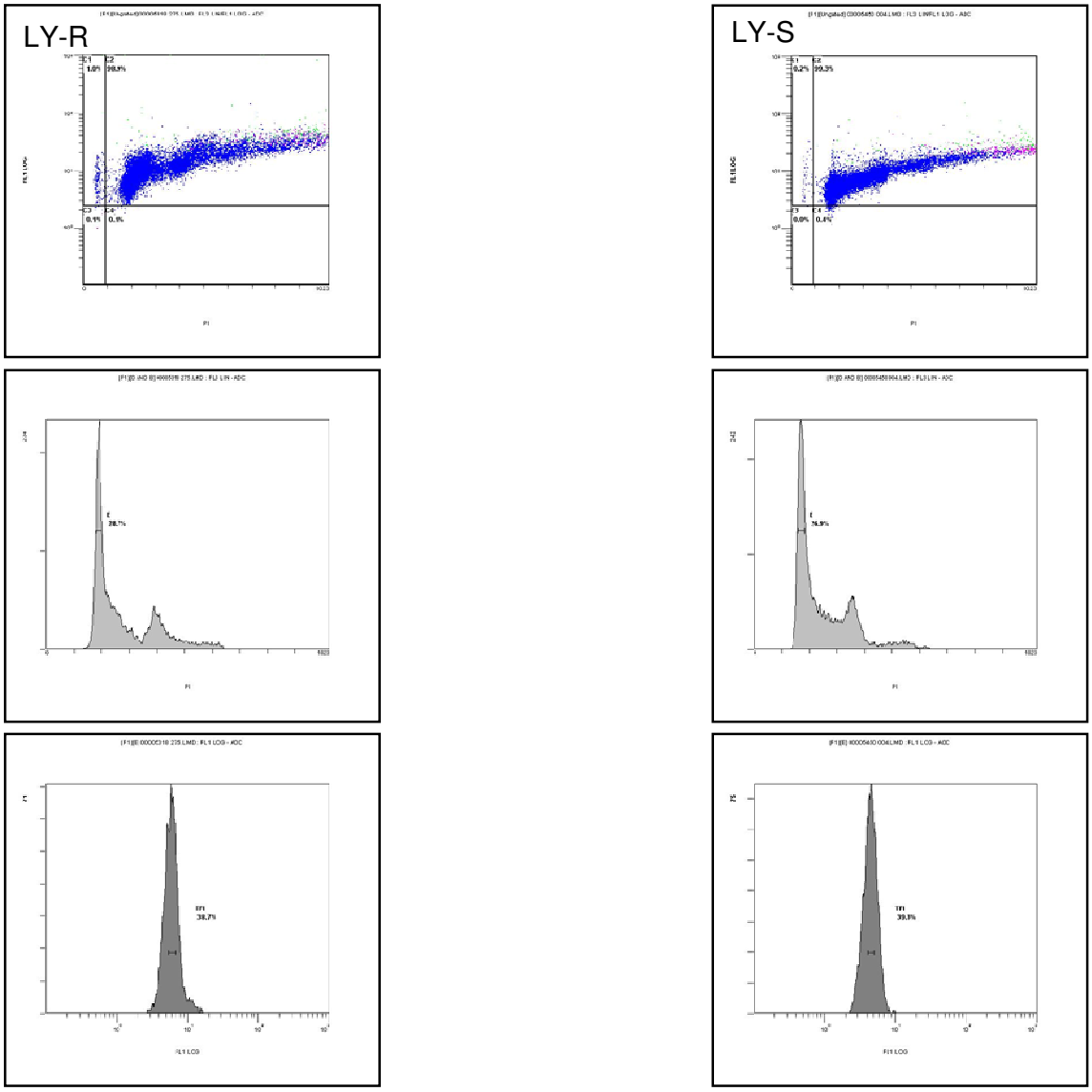

Figure 5.3 Examples of a typical flow cytometry profile of untreated LY-R (left) and untreated LY-S (right) cell lines.
FL1 versus FL3 dot plot distinguishes each population of cells (top panels). A histogram of a cell cycle was then plotted and only cells in the G0/G1 phase were gated for telomere measurement (middle panels). TFI (Telomere Fluorescence Intensity) units were measured within the middle part of the histogram on the FL1 channel (bottom panels). Twenty thousand cells were detected in five minutes and on average at least 1,000 cells were used to measure TFI units.

Table 5.2 and Figure 5.4 show the summary of telomere length measurements. Our results show ~ 5-fold difference in telomere length between untreated LY-R and LY-S cells. This is different from ~ 6.9-fold difference between the same lines observed by McIlrath et al. (2001) after Q-FISH analysis. The difference may be explained by natural variation of telomere length in these two cell lines. For example, Cabuy et al. (2004) found that average telomere length in LY-R cells vary 40-60%. We confirmed this fluctuation in LY-R cells as shown in Figure 5.5. DNA-PKcsi caused a reduction in average telomere length by around 27% and 21% in LY-S and LY-R cell lines respectively relative to their untreated counterparts following a twenty-four hour treatment with DNA-PKcsi. The percentage difference in telomere length between treated and untreated cell lines was statistically significant ($p<0.05$) (Figure 5.4). Therefore, our results show that DNA-PKcsi, through exposure of cells to IC86621, causes not only loss of telomere function (Table 5.1 and Figure 5.1) but also telomere shortening in mouse LY-R and LY-S cells.

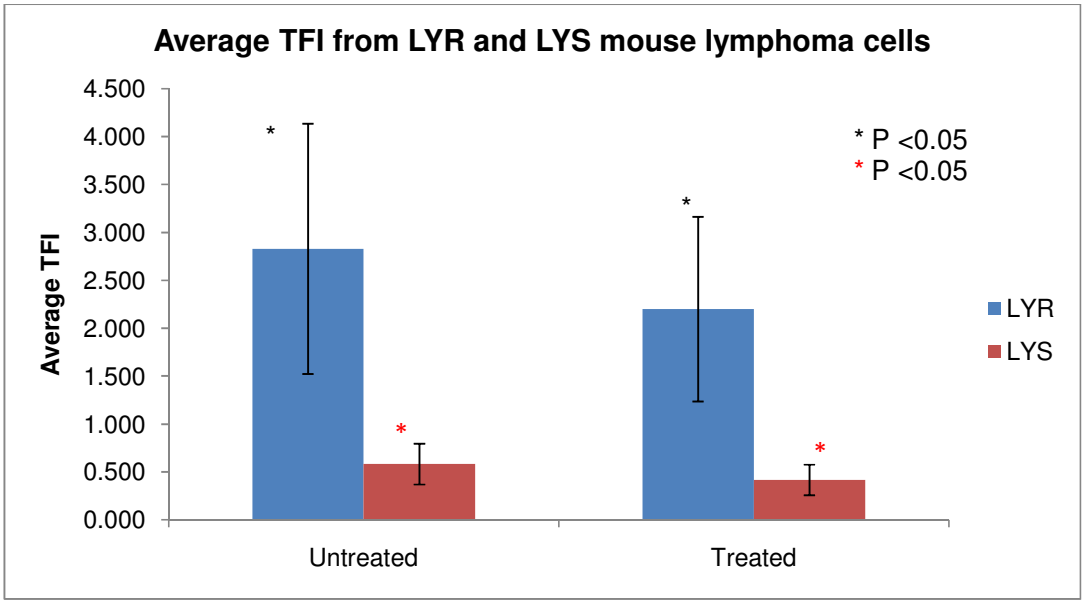

Figure 5.4. Average TFI in treated and untreated LY-R and LY-S cell lines. The difference in TFI was statistically significant. The error bars represent SD, n=6-7

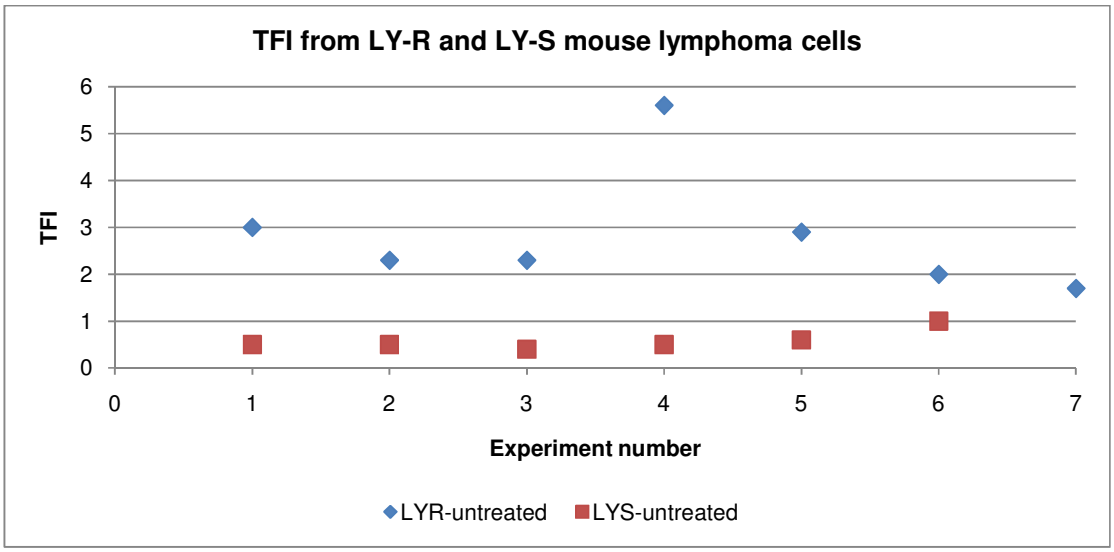

Figure 5.5 TFI values from each experiment in untreated LYR and LYS cell lines.

Table 5.2. Summary of TFI in treated and untreated mouse cell lines
Telomere length measurement using Flow-FISH in LY-S (top panel) and LY-R (bottom panel) cell line. Six continuous experiments were conducted to measure the average telomere fluorescence intensity (TFI) in treated and untreated LY-S and LY-R cell lines. The data below are based on, at minimum 5,000 and maximum of 20,000 cells, depending on the cell population at the time of experiment.

LY-S Cell line

Experiment Number	PD	Untreated TFI	Treated TFI	% change in TFI
1	N/A	0.5	0.4	20
2	N/A	0.5	0.2	60
3	N/A	0.4	0.4	0
4	N/A	0.5	0.4	20
5	2	0.6	0.4	40
6	4	1.0	0.7	30
	Mean	**0.58**	**0.42**	**27.60**
	SD	**0.21**	**0.16**	***P<0.05***

LY-R Cell line

Experiment Number	PD	Control TFI	Treated TFI	% change in TFI
1	N/A	3.0	2.1	30
2	N/A	2.3	1.8	21
3	N/A	2.3	1.7	26
4	2	5.6	4.2	25
5	4	2.9	2.6	10
6	8	2	1.5	25
7	10	1.7	1.5	12
	Mean	**2.83**	**2.20**	**21.30**
	SD	**1.3**	**0.96**	***P<0.05***

5.2.2 DNA-PKcsi in Artemis defective human cell lines

5.2.2.1 Western blot analysis

After the successful demonstration that DNA-PKcsi in mouse lymphoma cell lines generates both telomere dysfunction phenotype (Figure 5.1) and telomere shortening (Figure 5.4) the attention was turned to DNA-PKcsi in human cell lines defective in Artemis.

Each of three human primary fibroblast cell lines (two Artemis defective and one normal) were subjected to DNA-PKcsi (20µM of IC86621) for a period of 24 hours and levels of DNA-PKcs were quantified using western blot (Figure 5.6). DNA-PKcsi resulted in 45 % reduction in DNA-PKcs levels in all three cell lines as seen after image Quant 5.0 densitometry analysis of Western blot images. Reduction in the level of DNA-PKcs was quantified relative to the level of beta-actin. For details of the western blot technique, quantitation, primary and secondary antibodies, see Chapter 2.7.

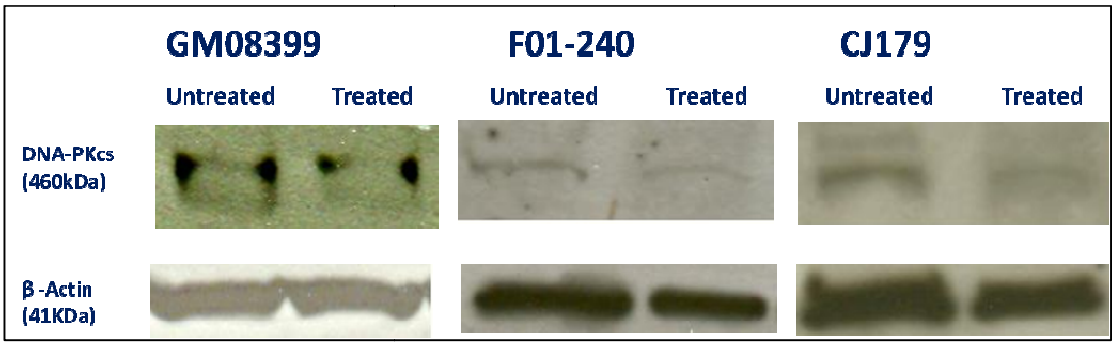

Figure 5.6. Western blot in three human cell lines before and after DNA-PKcsi.

5.2.2.2 DNA-PKcsi generates increased levels of telomeric fusion in Artemis defective cell lines

We next analysed levels of Type 1 chromosome fusion, representative of telomeric dysfunction, in all three human primary cell lines subjected to DNA-PKcsi. Our analysis, shown in Table 5.3, was based on two independent experiments.

The levels of Type 1 chromosome fusions in untreated cell lines (Figure 5.7A) were similar to those observed in Chapter 3.2.1., (Figure 3.4). There was a significant increase in frequencies of Type 1 chromosome fusions in all cell lines following DNA-PKcsi relative to their untreated counterparts ($p<0.05$) (Figure 5.7B). Also there was a similar increase in levels of chromosome breaks (Figure 5.7 B). The majority of Type 1 chromosome fusions observed in treated cell lines was of chromatid type similar to results of Bailey et al. (2004) (Figure 5.7 C).

Table 5.3 Summary of telomeric fusion in human cell lines.
Type 1 chromosome fusions and chromosome breaks in individual cell lines. Two independent experiments were performed. The frequencies shown represent number of events per cell.

		Metaphase cells analyzed	Type 1 chromsome fusions	Breaks/Fragments
GM08399 (WT)	Untreated	111	0.018	0.000
	Treated	150	0.087	0.067
CJ179 (Art)	Untreated	194	0.067	0.015
	Treated	182	0.203	0.104
F01/240 (Art)	Untreated	174	0.081	0.017
	Treated	140	0.136	0.157

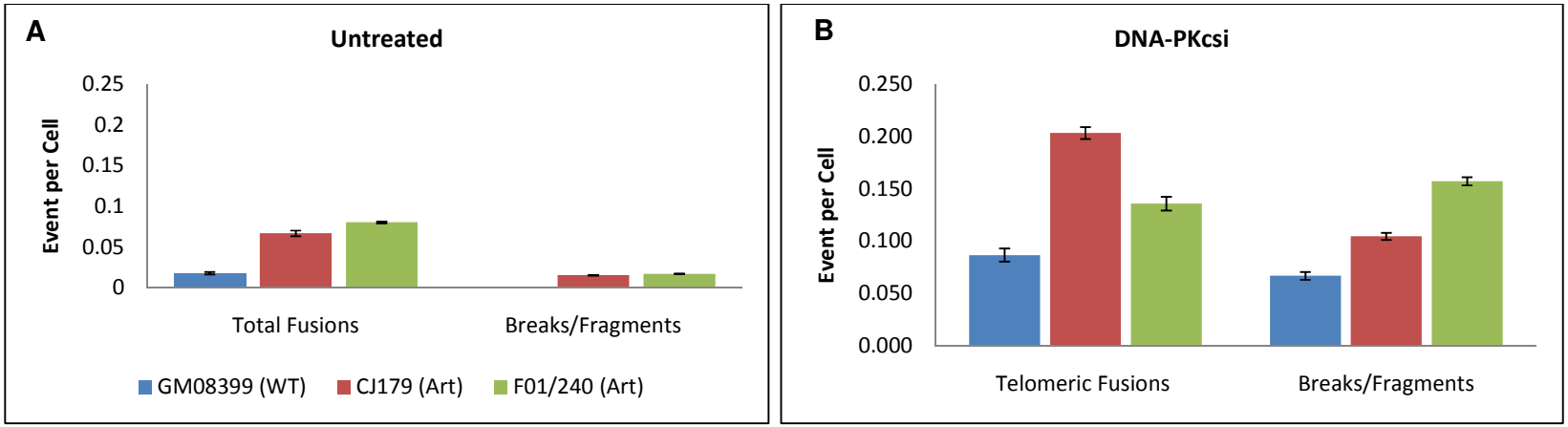

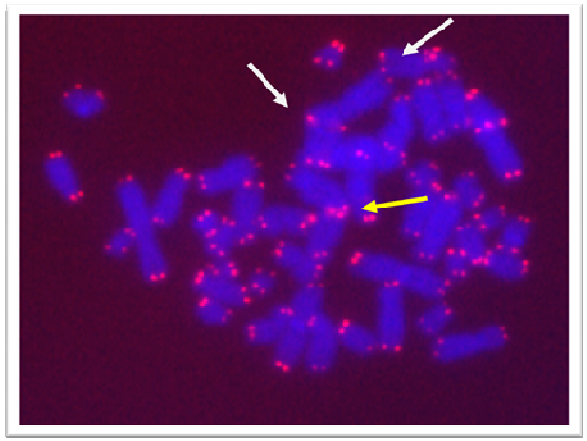

Figure 5.7. Type 1 chromosome fusions in three cell lines.
A| Levels of type 1 chromosome fusion and chromosome breaks in untreated cell lines. **B**| The frequency of Type 1 chromosome fusion and chromosome breaks in treated cell lines. **C**| Telo-FISH image of a metaphase cell from the CJ179 cel line (Artemis defective) showing Type 1 chromosome fusions of chromosome type (yellow arrow) and of chromatid type (white arrows). Error bars are SEM

5.2.3 Telomere length measurements of DNA-PKcs inhibited Artemis defective cell lines using flow-FISH

The next experiment involved the measurement of telomere length in all three cell lines after DNA-PKcsi. We previously found that DNA-PKcsi in mouse lymphoma cell lines caused a marked decrease in telomere length, suggesting the importance of DNA-PKcs in telomere length regulation (section 5.2.1). A total of five experiments were carried out to measure telomere length in human primary fibroblast using the flow-FISH protocol (Table 5.4). Average telomere length values based on all experiments are presented in Figure 5.8 and Table 5.5). The treatment of all three cell lines with the DNA-PKcs inhibitor for a period of 24 hour caused a reduction in the telomere length (Table 5.5, Figure 5.8). However, the difference in telomere length between untreated and treated cell lines was not significant ($p<0.164$ for GM08399, $p<0.265$ for CJ179) in contrast to mouse cell lines (see Figure 5.4).

Table 5.4. Telomere length measurements after DNA-PKcsi.

	Telomere Length Fluorescence (TFI)					
	Exp Number	Passage	PD	Untreated TFI	Treated TFI	% change (Δtreated – untreated)
F01-240	1	P14	22	1.9	-	-
CJ179	1	P+17	27	2	-	-
GM08399	1	P16	25	1.2	-	-
CJ179	2	P+20	32	0.9	0.5	44
F01-240	2	P16	25	1	0.6	40
GM08399	2	P18	29	1.1	0.7	36
CJ179	3	P+23	36	0.7	0.4	43
CJ179	4	P+25	40	-	0.6	-
GM08399	4	P20	32	0.7	-	-
GM08399	5	P21	33	0.3	0.2	33
CJ179	5	P+26	41	0.2	0.1	50

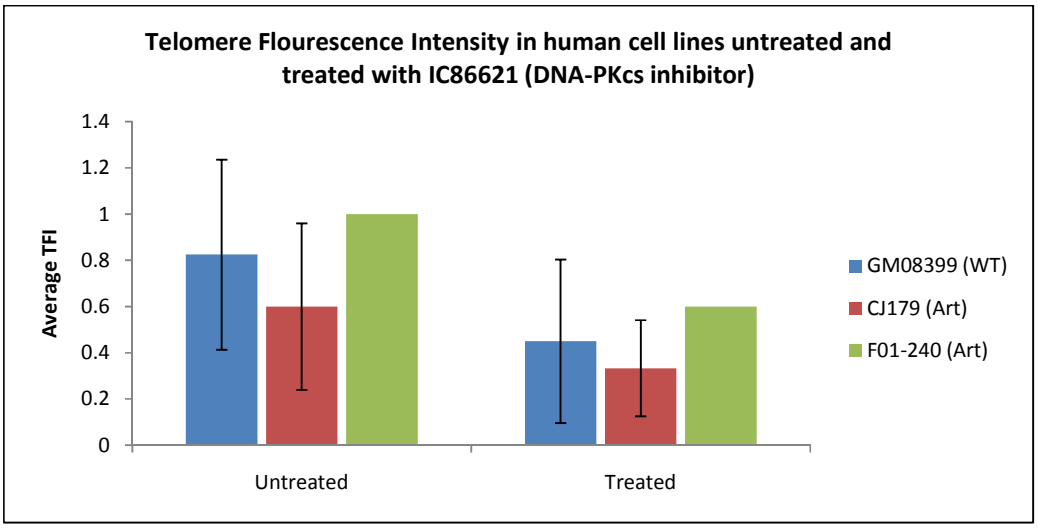

Figure 5.8. Telomere length in (TFI) units in treated versus untreated human primary cell lines.

Table 5.5. Average telomere length in untreated and treated human primary cell lines inhibited with DNA-PKcs.

Telomere length in (kb)			
	Untreated	Treated	% change
GM08399 (WT)	5.97	4.42	26
CJ179 (Art)	5	3.94	21
F01-240 (Art)	6.69	5.04	25

5.2.4 IF TIF analysis following DNA-PKcsi

We next examined levels of IR induced DNA damage before and after DNA-PKcsi. All three human cell lines were irradiated with 1.0 Gy of gamma rays after DNA-PKcsi that lasted for 24 hours and frequencies of γH2AX positive foci, as well as TIFs were assessed (Figures 5.9-5.11). All cell lines were at PDs ranging from 13-21 (“younger” cells) at the time of irradiation. (Table 5.11 Appendix I).

Figure 5.9 shows frequencies of γH2AX positive foci in three cell lines up to 24 h after irradiation. In Table 5.6 we presented repair efficiencies of three cell lines before and after DNA-PKcsi as measured by calculating percentage of remaining γH2AX positive foci 24 h

after IR exposure relative to percentage of the same foci as observed immediately after IR (100%). From results observed in the normal control cell line it is clear that DNA-PKcsi caused delayed DSB repair as shown by 15 % difference in repair capacity when comparing γH2AX foci before the treatment and after incubation with DNA-PKcsi (Table 5.6). Artemis defective cells showed similar differences between DNA-PKcsi positive and DNA-PKcsi negative cells (9.8 – 12.6%) (see Table 5.6.). Figure 5.9 also shows less efficient repair at 5 h post IR in DNA-PKcsi positive cells relative to their DNA-PKcsi negative counterparts.

Table 5.6. DNA DSB repair efficiency
DSB repair efficiencies of treated and untreated cell lines as measured by subtracting % of γH2AX positive foci 24 h after IR from % of foci immediately after IR exposure (100%).

Cell line	DNA-PKcs inhibitor	DNA DSB repair efficiency (%) of remaining DNA DSB 24 hrs post IR
GM08399 (WT)	Untreated	6.0
	Treated	21.5
CJ179 (Art)	Untreated	13.0
	Treated	25.6
F01-240 (Art)	Untreated	16.2
	Treated	26.0

Differences between DSB repair efficiencies of (a) Artemis defective cell lines before and after DNA-PKcsi ($p<0.013$ for CJ179 treated and $p<0.001$ for F01-240) and (b) the normal cell line before and after DNA-PKcsi ($p< 0.001$) were statistically significant.

5.2.4.2 DNA-PKcsi increases levels of TIF in Artemis defective cells

Next, we examined frequencies of DNA damage at telomeres using IF TIF. Analysis of TIF frequencies before and after DNA-PKcsi but without exposure of cells to IR is shown in Figure 5.9. There was an increase in TIF frequencies after DNA-PKcsi in all cell lines but this effect was not statistically significant.

Frequencies of TIFs after DNA-PKcsi and IR exposure are shown in Figure 5.11. The two Artemis defective cell lines (CJ179 and F01-240) repaired only 1 - 6 % of DSBs within telomeres compared to 41% repaired DSBs within telomeres in the normal cell line after DNA-PKcsi and five hours post IR. Twenty four hours post IR the two Artemis cell lines had an average of ~ 50 % of TIFs unrepaired, whereas in normal cell line 38 % of TIFs remained unrepaired after DNA-PKcsi. The difference in TIFs levels 24 hours post IR was statistically significant: (a) between the two Artemis defective treated and untreated cell lines and (b) normal control treated and untreated cells ($P<0.001$) (Figure 5.11).

These results demonstrate two points. First, DNA-PKcsi increased levels of unrepaired TIFs 24 hours post IR in both normal and Artemis defective cell lines. Second, DNA-PKcsi positive Artemis defective cell lines showed higher levels of TIFs than Artemis defective DNA-PKcsi negative cells or DNA-PKcsi positive normal cells, suggesting cumulative effects of DNA-PKcs and Artemis deficiencies on telomeres.

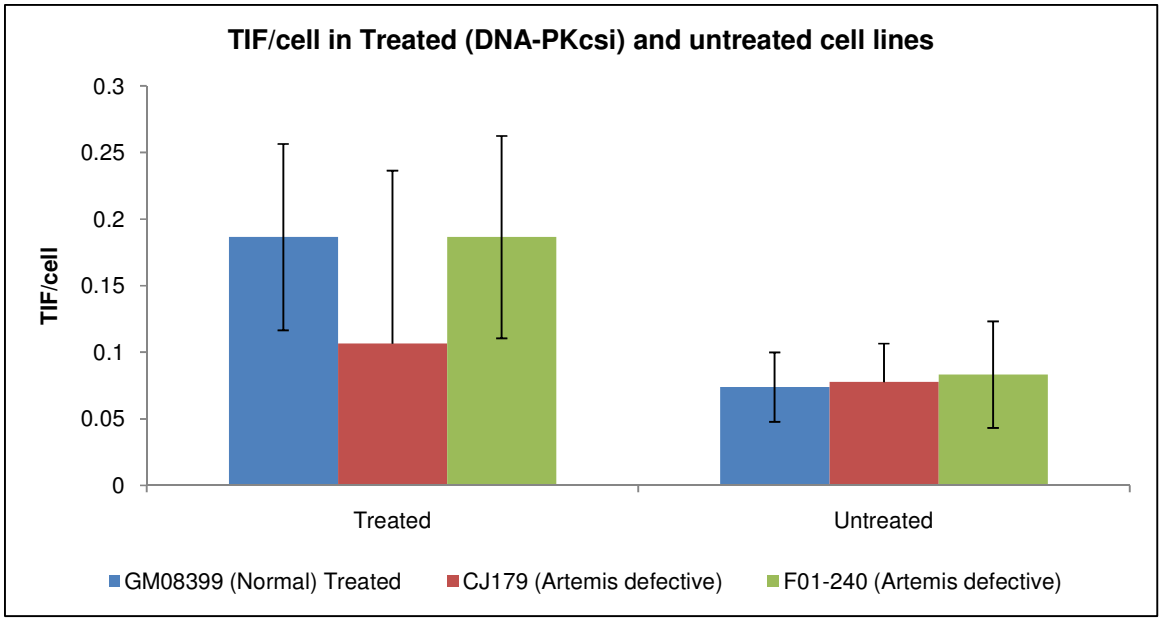

Figure 5.9 Frequencies of TIFs in three cell lines before (untreated) and after (treated) DNA-PKcsi. Error bars represent S.D., n=3.

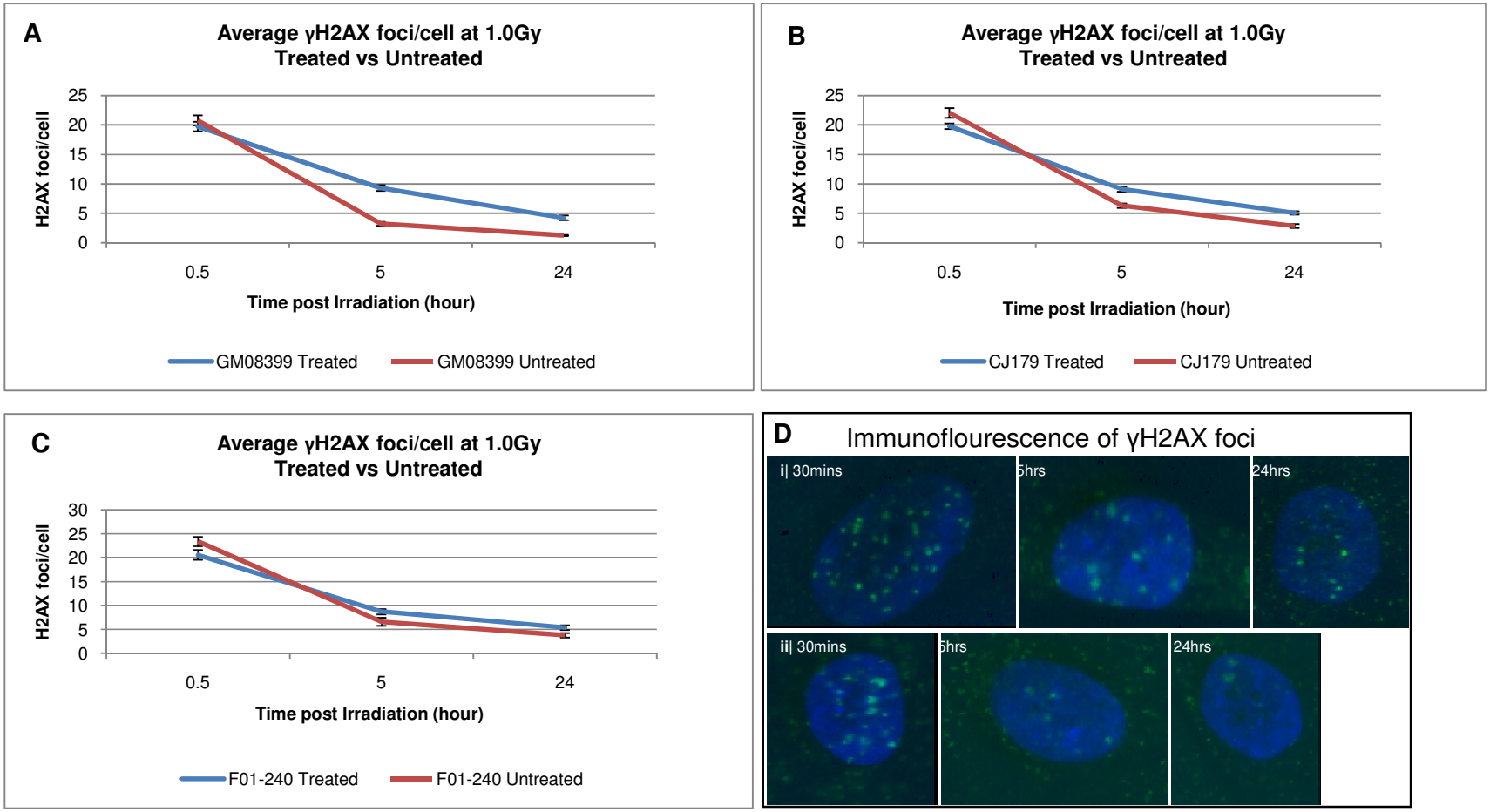

Figure 5.10. DSB repair kinetics of in three cell lines before and after DNA-PKcsi (20μM IC86621).
A| GM08399 (normal control). **B**| CJ179 (Artemis defective) **C**| F01-240 (Artemis defective) **D**| Examples of treated (top panel, i) and untreated (bottom panel, ii) cells stained with γH2AX antibody. Please note that the terms "Treated" and "Untreated" refer to treatment with IC86621.

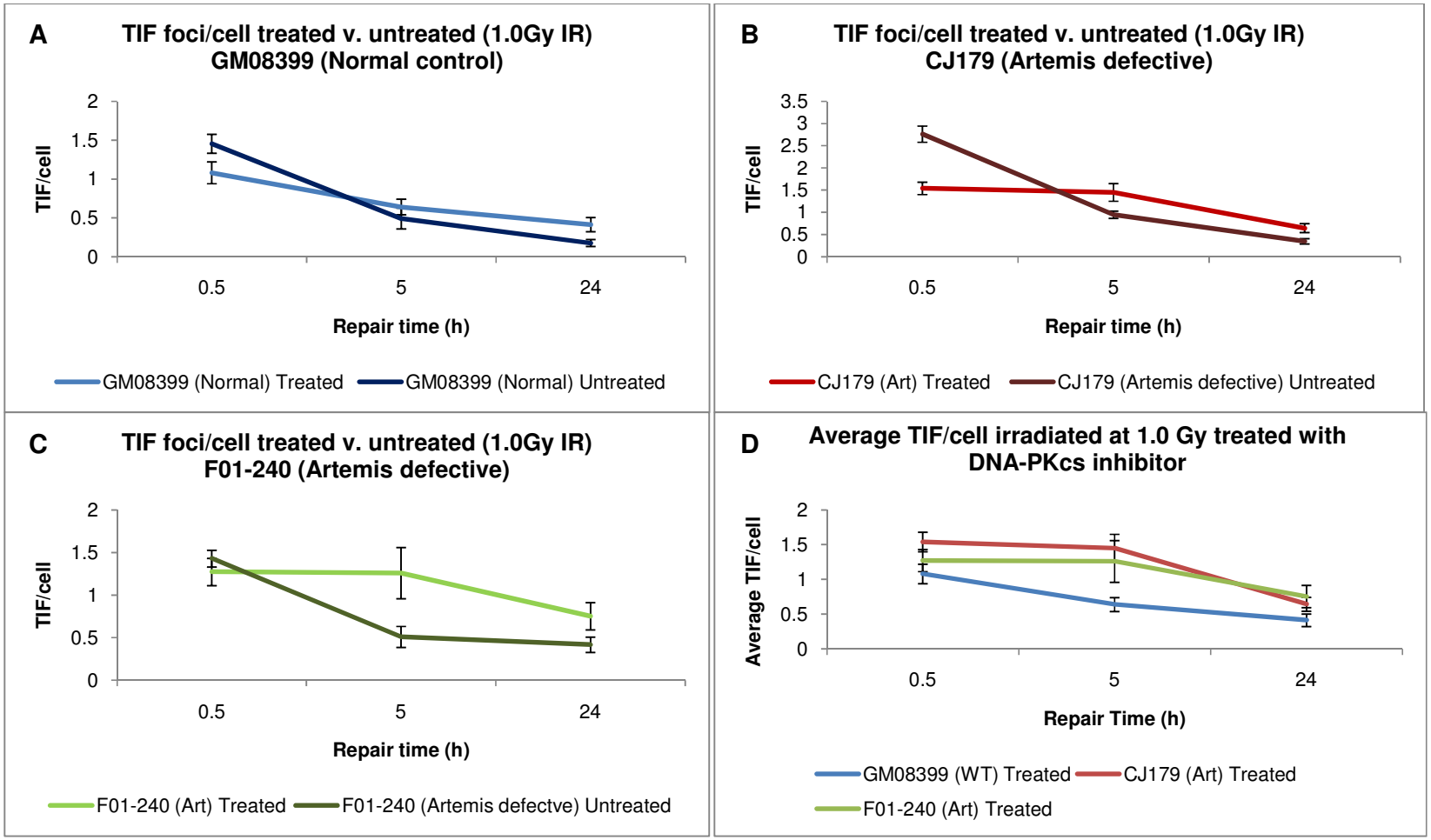

Figure 5.11. Frequency of TIFs in treated (DNA-PKcsi) and untreated cell lines induced with 1.0Gy IR.
A| GM08399 (normal control) **B**| CJ179 (Artemis defective). **C**| F01-240 (Artemis defective) **D**| Merged TIFs in treated (DNA-PKcsi) normal control and two Artemis defective cell lines.

5.3 Discussion

In this chapter we employed a highly specific inhibitor of DNA-PKcs, IC86621, to reduce DNA-PKcs levels in human fibroblast cell lines and to examine effects of this inhibition on telomeres in Artemis defective cell. Our results show that DNA-PKcsi caused (a) elevated frequencies of telomeric fusions and (b) telomere shortening in mouse LY-R and LY-S cell lines (Figures 5.1 and 5.3). Effect of DNA-PKcsi on telomeres in human cells caused similar effects with the exception that the observed telomere shortening was not statistically significant relative to untreated human cells (Figure 5.8). Therefore, these results are in line with results published by Bailey et al (2004) which revealed that the same inhibitor caused telomeric fusions in normal mouse embryonic fibroblasts. Similarly to Bailey et al. (2004) the large majority of telomeric fusions observed in our study were of chromatid type.

There are no reports in the literature on the effects of DNA-PKcsi on telomere length. To the best of our knowledge telomere length analysis by flow-FISH after DNA-PKcsi (Figures 5.4 and 5.8) is the first such report. We found that DNA-PKcsi causes telomere shortening in mouse and human cells (Figure 5.4 and 5.8), but the effect was statistically significant only in mouse cells. It seems likely that the treatment of human cells with IC86621 should be longer in order that telomere length values reach statistically significant differences when analyzing telomere length before and after DNA-PKcsi. Nevertheless, our results argue that DNA-PKcs has an effect on telomere length regulation *in vitro*. This is in line with previous studies which suggested that DNA-PKcs affects telomere length *in vivo* (Espejel et al., 2002b). However, it is important to note that DNA-PKcs deficiency *in vivo* causes abnormally longer telomeres in mouse cells (Hande et al., 1999).

Having established clear effects of DNA-PKcsi on telomeres in normal cells we analyzed behaviour of Artemis defective human cells subjected to DNA-PKcsi. Our results show that

DNA-PKcsi causes (a) increase in telomeric fusions in Artemis defective cell lines relative to both normal cell lines after DNA-PKcsi and Artemis cell lines without DNA-PKcsi and (b) elevated levels of DNA damage at telomeres (TIFs) following IR relative to both irradiated normal cells exposed to DNA-PKcsi and irradiated Artemis defective cells but not exposed to DNA-PKcsi. These results suggest that the effects of Artemis and DNA-PKcs on telomeres are cumulative. For example, analysis presented in Figure 5.11 show statistically significant differences between percentages of TIFs immediately after IR and 24 h after IR in relevant comparisons between cell lines.

What do these results mean from the perspective of mechanisms by which Artemis causes telomere dysfunction? We would like to argue that Artemis affects telomere maintenance independently of DNA-PKcs. This argument is based on the following observations. Both deficiencies cause similar levels of unrepaired TIFs 24 h after irradiation and when two deficiencies are present in the same cell environment their effect is cumulative. Given that DNA-PKcs regulates Artemis through phosphorylation and that Artemis defect on telomeres was still apparent after DNA-PKcsi it seems logical to conclude that DNA-PKcs is not required to mediate Artemis effect on telomeres. We would like to suggest that Artemis may exert its effect on telomere length either through an ATM dependent pathway, or through a pathway that involves its close homologue, Apollo. The two hypothetical scenarios are briefly discussed below.

It has been conclusively demonstrated that ATM plays an active role at telomeres. ATM defective human or mouse cells show increased frequencies of telomeric fusions, accelerated telomere shortening relative to control cells and increased frequencies of extra-chromosomal telomeric fragments which are most likely generated by DSBs occurring within telomeric sequences (Karlseder et al., 2004, Takata et al., 2004, Verdun et al., 2005, Guo X

et al., 2007). Biochemical characterization of ATM from the perspective of telomere maintenance revealed molecular interactions with TRF2, a protein that is part of shelterin. ATM phosphorylates TRF2 at T188 and that this phosphorylation plays a role in the fast repair of DSBs (Huda et al., 2009). It is also interesting to mention that TRF2 is involved in the repair of photo induced DSBs (Bradshaw et al., 2005). These observations highlight the importance of a functional interplay between DNA damage response pathways and pathways that regulate telomere maintenance. Given the fact that Artemis is involved in the repair of approximately 10% IR induced DSBs in an ATM dependent manner it is of interest to search for potential mechanisms by which Artemis affects telomeres in this context. Recent studies suggest that DSBs generated within the heterochromatic parts of the human genome are repaired much more slowly than DSBs generated within euchromatin and that ATM is required for the repair of heterochromatic DSBs (Goodarzi et al. 2008). Telomeres are typical heterochromatic parts of the human genome. This notion is supported by the observations that mammalian telomeric chromatin also has heterochromatin features (Garcia-Cao et al, 2004, Gonzalo and Blasco, 2005) and this influences telomere length regulation and telomere function (Schoeftner and Blasco, 2009). The fact that Artemis defective cells fail to repair IR induced TIFs as efficiently as normal cells argue that these cells have problems with repairing DSBs within telomeres. This could be due to specific heterochromatic organization of telomeres which may require functional ATM and functional Artemis for efficient DSB repair. It would be of interest to test this hypothesis in future studies.

Alternatively, Artemis could affect telomere maintenance through its interactions with its close homologue, Apollo. Apollo is known to interact with TRF2 to protect telomeres during S-phase but its role in DNA damage response is somewhat conflicting (Lenain et al., 2006,

van Overbeek and de Lange, 2006, Demuth et al., 2004, Bae et al., 2008). However, recent findings indicate that Apollo stimulates ATM in response to IR (Demuth et al., 2008) and functional interaction between Apollo and DNA damage response via ATR in UV induced damage have been described (Anders et al., 2009). The recent findings therefore, suggest a clearer role of Apollo in DNA damage response although its precise role is still unclear. Nevertheless, these findings on Apollo's role in DNA damage response and telomeres can strengthen the scenario discussed in this chapter that Artemis and Apollo may interact in an ATM dependent manner in telomere maintenance.

Chapter 6 :
Effects of DNA-PKcs and Artemis knock-down on telomeres in Artemis and DNA-PKcs defective cell lines

6.1 Introduction

In the previous chapter we have shown that DNA-PKcsi resulted in increased levels of a) Type 1 chromosome fusions, indicative of telomere dysfunction and b) increased IR induced TIF frequencies in Artemis defective cells relative to normal control cells. Given cumulative effects of Artemis and DNA-PKcs deficiencies on TIF frequencies it is possible that DNA-PKcs and Artemis affect telomere function independently of each other.

Using the quantitative western blot technique (section 5.2.2.1) we found only partial reduction in the level of the DNA-PKcs protein after DNA-PKcsi (45% reduction, Figure 5.6). To generate a stronger reduction of the DNA-PKcs protein, in this chapter we employed short interfering RNA (siRNA) to target, bind and degrade the product of the *PRKDC* gene. Moreover, we knocked-down Artemis in a DNA-PKcs defective human glioblastoma cell line. This cell line has a frameshift mutation in exon 32 corresponding to the first nucleotide codon 1351 (ACC,Thr) with the consequence of early termination of the *PRKDC* gene in exon 33 (Anderson et al., 2001).

By investigating effects a) DNA-PKcs knock-down in Artemis defective cell lines and b) Artemis knock-down in DNA-PKcs defective cells it is hoped that mechanisms by which Artemis affects telomere dysfunction will be probed further.

6.2 Results and discussion

6.2.1 Knock-down of human *PRKDC* (DNA-PKcs) expression using short interfering RNA (siRNA) technology in an Artemis defective human cell line

DNA-PKcsi using a synthetic drug IC86621 and effects of this inhibition on Artemis defective cells was described in the previous section (5.2). However, only a 45% inhibition of DNA-PKcs was achieved. In this section we employed a different technique

to reduce the level of DNA-PKcs protein - short interfering RNA (siRNA). The entire protocol used in this section has been described in chapter 2. A pool of four separate siRNA binding to four separate locations within the DNA-PKcs mRNA (Table 6.1) was purchased from Dharmacon. We quantified mRNA levels of DNA-PKcs gene using real-time qPCR technique. In all experiments, dissociation curves were plotted to check quality of each primer set (Figure 6.3B).

Table 6.1 Summary of DNA-PKcs siRNA
Sequences of Dharmacon Accell smart pool siRNA targeting four regions of the human DNA-PKcs gene. Human GAPDH siRNA was used to test the efficiency and viability of the Accell transfection medium

Dharmacon Accell Smart Pool	**Target Sequence**
Human *PRKDC* (DNA-Pkcs) Seq. 1	UCUUGUGUUUAUUGGAUC
Human *PRKDC* (DNA-Pkcs) Seq. 2	GGAAGAAGCUCAUUUGAUU
Human *PRKDC* (DNA-Pkcs) Seq. 3	CGAUCAACACGGAAUUAUU
Human *PRKDC* (DNA-Pkcs) Seq. 4	CUUUUACAUAGCAUGGUUA
Human *GAPDH*	GUGUGAACCAUGAGAAGUA

We started with a pilot experiment using only GAPDH siRNA and quantified GAPDH at three separate time points, 3 days, 5 days and 7 days post transfection. As can be seen from Figure 6.1A, on average an 80% reduction in GAPDH level was achieved over a three days period. We next used GAPDH siRNA and PRKDC pool siRNA together and quantified levels of proteins at four separate time points (3 days, 5 days, 7 days and 9 days post transfection) in two independent experiments. Again, over 70% knock-down of target mRNAs was achieved over three days (Figure 6.2).

A scrambled siRNA was used as a negative control to show that the knock-down was not random and was due to degradation of target mRNA.

Lowest levels of DNA-PKcs were measured 3 days after transfection and the percentage of knock-downs were between 70% and 78% (Figure 6.2). Levels of DNA-PKcs mRNA stayed low for 7 days post transfection before a recovery by day 9 measuring between 85% and 95% of the endogenous DNA-PKcs levels. To verify qPCR results we employed another technique, immunocytochemistry. A DNA-PKcs specific antibody (Neomarker) was used to detect levels of DNA-PKcs in cell lines transfected with PRKDC siRNA and in untransfected control cells Figure 6.3 C-E. Results (Figure 6.3 C-E) showed complete or partial reduction in DNA-PKcs levels in cell nuclei from transfected samples confirming that knock-down of DNA-PKcs gene has resulted in reduction of DNA-PKcs protein.

6.2.1.2 Delayed repair of endogenous DNA-damage in DNA-PKcs Knock-down Artemis defective cells

We next examined effects of DNA-PKcs knock-down on TIF frequencies. For this purpose we used only one Artemis defective cell line. Furthermore, the price of siRNA oligonucleotides and other reagents required prevented us from generating repair kinetics curves after exposure of cells to IR as in previous chapters. We observed increased frequencies of γH2AX foci in normal cells 3 days post transfection only, whereas Artemis defective cells exhibited more sustained and longer lasting effect showing elevated frequencies of γH2AX foci 3, 5 and 7 days after transfection (Figure 6.4). The difference in average frequencies of γH2AX foci per cell 5 days post transfection between Artemis defective and normal cell lines were significant ($p<0.001$), but not significant for 3 and 7 days post transfection ($p<0.0263$ and $p<0.086$ respectively).

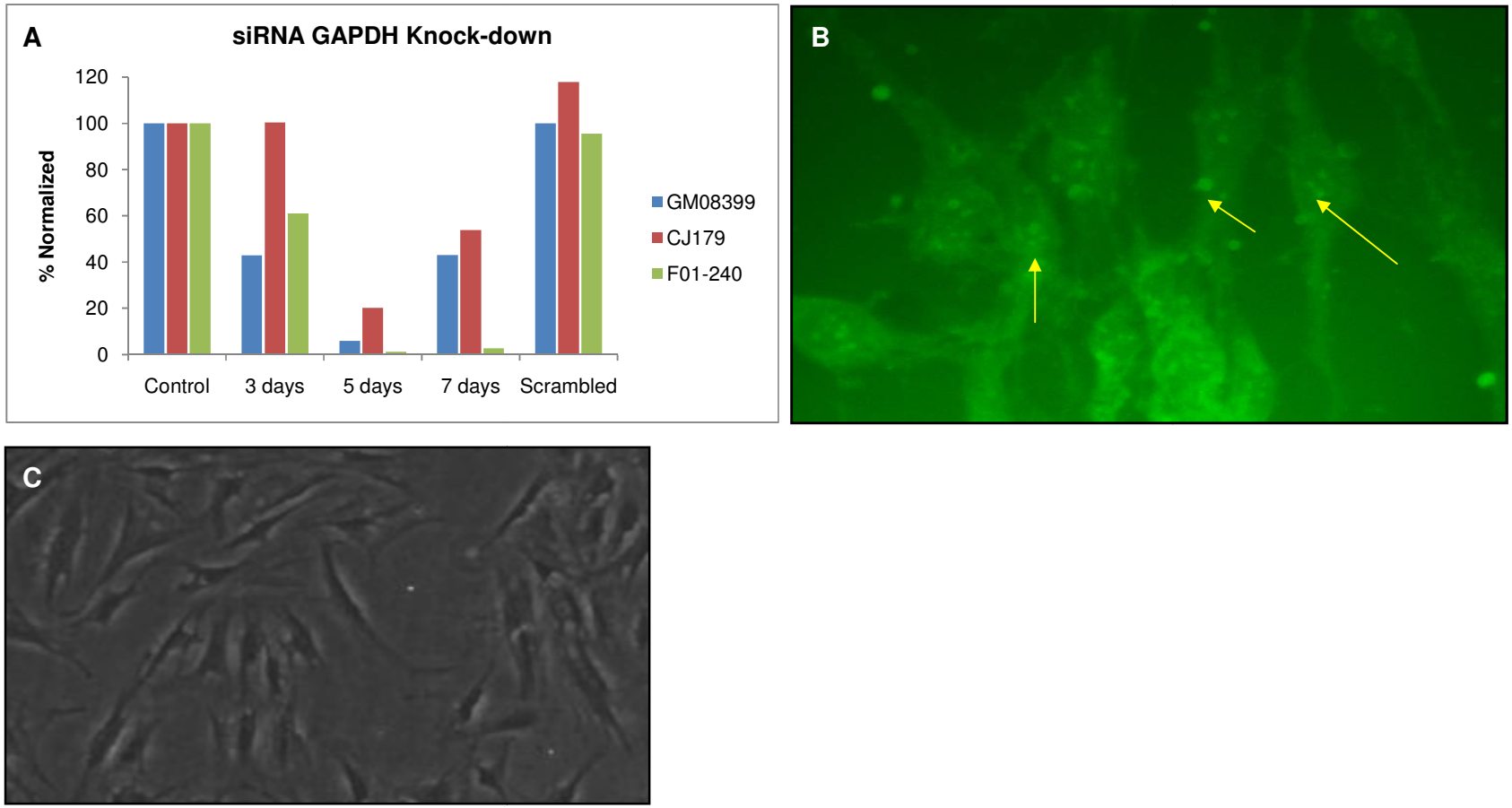

Figure 6.1.Over 80% knock-down was achieved in control GAPDH experiment.
A| Showing relative percentage of GAPDH knock-down in all three cell lines transected for seven days. Scrambled siRNA is a non-targeting siRNA sequence used as a negative control. **B**| Transfection efficiency was observed using a FITC-conjagated non-targeting control siRNA. The image shows the cytoplasmic localization of NTC (non-template control or scrambled control) siRNA (yellow arrows). in normal human primary fibroblast cell line (GM08399).**C**| Cells were plated initially at 30 – 40 % confluency and were transfected with siRNA of interest in Accell delivery medium for a period for three days (96 hours)

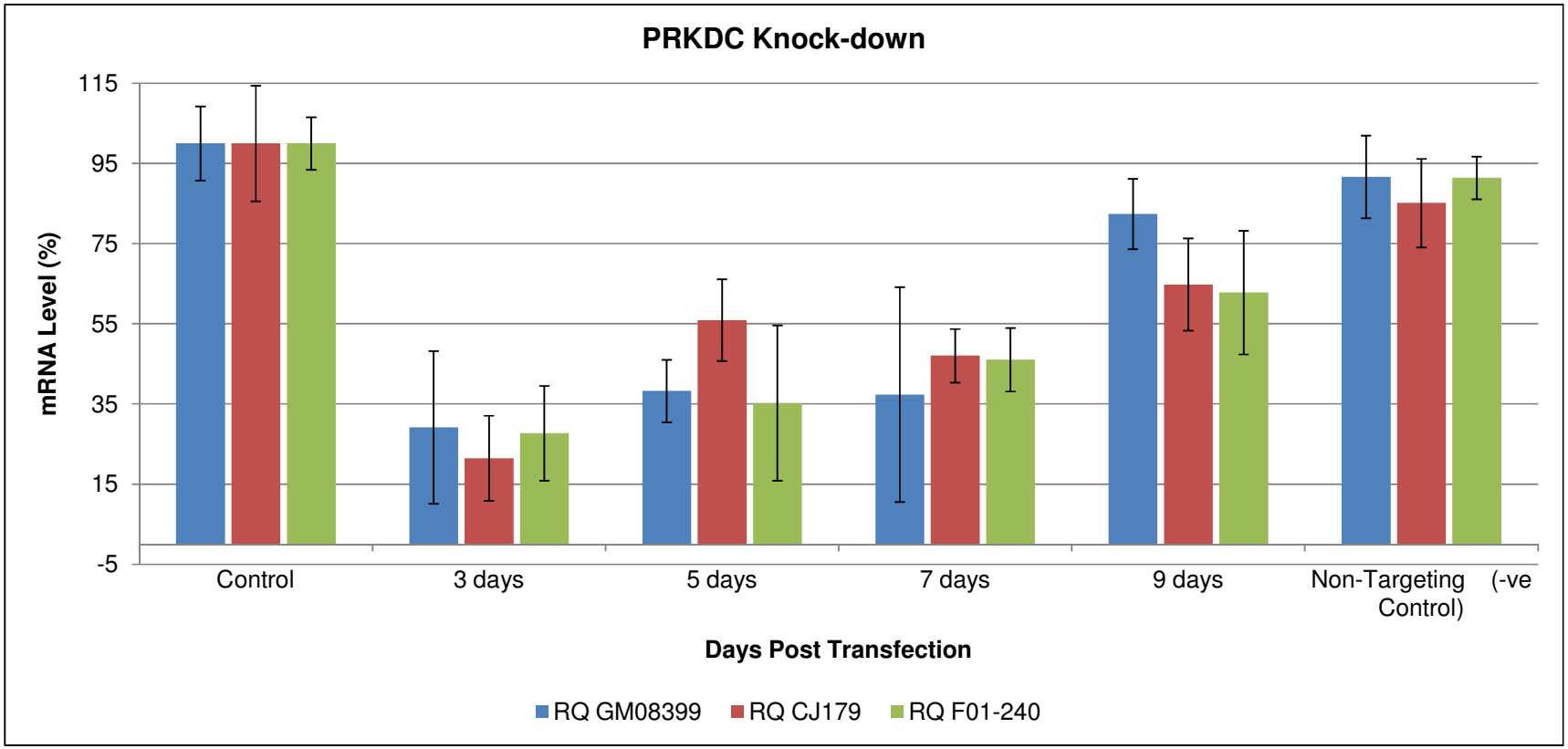

Figure 6.2. 80% knock-down in DNA-PKcs mRNA level were measured at 3-days post transfection.
The knock-down levels were normalized against endogenous GAPDH mRNA level in two independent experiments. Please note that levels of PRKDC mRNA recovered 9 days post transfection. A negative control of non-targeting scrambled siRNA sequence was also used in all three experiments. Error bars indicate S.D. RQ: Relative quantification.

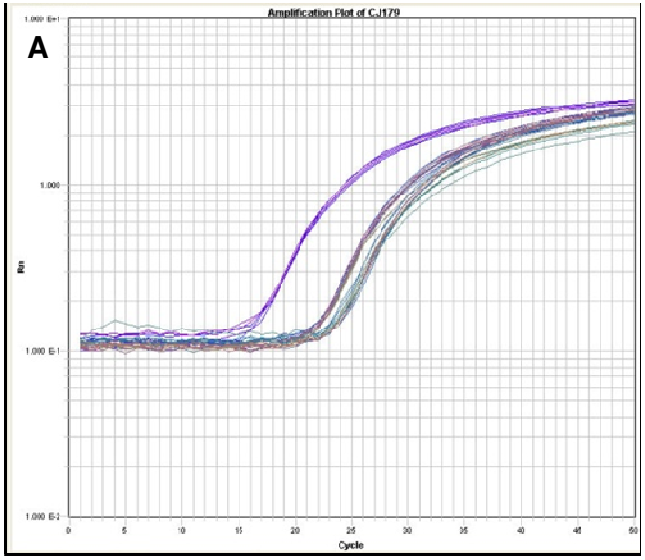

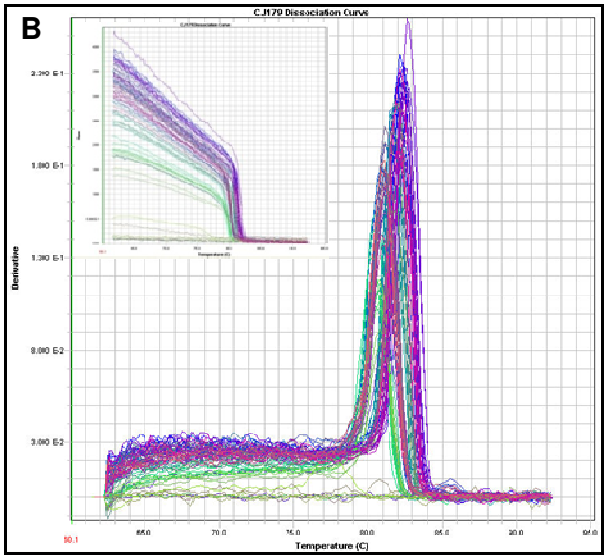

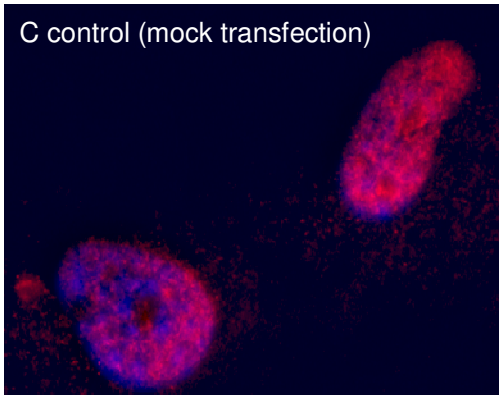

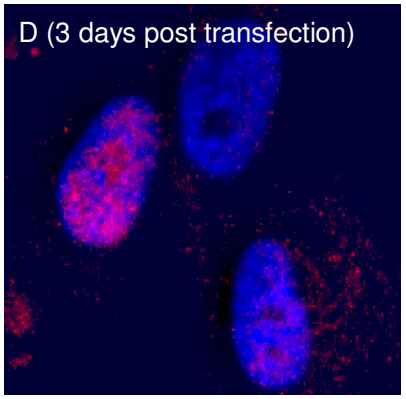

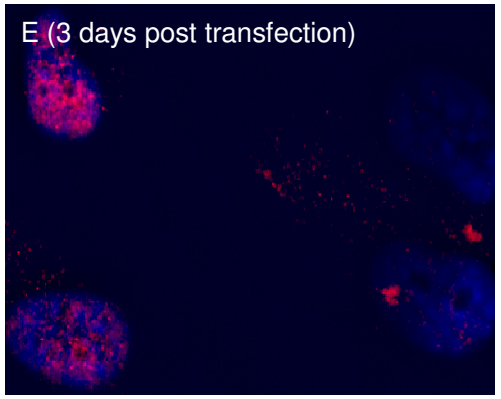

Figure 6.3 Immunofluorescence and real-time qPCR amplification curve showing reduced levels of PRKDC gene.

A| Real-Time qPCR Amplification curve of CJ179 (Art) 3 days post-transfection. **B**| Dissociation curve of CJ179 (Art) from the above real-time amplification curve showing melting temperature and specificity of the GAPDH and PRKDC primers. **C**| Cell nuclei stained with anti-DNA-PKcs antibody conjugated with Cy3 (red) showing nuclear localization of DNA-PKcs protein in mock transfection (control) and **D**| and **E**| 3 days post transfection showing reduced levels of DNA-PKcs protein in some nuclei and complete reduction of DNA-PKcs in others. Cell nuclei are stained with DAPI in (blue) DNA-PKcs is in (red).

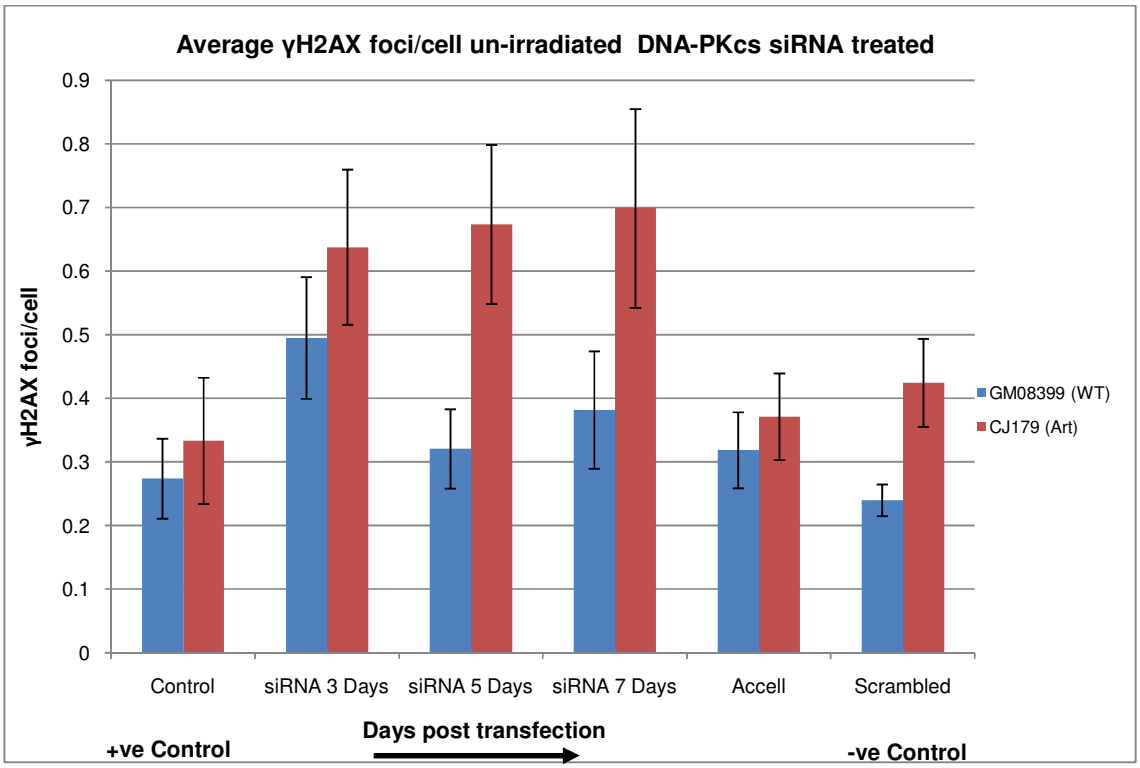

Figure 6.4. Frequencies of γH2AX foci in Artemis defective cell lines before and after transfection.
DNA-PKcs siRNA oligonucleotides were added in each sample in an Accell transfection medium for 3 days after which the medium was replaced with normal growth medium. A non-targeting (scrambled) siRNA was also used as a negative control alongside a mock transfection using Accell transfection medium only. The data are pooled results from two independent experiments with at least 100 nuclei scored per point per experiment. The error bars represent SEM.

6.2.1.1 Increased levels of TIF in DNA-PKcs knock-down Artemis defective cells

We next analyzed TIF frequencies in the two cell lines. Through analysis of at least 100 cell nuclei per cell line in two independent experiments we found that TIF levels increased in normal cells only 3 days after transfection relative to control cells, whereas Artemis defective cells showed more sustained and longer lasting effect with TIF frequencies being higher 3 and 5 days post-transfection relative to TIF frequencies in a) control Artemis cells and b) DNA-PKcs knocked-down normal cells (Figure 6.5).

These results show that DNA-PKcs knock-down has a stronger effect on telomeres in Artemis defective cells than in normal cells.

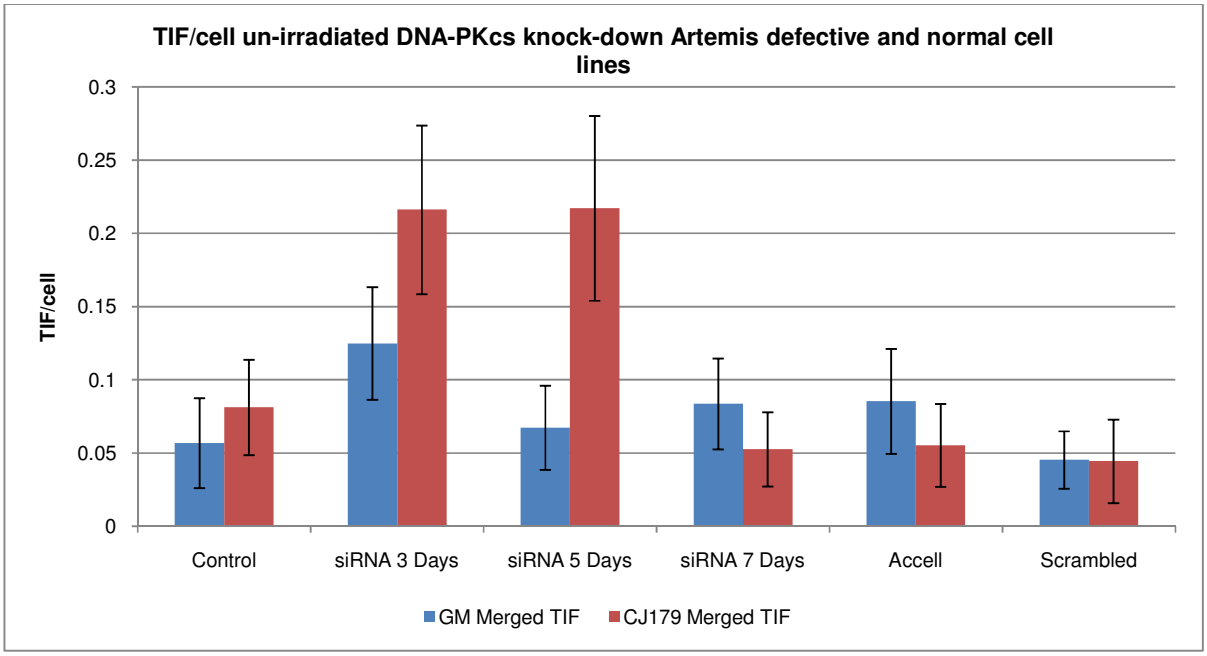

Figure 6.5. Frequencies of TIFs in DNA-PKcs knocked-down Artemis deficient and normal control cell lines.
The data are pooled results from two independent experiments. Error bars represent SEM. The difference in TIF between the two lines are significant at 5 days post transfection ($p<0.012$).

6.2.2 Human Glioblastoma cell line deficient in DNA-PKcs

The two human glioblastoma cell lines (MO59K and MO59J) were derived from a glioblastoma multiform (GBM) patient (Anderson et al., 2001). It has been shown that MO59J is hypersensitive to IR and also to bleomycin, nitrogen mustard and N,N-bis(2-chloroethyl)-N-nitrosourea (Allalunis-Turner et al., 1993), and that it lacks proper rejoining of DSBs (Lees-Miller et al., 1995), whereas MO59K was found to have normal DNA-PK activity and was not radiosensitive (Anderson et al., 2001).

6.2.2.2 Knock-down of *DCLRE1C* (Artemis) in MO59K and MO59J through siRNA

The complete protocol for knock-down of *DCLRE1C* gene (Artemis) through siRNA has been described fully in chapter 2. A smart pool siRNA were purchased from Dharmacon and transfected using Accell delivery medium. Details of four siRNA oligonucleotides corresponding to the Artemis gene are listed in Table 6.2.

Table 6.2. All four sequences of siRNA used in knock-down of Artemis gene (*DCLRE1C*) and the sequence of human *GAPD* siRNA used as a control.

Dharmacon Accell Smart Pool	**Target Sequence**
Human *DCLRE1C* (Artemis) Seq. 1	UCUUGUGUUUAUUGGAUC
Human *DCLRE1C* (Artemis) Seq. 2	GGAAGAAGCUCAUUUGAUU
Human *DCLRE1C* (Artemis) Seq. 3	CGAUCAACACGGAAUUAUU
Human *DCLRE1C* (Artemis) Seq. 4	CUUUUACAUAGCAUGGUUA
Human *GAPDH*	GUGUGAACCAUGAGAAGUA

The levels of Artemis mRNA were quantified using real-time qPCR and normalised against endogenous GAPDH. Four time points were selected and total mRNA extracted at each time point post-transfection (Figure 6.6C). In every qPCR experiments, dissociation curves were plotted to check quality of each primer set (Figure 6.6AB). We achieved a 76 % knock-down in MO59K (normal control) and 57 % in MO59J (DNA-PKcs defective) three days post transfection (Figure 6.6C). We observed increase in the level of Artemis mRNA starting five days post transfection. This increase proves the fact that the knock-down was transient and that both cell lines were able to recover Artemis mRNA levels.

6.2.2.3 Preliminary analysis of endogenous γH2AX and TIF foci in Artemis knock-down DNA-PKcs defective cells

We then recorded levels of endogenous γH2AX foci at three points post transfection (3 days, 5 days and 9 days). We would like to stress that because of time constrains experiments described in this session are performed only once and should be considered preliminary.

Our analysis showed a significant difference in γH2AX frequencies between DNA-PKcs defective cells (MO59J) compared to the normal control cells (MO59K) prior to transfection (Figure 6.6D). The four-fold difference in frequency of γH2AX foci is consistent with the published finding that MO59J cell line show reduced ability to rejoin DNA DSBs and increased radiosensitivity (Allalunis-Turner et al., 1993 & 1995, Lees-Miller et al., 1995). Frequency of γH2AX increased three days post-transfection in MO59J cells, but remained the same in MO59K cells relative to control cells throughout the experiment (Figure 6.6D)

Furthermore, TIF levels increased in MO59J cells 3 days post transfection, whereas TIF remained at normal level in MO59K cells throughout the experiment (Figure 6.6E).

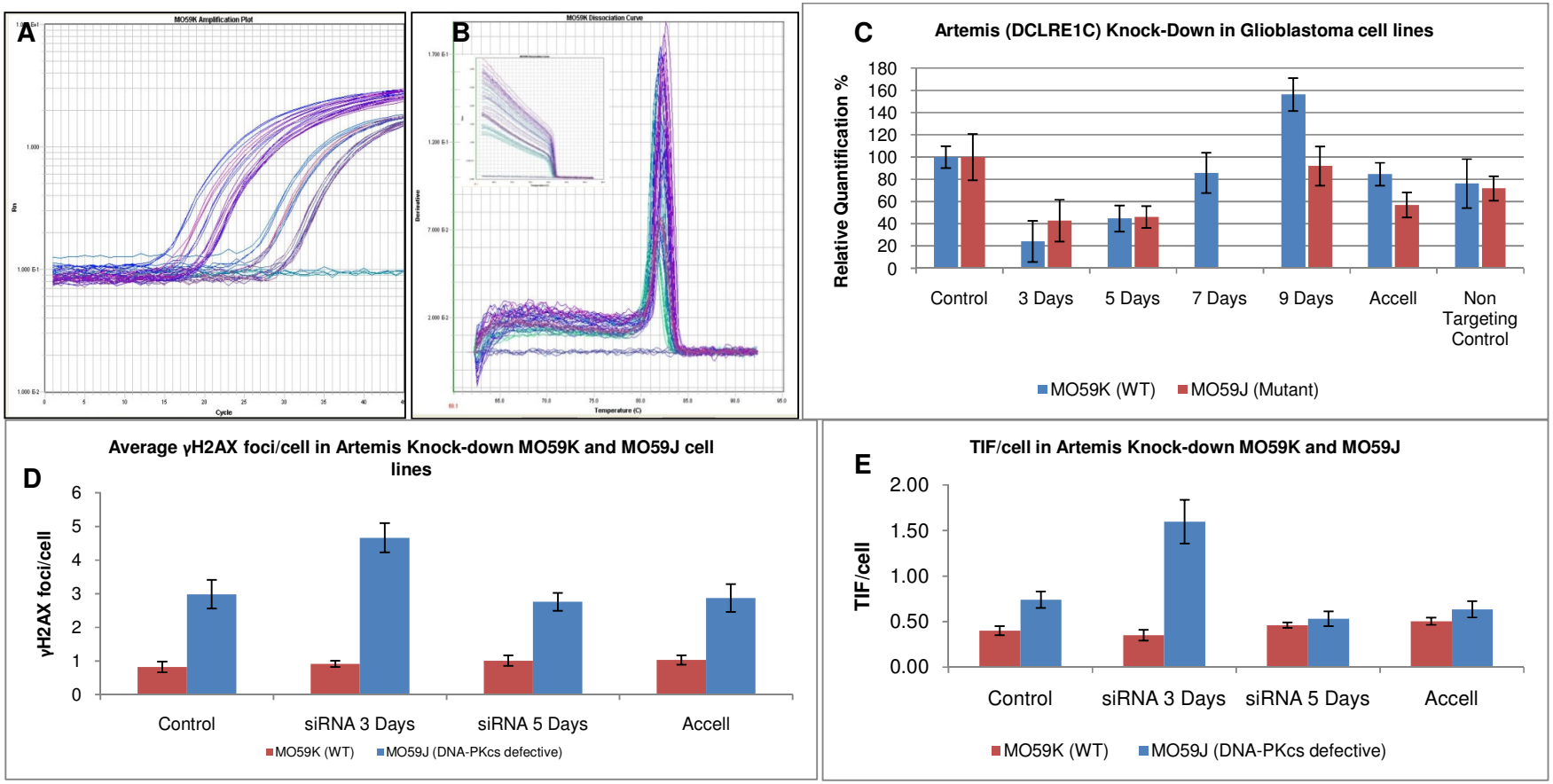

Figure 6.6. Knock-down of the Artemis gene in MO59K and MO59J human glioblastoma cell lines.
A| Real-time qPCR curve showing reduced levels of Artemis in both MO59K and MO59J cells. All results were normalised to endogenous GAPDH. **B**| Dissociation curve showing the specificity of the primer used in real-time qPCR. **C**| Graph showing relative percentage of Artemis mRNA in the two cell lines. A 76 % knock-down was achieved in the MO59K cell and 57 % in the MO59J cell line. **D**| Frequencies of γH2AX foci/cell in MO59K and MO59J cells before and after Artemis knock-down. **E**| Frequencies of TIF foci per cell in MO59K and MO59J cell lines. 100 nuclei were scored / point in one round of experiment. The error bars represent SD. Accell is transfection medium only incubated for three days as positive control.

Taken together, in this chapter we have shown that DNA-PKcs knock-down has greater effect in Artemis defective cells than normal control cells on a) spontaneous levels of DNA damage and b) frequencies of TIFs. This finding further supports our speculation that effects of DNA-PKcs and Artemis on telomeres are separate. If DNA-PKcs controls Artemis in telomere maintenance-related processes one may argue that knock-down of DNA-PKcs in Artemis defective cells should only cause the effect equivalent to that in Artemis proficient cells and the pattern of effect would be similar in both cell types. This is clearly not the case. DNA-PKcs knock-down causes elevated γH2AX and TIF levels in normal cells only 3 days post transfection (Figure 6.4, Figure 6.5). By contrast, γH2AX levels are elevated 3, 5 and 7 days post transfection whereas TIF levels are elevated 3 and 5 days post-transfection in Artemis defective cells (Figure 6.6 D, E).

Our speculation that Artemis and DNA-PKcs have separate effects on telomeres is further supported by a set of preliminary results employing Artemis specific siRNA oligonucleotides. However, these results have to be confirmed by further experiments.

Chapter 7 :

General Discussion

7.1 General Discussion

The work presented in this thesis aimed to examine whether Artemis, a protein involved in NHEJ, plays any role in telomere maintenance. The reasoning behind this was that at least two NHEJ proteins, Ku and DNA-PKcs, play active roles in telomere maintenance and that DNA-PKcs regulates Artemis through phosphorylation. Furthermore, a relatively high number of other DNA damage response proteins, not involved in NHEJ, seem to actively participate in telomere maintenance suggesting a close relationship between DNA damage response mechanisms and mechanisms that regulate telomere maintenance.

This thesis generated three novel findings. Firstly, Artemis defective cells show mild telomere dysfunction suggesting the role of this protein in telomere maintenance. Secondly, Artemis defective cells show increased incidence of IR induced DNA damage at telomeres only when they undergo above 30 PD but do not reach senescence yet. Thirdly, DNA damage at telomeres following IR was also observed in normal “older” cells suggesting that cell ageing can potentially enhance DNA damage. These three findings are briefly discussed below.

7.2 The role of Artemis at telomeres

The mechanism of telomere maintenance is somewhat “paradoxical” (Slijepcevic, 2006) given that telomeres are supposed to hide natural DNA ends from being recognized as DSBs and yet two key NHEJ proteins, DNA-PKcs and Ku, are physically present at telomeres and they interact with shelterin (de Lange, 2005). A recently proposed model suggests that telomere maintenance is an integral part of DNA damage response (Slijepcevic, 2006, Slijepcevic, 2008). This model makes a distinction between DNA repair, which can be viewed as the restoration of DNA

sequence integrity and fidelity, and "chromosome repair" which represents restoration of chromosome structure and function, a part of which is de novo acquisition of telomeres and centromeres (Slijepcevic, 2008). The model predicts that NHEJ is not only a DNA repair process but also a process which contributes to restoring chromosome function (Slijepcevic 2006). The model also eliminates the above paradox as the presence of Ku and DNA-PKcs at telomeres may be required to initiate the acquisition of a new telomere at the site of DNA DSB that cannot be repaired by other means. There is clear evidence in the literature that de novo acquisition of telomeres or chromosome "healing" is operational in both yeast and humans (for review see Slijepcevic, 2006). One of the key molecules in this process is Ku which induces local chromatin condensation prior to chromosome healing (Fisher and Zakian, 2005) and recruits telomerase which will synthesize a new telomere. It has been postulated that DNA-PKcs is also involved in chromosome healing (Slijepcevic, 2006).

Our observation that an Artemis defect causes a mild telomere dysfunction phenotype is in line with the above model. However, we do not have any evidence as to how exactly Artemis may affect telomere maintenance. In the case of Ku and DNA-PKcs it was conclusively demonstrated that cells or mice defective in these proteins show high frequencies of telomeric fusions and clear biochemical interaction between these two proteins and shelterin. We calculated that the level of telomeric fusions observed in Artemis defective cells is approximately 10 times lower than in Ku or DNA-PKcs defective cells. However, we have not carried out biochemical experiments to find out whether Artemis directly interacts with shelterin and this line of research should be pursued in the future. It is interesting in this context that a

close relative of Artemis, a protein recently named Apollo (in Greek mythology Apollo and Artemis are twins) directly interacts with shelterin, more specifically with TRF2.

An obvious question is why Artemis is required for telomere maintenance? If the prediction that DNA-PKcs is required for “chromosome healing” (see above) is true and given that DNA-PKcs phosphorylates Artemis, a protein with endonucleolytic activity, it is tempting to speculate that Artemis may be required to prepare the substrate for telomerase before “chromosome healing” takes place. This seems to be an attractive scenario particularly in the view of the fact that telomerase requires a single strand DNA end to synthesize telomeric DNA. In this scenario Ku would be the key initiator of “chromosome healing” as suggested by experimental evidence (Fisher and Zakian, 2005). If the conventional NHEJ fails, Ku will a) “heterochromatinize” the site of DSB and b) recruit telomerase. As telomerase cannot operate on double stranded DNA, DNA-PKcs would need to activate Artemis which will process DSBs so that a single stranded DNA overhang is available for telomerase to act upon and synthesize new telomeric DNA. It is important to stress that telomerase does not need a high level of homology to the conventional telomeric sequence to start the synthesis. When a new telomeric sequence at the site of chromosome break is synthesized Ku will recruit shelterin so that a functional telomere is generated.

Given that we have no evidence that Artemis biochemically interacts with shelterin we have to consider an alternative scenario, namely that Artemis is not directly involved in telomere maintenance but that the mild telomere dysfunction phenotype observed is simply an indirect consequence of defective DNA repair. This possibility is supported by our earlier prediction (see Chapter 5) that the role of Artemis at

telomeres is independent from DNA-PKcs. However, the observation of telomere dysfunction phenotype in mice defective in Artemis (Rooney et al., 2003) argues against this possibility.

In conclusion for this part, future research is required to establish, through biochemical experiments, whether Artemis interacts with shelterin and if so how exactly this protein affects telomere maintenance.

7.2 Reduced DNA repair efficiency at telomeres

In chapter 4.3 we presented and discussed two novel findings based on the IF-TIF assay. Firstly, “older” cells, whether normal or Artemis defective, cannot efficiently repair DNA damage at telomeres (Figure 4.4). Secondly, the level of DNA damage at telomeres after IR was significantly higher in Artemis defective “older” cells than in normal “older” cells. These findings suggest that DNA repair efficiency within telomeric DNA is lower in “older” cells than in “younger” cells. The finding is relevant for understanding how telomeres affect cellular ageing but also from the perspective of understanding efficiency of repair mechanisms in the context of cellular ageing. Previous works based on Chinese hamster cells have shown that interstitial telomeric sequences are hypersensitive to DNA damaging agents such as IR and prompted several authors to consider telomeres as fragile sites (see for example Balajee et al., 1994, Slijepcevic et al., 1996). A recent study has conclusively demonstrated that telomeres behave as classical fragile sites (Sfeir et al., 2009). A work by Kruk et al., (1995), has shown that DNA damage at telomeres induced by UV was repaired less efficiently than DNA damage induced in actively transcribed DNA. Importantly, Kruk et al., (1995) found that cells from older donors were less efficient in DNA repair than cells from younger donors, which is similar to our finding

that “older” cells process DNA damage at telomeres less efficiently than “younger” cells (Figure 4.4). Our finding therefore may further enhance the link between telomere maintenance and cellular aging (Slijepcevic, 2008). Almost all human syndromes characterized by defective DNA damage response show defective telomere maintenance (Slijepcevic, 2008). These include Ataxia telangiectaisa, Nijmegen brekage syndrome, Fanconi anemia, Bloom syndrome, RS-SCID, Xeroderma pigmentosum etc. All these syndromes are also characterized by signs of premature aging.

However, it has been suggested that the cause of the fragility within telomeric DNA is altered packaging and/or condensation of the chromatin rather than the presence of DNA DSBs (Sfeir et al., 2009). If that is the case, then what is the cause of persistent TIFs, observed in “older” cells relative to “younger” cells (Figure 4.4)? We have not carried out experimental work to address this issue. However, given that telomeres are classical heterochromatic regions, one might speculate that if Artemis directly contributes to elevated TIFs observed in our study (Figure 4.4) this is likely to happen in an ATM dependent fashion. It has recently been shown that ATM and Artemis participate in a pathway responsible for repair of DSBs in heterochromatic regions of the genome (Goodarzi et al., 2008).

It is interesting to note that Artemis defective cell lines showed accelerated rate of telomere shortening (Cabuy et al., 2005). Critically short telomeres activate DNA damage response which in turn can activate cellular senescence which is an evolutionary mechanism that prevents genome instability (d’Adda di Fagagna et al., 2003, Shay et al., 1992). Therefore, one might argue that increased level of TIFs observed in “older” Artemis defective cells may have resulted from the activation of

DNA damage response due to accelerated telomere shortening rather than from the active role of Artemis at telomeres.

7.1 7.3 Future research

Results presented in this thesis open at least two interesting avenues for future research. The first avenue should focus on exploring biochemical characterization of Artemis relative to its interaction with shelterin. Assays that can be used to explore the above possibility include two yeast hybrid screen and chromatin immunoprecipitation (ChIP) assay. In a typical two yeast hybrid screen a known protein is selected which serves as a bait for the test protein. When examining shelterin interaction with other proteins the usual protein selected as shelterin representative is TRF2. If TRF2 proves to be the wrong candidate for interaction with Artemis all other shelterin proteins should be tested. Alternatively, the ChIP assay can be performed in which all proteins binding to a particular DNA sequence, in this case telomeric DNA, are detected.

The second avenue should focus on how DNA damage is induced and processed within telomeric DNA relative to cell age status. The key assay here is IF TIF. A number of experiments can be designed to determine in several systems the repair efficiency of telomeric DNA in old versus young cells. In particular, it is important to use mouse cells in addition to human cells. Mouse cells have much longer telomeres and it is easier to induce higher levels of DNA damage at telomeres in mouse than in human cells, given the size of the mouse telomeres. Another important point is to use an assay that is different from IF TIF to verify our findings. We believe that the comet assay should be a good alternative given that a number of DNA probes can be used in parallel to the telomeric probe.

It will also be important to follow up analysis of telomere status in DNA-PKcs defective human cell lines at cytological level to look for evidence of telomere fusions occurring either spontaneously or as a result of exposure to IR. Furthermore, TIF analysis using DNA-PKcs defective cell lines with knocked-down Artemis should be repeated and if possible experiments carried out in which cells will be exposed to IR. These experiments may be critical for testing whether effects of DNA-PKcs and Artemis on telomere maintenance are independent or not. It will also be of interest to extend TIF analysis using Artemis defective cell lines and examine whether DNA damage at telomeres persists 48hrs and 72hrs post IR. By analysing TIFs for longer periods (2-3 days post IR) we may be able to understand the extent and efficiency of telomere repair kinetics in Artemis defective "older" cells. Understanding how damaged telomeres are repaired is important in aging and cancer.

Finally, the link between ATM and Artemis needs to be further examined from the telomere prospective. It has been shown previously that a subset of 10% of DSBs is repaired by ATM and Artemis and these occur within heterochromatin regions (Goodarzi et al., 2008). Telomeres are typical heterochromatin regions and the use of an ATM inhibitor in an Artemis defective environment should provide important information about the link between Artemis and ATM in telomere maintenance.

References

ABE, T., ISHIAI, M., HOSONO, Y., YOSHIMURA, A., TADA, S., ADACHI, N., KOYAMA, H., TAKATA, M., TAKEDA, S., ENOMOTO, T. & SEKI, M. (2008) Ku70/80, DNA-PKcs, and Artemis are essential for the rapid induction of apoptosis after massive DSB formation. *Cellular Signalling,* 20**,** 1978-1985.

AHNESORG, P., SMITH, P. & JACKSON, S. P. (2006) XLF interacts with the XRCC4-DNA Ligase IV complex to promote DNA nonhomologous end-Joining. *Cell,* 124**,** 301-313.

AL-WAHIBY, S. & SLIJEPCEVIC, P. (2005) Chromosomal aberrations involving telomeres in BRCA1 deficient human and mouse cell lines. *Cytogenetics and Genome Research,* 109**,** 491-496.

ALBERTS, B., BRAY, D., LEWIS, J., RAFF, M., ROBERTS, K. & WATSON, J. D. (1994) *Molecular Biology of the Cell,* New York & London, Garland Publishing.

ALEXANDER, P. (1961) Mouse lymphoma cells with different radiosensitivities. *Nature,* 192**,** 572-573.

ALLALUNIS-TURNER, M., BARRON, G., DAY, R. R., . , DOBLER, K., . & MIRZAYANS, R. (1993) Isolation of two cell lines from a human malignant glioma specimen differing in sensitivity to radiation and chemotherapeutic drugs. *Radiation Research,* 134**,** 349-54.

ALLALUNIS-TURNER, M., ZIA PK, BARRON GM, MIRZAYANS R & 3RD., D. R. (1995) Radiation-induced DNA damage and repair in cells of a radiosensitive human malignant glioma cell line. *Radiation Research,* 144**,** 288-93.

ALLSOPP, R. C., CHANG, E., KASHEFI-AAZAM, M., ROGAEV, E. I., PIATYSZEK, M. A., SHAY, J. W. & HARLEY, C. B. (1995) Telomere shortening is associated with cell division in vitro and in vivo. *Experimental Cell Research,* 220**,** 194-200.

ALVAREZ, L., EVANS, W. J., WILKS, R., LUCAS, J. N., BROWN, M. J. & GIACCIA, J. M. (1993) Chromosomal radiosensitivity at intrachromosomal telomeric sites. *Genes, Chromosomes and Cancer,* 8**,** 8-14.

ANDERS, M., JENS, M., MARTIN DIGWEED & DEMUTH, I. (2009) Evidence for hSNM1B/Apollo functioning in the HSP70 mediated DNA damage response. *Cell Cycle,* 8**,** 1725-1732.

ANDERSON, C. W., DUNN, J. J., FREIMUTH, P. I., GALLOWAY, A. M. & ALLALUNIS-TURNER, M. J. (2001) Frameshift mutation in PRKDC, the gene for DNA-PKcs, in the DNA repair-defective, human, glioma-derived cell line M059J. *Radiation Research,* 156**,** 2-9.

AYOUAZ, A., RAYNAUD, C., HERIDE, C., REVAUD, D. & SABATIER, L. (2008) Telomeres: Hallmarks of radiosensitivity. *Biochimie,* 90**,** 60-72.

BAE, J., MUKHOPADHYAY, S., LIU, L., ZHANG, N., TAN, J., AKHTER, S., LIU, X., SHEN, X., LI, L. & LEGERSKI, R. (2008) Snm1B/Apollo mediates replication fork collapse and S-phase checkpoint activation in response to DNA interstrand cross-links. *Oncogene,* 27**,** 5045-5056.

BAILEY, S., BRENNEMAN, M., HALBROOK, J., NICKOLOFF, J., ULLRICH, R. & GOODWIN, E. (2004a) The kinase activity of DNA-PK is required to protect mammalian telomeres. *DNA Repair,* 3**,** 225-233.

BAILEY, S., CORNFORTH, M., KURIMASA, A., CHEN, D. & GOODWIN, E. (2001) Strand-specific postreplicative processing of mammalian telomeres. *Science,* 293**,** 2462-2465.

BAILEY, S., CORNFORTH, M., ULLRICH, R. & GOODWIN, E. (2004b) Dysfunctional mammalian telomeres join with DNA double-strand breaks. *DNA Repair,* 3**,** 349-357.

BAILEY, S. & GOODWIN, E. (2004) DNA and telomeres: beginnings and endings. *Cytogenetics and Genome Research,* 104**,** 109-115.

BAILEY, S., GOODWIN EH. & CORNFORTH MN. (2004c) Strand-specific fluorescence in situ hybridization: the CO-FISH family. *Cytogenetics and Genome Research,* 107**,** 14-17.

BAILEY, S., MEYNE, J., CHEN, D., KURIMASA, A., LI, G., LEHNERT, B. & GOODWIN, E. (1999) DNA double-strand break repair proteins are required to cap the ends of mammalian chromosomes. *Proc. Natl. Acad. Sci. (USA),* 96**,** 14899-14904.

BALAJEE, A., OH, H. & NATARAJAN, A. (1994) Analysis of restriction enzyme-induced chromosome aberrations in the interstitial telomeric repeat sequences of CHO and CHE cells by FISH. *Mutation Research/Fundamental and Molecular Mechanisms of Mutagenesis,* 307**,** 307-313.

BLASCO, M. (2005) Telomeres and human disease: ageing, cancer and beyond. *Nat. Rev. Genet.,* 6**,** 611-622.

BLASCO, M. (2007) Telomere length, stem cells and aging. *Nat. Chem. Biol.,* 3**,** 640-649.

BLASCO, M., LEE, H., HANDE, M., SAMPER, E., LANSDORP, P., DEPINHO, R. & GREIDER, C. (1997) Telomere shortening and tumor formation by mouse cells lacking telomerase RNA. *Cell,* 91**,** 25-34.

BUCK, D., MALIVERT, L., DE CHASSEVAL, R., BARRAUD, A., FONDANECHE, M., SANAL, O., PLEBANI, A., STEPHAN, J., HUFNAGEL, M., LE DEIST, F., FISCHER, A., DURANDY, A., DE VILLARTAY, J. & REVY, P. (2006) Cernunnos, a novel nonhomologous end-joining factor, is mutated in human immunodeficiency with microcephaly. *Cell,* 124**,** 287-299.

BURMA, S. & CHEN, D. (2004) Role of DNA-PK in the cellular response to DNA double-strand breaks. *DNA Repair,* 3**,** 909-918.

CABUY, E., NEWTON, C., JOKSIC, G., WOODBINE, L., KOLLER, B., JEGGO, P. & SLIJEPCEVIC, P. (2005) Accelerated telomere shortening and telomere abnormalities in radiosensitive cell lines. *Radiation Research,* 164**,** 53-62.

CABUY, E., NEWTON, C., ROBERTS, T., NEWBOLD, R. & SLIJEPCEVIC, P. (2004) Identification of subpopulations of cells with differing telomere lengths in mouse and human cell lines by flow FISH. *Cytometry,* 62A**,** 150-161.

COLLIS, S., DEWEESE, T., JEGGO, P. & PARKER, A. (2004) The life and death of DNA-PK. *Oncogene,* 24**,** 949-961.

D'ADDA DI FAGAGNA, F., HANDE, M., TONG, W., ROTH, D., LANSDORP, P., WANG, Z. & JACKSON, S. (2001) Effects of DNA nonhomologous end-joining factors on telomere length and chromosomal stability in mammalian cells. *Current Biology,* 11**,** 1192-1196.

D'ADDA DI FAGAGNA, F., REAPER, P., CLAY-FARRACE, L., FIEGLER, H., CARR, P., VON ZGLINICKI, T., SARETZKI, G., CARTER, N. & JACKSON, S. (2003) A DNA damage checkpoint response in telomere-initiated senescence. *Nature,* 426**,** 194-198.

DARROUDI, F., WIEGANT, W., MEIJERS, M., FRIEDL, A., VAN DER BURG, M., FOMINA, J., VAN DONGEN, J., VAN GENT, D. & ZDZIENICKA, M. (2007) Role of Artemis in DSB repair and guarding chromosomal stability following exposure to ionizing radiation at different stages of cell cycle. *Mutation Research/Fundamental and Molecular Mechanisms of Mutagenesis,* 615**,** 111-124.

DE BOECK, G., FORSYTH, R., PRAET, M. & HOGENDOORN, P. (2009) Telomere-associated proteins: cross-talk between telomere maintenance and telomere-lengthening mechanisms. *The Journal of Pathology,* 217**,** 327-344.

DE LANGE, T. (2002) Protection of mammalian telomeres. *Oncogene,* 21**,** 532.

DE LANGE, T. (2005) Shelterin: the protein complex that shapes and safeguards human telomeres. *Genes & Development,* 19**,** 2100-2110.

DE LANGE, T., LUNDBLAD, V. & BLACKBURN, E. (2006) *Telomeres*, Cold Spring Harbor Laboratory Press.

DE LANGE, T., SHIUE, L., MYERS, R., COX, D., NAYLOR, S., KILLERY, A. & VARMUS, H. (1990) Structure and variability of human chromosome ends. *Mol. Cell. Biol.,* 10**,** 518-527.

DEMUTH, I., BRADSHAW, P., LINDNER, A., ANDERS, M., HEINRICH, S., KALLENBACH, J., SCHMELZ, K., DIGWEED, M., MEYN, M. & CONCANNON, P. (2008) Endogenous hSNM1B/Apollo interacts with TRF2 and stimulates ATM in response to ionizing radiation. *DNA Repair,* 7**,** 1192-1201.

DEMUTH, I., DIGWEED, M. & CONCANNON, P. (2004) Human SNM1B is required for normal cellular response to both DNA interstrand crosslink-inducing agents and ionizing radiation. *Oncogene,* 23**,** 8611-8618.

DIMITROVA, N. & DE LANGE, T. (2006) MDC1 accelerates nonhomologous end-joining of dysfunctional telomeres. *Genes & Development,* 20**,** 3238-3243.

DROUET, J., FRIT, P., DELTEIL, C., DE VILLARTAY, J., SALLES, B. & CALSOU, P. (2006) Interplay between Ku, Artemis, and the DNA-dependent protein kinase catalytic subunit at DNA ends. *J. Biol. Chem.,* 281**,** 27784-27793.

EDITORIAL (2003) Whither RNAi? *Nat. Cell Biol.,* 5**,** 489-490.

EGE, M., MA, Y., MANFRAS, B., KALWAK, K., LU, H., LIEBER, M., SCHWARZ, K. & PANNICKE, U. (2005) Omenn syndrome due to Artemis mutations. *Blood,* 105**,** 4179-4186.

ESPEJEL, S. & BLASCO, M. (2002) Identification of telomere-dependent "Senescence-like" arrest in mouse embryonic fibroblasts. *Exp. Cell Res.,* 276**,** 242-248.

ESPEJEL, S., FRANCO, S., RODRIGUEZ-PERALES, S., BOUFFLER, S., CIGUDOSA, J. & BLASCO, M. (2002a) Mammalian Ku86 mediates chromosomal fusions and apoptosis caused by critically short telomeres. *EMBO J.,* 21**,** 2207-2219.

ESPEJEL, S., FRANCO, S., SGURA, A., GAE, D., BAILEY, S., TACCIOLI, G. & BLASCO, M. (2002b) Functional interaction between DNA-PKcs and telomerase in telomere length maintenance. *EMBO J.,* 21**,** 6275-6287.

EVANS, P., WOODBINE, L., RIBALLO, E., GENNERY, A., HUBANK, M. & JEGGO, P. (2006) Radiation-induced delayed cell death in a hypomorphic Artemis cell line. *Hum. Mol. Genet.,* 15**,** 1303-1311.

FERNANDEZ-CAPETILLO, O., CELESTE, A. & NUSSENZWEIG, A. (2003) Focusing on foci: H2AX and the recruitment of DNA-damage response factors. *Cell Cycle,* 2**,** 426-427.

FIRE, A., XU, S., MONTGOMERY, M., KOSTAS, S., DRIVER, S. & MELLO, C. (1998) Potent and specific genetic interference by double-stranded RNA in Caenorhabditis elegans. *Nature,* 391**,** 806-811.

FISHER, TS. and Zakian VA. (2005) Ku: a multifunctional protein involved in telomere maintenance. *DNA Repair,* 4, 1215-1256.

FRANCO, S., MURPHY, M., LI, G., BORJESON, T., BOBOILA, C. & ALT, F. (2008) DNA-PKcs and Artemis function in the end-joining phase of immunoglobulin heavy chain class switch recombination. *J. Exp. Med.,* 205**,** 557-564.

GARCIA-CAO, M., O'SULLIVAN, R., PETERS, A., JENUWEIN, T. & BLASCO, M. (2004) Epigenetic regulation of telomere length in mammalian cells by the Suv39h1 and Suv39h2 histone methyltransferases. *Nat. Genet.,* 36**,** 94-99.

GHILDIYAL, M. & ZAMORE, P. (2009) Small silencing RNAs: an expanding universe. *Nat. Rev. Genet.,* 10**,** 94-108.

GILSON, E. & GELI, V. (2007) How telomeres are replicated. *Nat. Rev. Mol. Cell Biol.,* 8**,** 825-838.

GONZALO, S., GARCIA-CAO, M., FRAGA, M., SCHOTTA, G., PETERS, A., COTTER, S., EGUIA, R., DEAN, D., ESTELLER, M., JENUWEIN, T. & BLASCO, M. (2005) Role of the RB1 family in stabilizing histone methylation at constitutive heterochromatin. *Nat. Cell Biol.,* 7**,** 420-428.

GOODARZI, A., NOON, A., DECKBAR, D., ZIV, Y., SHILOH, Y., LÖBRICH, M. & JEGGO, P. (2008) ATM signaling facilitates repair of DNA double-strand breaks associated with heterochromatin. *Molecular Cell,* 31**,** 167-177.

GOYTISOLO, F., SAMPER, E., EDMONSON, S., TACCIOLI, G. & BLASCO, M. (2001) The Absence of the DNA-dependent protein kinase catalytic subunit in mice results in anaphase bridges and in increased telomeric fusions with normal telomere length and G-strand overhang. *Mol. Cell. Biol.,* 21**,** 3642-3651.

GREIDER, C. & BLACKBURN, E. (1985) Identification of a specific telomere terminal transferase activity in tetrahymena extracts. *Cell,* 43**,** 405-413.

GRIFFIN, C. & THACKER, J. (2004) The role of homologous recombination repair in the formation of chromosome aberrations. *Cytogenetic & Genome Research,* 104**,** 21-27.

GRIFFITH, J., COMEAU, L., ROSENFIELD, S., STANSEL, R., BIANCHI, A., MOSS, H. & DE LANGE, T. (1999) Mammalian telomeres end in a large duplex loop. *Cell,* 97**,** 503-514.

GRUNSTEIN, M. (1992) Histones as regulators of genes. *Scientific American,* 267**,** 68-74.

GUO, X., DENG, Y., LIN, Y., COSME-BLANCO, W., CHAN, S., HE, H., YUAN, G., BROWN, E. & CHANG, S. (2007) Dysfunctional telomeres activate an ATM-ATR-dependent DNA damage response to suppress tumorigenesis. *EMBO J.,* 26**,** 4709-4719.

HANDE, M., BALAJEE, A., TCHIRKOV, A., WYNSHAW-BORIS, A. & LANSDORP, P. (2001) Extra-chromosomal telomeric DNA in cells from Atm-/- mice and patients with ataxia-telangiectasia. *Hum. Mol. Genet.,* 10**,** 519-528.

HANDE, M., SLIJEPCEVIC, P., SILVER, A., BOUFFLER, S., VAN BUUL, P., BRYANT, P. & LANSDORP, P. (1999) Elongated telomeres in scid mice. *Genomics,* 56**,** 221-223.

HARLEY , C., BA., F. & GREIDER, C. (1990) Telomeres shorten during ageing of human fibroblasts. *Nature,* 345**,** 458-460.

HERBIG, U., JOBLING, W., CHEN, B., CHEN, D. & SEDIVY, J. (2004) Telomere shortening triggers senescence of human cells through a pathway involving ATM, p53, and p21CIP1, but Not p16INK4a. *Cell,* 14**,** 501-513.

HSU, H., GILLEY, D., BLACKBURN, E. & CHEN, D. (1999) Ku is associated with the telomere in mammals. *Proc. Natl. Acad. Sci. (USA),* 96**,** 12454-12458.

HSU, H., GILLEY, D., GALANDE, S., HANDE, M., ALLEN, B., KIM, S., LI, G., CAMPISI, J., KOHWI-SHIGEMATSU, T. & CHEN, D. (2000) Ku acts in a unique way at the mammalian telomere to prevent end joining. *Genes & Development,* 14**,** 2807-2812.

HUDA, N., TANAKA, H., MENDONCA, M. & GILLEY, D. (2009) DNA damage-induced phosphorylation of TRF2 is required for the fast pathway of DNA double-strand break repair. *Mol. Cell. Biol.,* 29**,** 3597-3604.

HUFFMAN, K., LEVENE, S., TESMER, V., SHAY, J. & WRIGHT, W. (2000) Telomere shortening is proportional to the size of the G-rich telomeric 3'-overhang. *J. Biol. Chem.,* 275**,** 19719-19722.

HULTDIN, M., GRONLUND, E., NORRBACK, K., ERIKSSON-LINDSTROM, E., JUST, T. & ROOS, G. (1998) Telomere analysis by fluorescence in situ hybridization and flow cytometry. *Nucl. Acids Res.,* 26**,** 3651-3656.

HUPPI, K., MARTIN, S. & CAPLEN, N. (2005) Defining and assaying RNAi in mammalian cells. *Mol. Cell,* 17**,** 1-10.

IWABUCHI, K., HASHIMOTO, M., MATSUI, T., KURIHARA, T., SHIMIZU, H., ADACHI, N., ISHIAI, M., YAMAMOTO, K., TAUCHI, H., TAKATA, M., KOYAMA, H. & DATE, T. (2006) 53BP1 contributes to survival of cells irradiated with X-ray during G1 without Ku70 or Artemis. *Genes to Cells,* 11**,** 935-948.

JACO, I., MUNOZ, P., GOYTISOLO, F., WESOLY, J., BAILEY, S., TACCIOLI, G. & BLASCO, M. (2003) Role of mammalian Rad54 in telomere length maintenance. *Mol. Cell. Biol.,* 23**,** 5572-5580.

JANEWAY, C. A., TRAVERS, P., WALPORT, M. & SHLOMCHIK, M. (2004) *ImmunoBiology,* New York, Garland Science.

JAWORSKA, A., SZUMIEL, I., DE ANGELIS, P., OLSEN, G. & REITAN, J. (2001) Evaluation of ionizing radiation sensitivity markers in a panel of lymphoid cell lines. *Int. J. Radiat. Biol.,* 77**,** 269 - 280.

JEGGO, P. (1997) DNA-PK: at the cross-roads of biochemistry and genetics. *Mutation Research/DNA Repair,* 384**,** 1-14.

JEGGO, P. & LÖBRICH, M. (2005) Artemis links ATM to double strand break rejoining. *Cell Cycle,* 4**,** 359-362.

JHAPPAN, C., MORSE, H., FLEISCHMANN, R., GOTTESMAN, M. & MERLINO, G. (1997) DNA-PKcs: a T-cell tumour suppressor encoded at the mouse scid locus. *Nat. Genet.,* 17**,** 483-486.

KARLSEDER, J., HOKE, K., MIRZOEVA, O., BAKKENIST, C., KASTAN, M., PETRINI, J. & DE LANGE, T. (2004) The telomeric protein TRF2 binds the ATM kinase and can inhibit the ATM-dependent DNA damage response. *PLoS Biol.,* 2**,** e240.

KIM, S., BEAUSEJOUR, C., DAVALOS, A., KAMINKER, P., HEO, S. & CAMPISI, J. (2004) TIN2 mediates functions of TRF2 at human telomeres. *J. Biol. Chem.,* 279**,** 43799-43804.

KINNER, A., WU, W., STAUDT, C. & ILIAKIS, G. (2008) gammaH2AX in recognition and signaling of DNA double-strand breaks in the context of chromatin. *Nucl. Acids Res.,* 36**,** 5678-5694.

KIPLING, D., WYNFORD-THOMAS, D., JONES, C., AKBAR, A., ASPINALL, R., BACCHETTI, S., BLASCO, M., BROCCOLI, D., DEPINHO, R., EDWARDS, D., EFFROS, R., HARLEY, C., LANSDORP, P., LINSKENS, M., PROWSE, K., NEWBOLD, R., OLOVNIKOV, A., PARKINSON, E., PAWELEC, G., PONTEN, J., SHALL, S., ZIJLMANS, M. & FARAGHER, R. (1999) Telomere-dependent senescence. *Nat. Biotech.,* 17**,** 313-313.

KOBAYASHI, N., AGEMATSU, K., SUGITA, K., SAKO, M., NONOYAMA, S., YACHIE, A., KUMAKI, S., TSUCHIYA, S., OCHS, H., SUGITA, K., FUKUSHIMA, Y. & KOMIYAMA, A. (2003) Novel Artemis gene mutations of radiosensitive severe combined immunodeficiency in Japanese families. *Human Genetics,* 112**,** 348-352.

KOIKE, M. & KOIKE, A. (2005) The Ku70-binding site of Ku80 is required for the stabilization of Ku70 in the cytoplasm, for the nuclear translocation of Ku80, and for Ku80-dependent DNA repair. *Experimental Cell Research,* 305**,** 266-276.

KREMPLER, A., DECKBAR, D., JEGGO, P. & LOBRICH, M. (2007) An imperfect G2M checkpoint contributes to chromosome instability following irradiation of S and G2 phase cells. *Cell Cycle,* 6**,** 1682-1686.

KRUK, P., RAMPINO, N. & BOHR, V. (1995) DNA damage and repair in telomeres: relation to aging. *Proc. Natl. Acad. Sci.,* 93**,** 258-262.

KUHNE, M., RIBALLO, E., RIEF, N., ROTHKAMM, K., JEGGO, P. & LOBRICH, M. (2004) A double-strand break repair defect in ATM-deficient cells contributes to radiosensitivity. *Cancer Research,* 64**,** 500-508.

LANSDORP, P., VERWOERD, N., VAN DE RIJKE, F., DRAGOWSKA, V., LITTLE, M., DIRKS, R., RAAP, A. & TANKE, H. (1996) Heterogeneity in telomere length of human chromosomes. *Hum. Mol. Genet.,* 5**,** 685-691.

LEES-MILLER, S. P., GODBOUT, R., CHAN, D. W., WEINFELD, M., DAY, R. S., 3RD, BARRON, G. M. & ALLALUNIS-TURNER, J. (1995) Absence of p350 subunit of DNA-activated protein kinase from a radiosensitive human cell line. *Science,* 267**,** 1183-1185.

LENAIN, C., BAUWENS, S., AMIARD, S., BRUNORI, M., GIRAUD-PANIS, M.-J. P. & GILSON, E. (2006) The Apollo 52 Exonuclease Functions Together with TRF2 to Protect Telomeres from DNA Repair. *Cell,* 16**,** 1303-1310.

LI, B., OESTREICH, S. & DE LANGE, T. (2000) Identification of Human Rap1: Implications for Telomere Evolution. *Cell,* 101**,** 471-483.

LI, L., MOSHOUS, D., ZHOU, Y., WANG, J., XIE, G., SALIDO, E., HU, D., DE VILLARTAY, J.-P. & COWAN, M. J. (2002a) A Founder Mutation in Artemis, an SNM1-Like Protein, Causes SCID in Athabascan-Speaking Native Americans. *J Immunol,* 168**,** 6323-6329.

LI, L., ZHOU, Y., WANG, J., HU, D. & COWAN, M. (2002b) Prenatal diagnosis and carrier detection for Athabascan severe combined immunodeficiency disease. *Prenatal Diagnosis,* 22**,** 763-768.

LIEBER, M. (2008) The mechanism of human nonhomologous DNA end joining. *J. Biol. Chem.,* 283**,** 1-5.
LOBRICH, M. & JEGGO, P. (2005) The two edges of the ATM sword: Co-operation between repair and checkpoint functions. *Radiother. Oncol. ,* 76**,** 112-118.
LOBRICH, M. & JEGGO, P. (2007) The impact of a negligent G2/M checkpoint on genomic instability and cancer induction. *Nat. Rev. Cancer,* 7**,** 861-869.
LU, H., SCHWARZ, K. & LIEBER, M. (2007) Extent to which hairpin opening by the Artemis:DNA-PKcs complex can contribute to junctional diversity in V(D)J recombination. *Nucl. Acids Res.,* 35**,** 6917-6923.
MA, Y., LU, H., TIPPIN, B., GOODMAN, M., SHIMAZAKI, N., KOIWAI, O., HSIEH, C., SCHWARZ, K. & LIEBER, M. (2004) A biochemically Ddefined system for mammalian nonhomologous DNA end joining. *Cell,* 16**,** 701-713.
MA, Y., PANNICKE, U., LU, H., NIEWOLIK, D., SCHWARZ, K. & LIEBER, M. (2005a) The DNA-dependent protein kinase catalytic subunit phosphorylation sites in human Artemis. *J. Biol. Chem.,* 280**,** 33839-33846.
MA, Y., PANNICKE, U., SCHWARZ, K. & LIEBER, M. (2002) Hairpin opening and overhang processing by an Artemis/DNA-dependent protein kinase complex in nonhomologous end joining and V(D)J recombination. *Cell,* 108**,** 781-794.
MA, Y., SCHWARZ, K. & LIEBER, M. (2005b) The Artemis:DNA-PKcs endonuclease cleaves DNA loops, flaps, and gaps. *DNA Repair,* 4**,** 845-851.
MAKAROV, V., HIROSE, Y. & LANGMORE, J. (1997) Long G tails at both ends of human chromosomes suggest a C strand degradation mechanism for telomere shortening. *Cell,* 88**,** 657-666.
MARTÍNEZ, P., THANASOULA, M., MUÑOZ, P., LIAO, C., TEJERA, A., MCNEES, C., FLORES, J., FERNÁNDEZ-CAPETILLO, O., TARSOUNAS, M. & BLASCO, M. (2009) Increased telomere fragility and fusions resulting from TRF1 deficiency lead to degenerative pathologies and increased cancer in mice. *Genes & Development,* 23**,** 2060-75.
MASUTOMI, K., YU, E., KHURTS, S., BEN-PORATH, I., CURRIER, J., METZ, G., BROOKS, M., KANEKO, S., MURAKAMI, S., DECAPRIO, J., WEINBERG, R., STEWART, S. & HAHN, W. (2003) Telomerase maintains telomere structure in normal human cells. *Cell,* 114**,** 241-253.
MATULI, M., SOPTA, M. & RUBELJ, I. (2007) Telomere dynamics: the means to an end. *Cell Proliferation,* 40**,** 462-474.
MCCLINTOCK, B. (1941) The stability of broken ends of chromosomes in *Zea mays*. *Genetics,* 26**,** 234-282.
MCILRATH, J., BOUFFLER, S., SAMPER, E., CUTHBERT, A., WOJCIK, A., SZUMIEL, I., BRYANT, P., RICHES, A., THOMPSON, A., BLASCO, M., NEWBOLD, R. & SLIJEPCEVIC, P. (2001) Telomere length abnormalities in mammalian radiosensitive cells. *Cancer Research,* 61**,** 912-915.
MCVEY, M. & LEE, S. (2008) MMEJ repair of double-strand breaks (director's cut): deleted sequences and alternative endings. *Trends in Genetics,* 24**,** 529-538.
MOSHOUS, D., CALLEBAUT, I., DE CHASSEVAL, R., CORNEO, B., CAVAZZANA-CALVO, M., LE DEIST, F., TEZCAN, I., SANAL, O., BERTRAND, Y., PHILIPPE, N., FISCHER, A. & DE VILLARTAY, J.-P. (2001) Artemis, a novel DNA double-strand break repair/V(D)J recombination protein, is mutated in human severe combined immune deficiency. *Cell,* 105**,** 177-186.
MOSHOUS, D., LI, L., CHASSEVAL, R., PHILIPPE, N., JABADO, N., COWAN, M., FISCHER, A. & DE VILLARTAY, J.-P. (2000) A new gene involved in DNA

double-strand break repair and V(D)J recombination is located on human chromosome 10p. *Hum. Mol. Genet.,* 9**,** 583-588.

MOYZIS, R. K., BUCKINGHAM, J. M., CRAM, L., DANI, M., DEAVEN, L., JONES, M., MEYNE, J., RATLIFF, R. & WU, J. (1988) A highly conserved repetitive DNA sequence, (TTAGGG)n, present at the telomeres of human chromosomes. *Proceedings of the National Academy of Sciences of the United States of America,* 85**,** 6622-6626.

MULLER, H. J. (1938) The remaking of chromosomes. *Collecting Net,* 8**,** 182-195.

MUSIO, A., MARRELLA, V., SOBACCHI, C., RUCCI, F., FARISELLI, L., GILIANI, S., LANZI, G., NOTARANGELO, L., DELIA, D., COLOMBO, R., VEZZONI, P. & VILLA, A. (2005) Damaging-agent sensitivity of Artemis-deficient cell lines. *Eur. J. Immunol.,* 35**,** 1250-1256.

NEWBOLD, R. (1997) Genetic controls of telomerase and replicative senescence in human and rodent cells. *Ciba found. Symp.,* 211**,** 177-189.

NIEWOLIK, D., PANNICKE, U., LU, H., MA, Y., WANG, L., KULESZA, P., ZANDI, E., LIEBER, M. & SCHWARZ, K. (2006) DNA-PKcs dependence of Artemis endonucleolytic activity, differences between hairpins and 5' or 3' overhangs. *J. Biol. Chem.,* 281**,** 33900-33909.

NOORDZIJ, J., VERKAIK, N., VAN DER BURG, M., VAN VEELEN, L., DE BRUIN-VERSTEEG, S., WIEGANT, W., VOSSEN, J., WEEMAES, C., DE GROOT, R., ZDZIENICKA, M., VAN GENT, D. & VAN DONGEN, J. (2003) Radiosensitive SCID patients with Artemis gene mutations show a complete B-cell differentiation arrest at the pre-B-cell receptor checkpoint in bone marrow. *Blood,* 101**,** 1446-1452.

O'DRISCOLL, M. & JEGGO, P. (2005) The role of double-strand break repair - insights from human genetics. *Nat. Rev. Genet.,* 7**,** 45-54.

OBE, G., PFEIFFER, P., SAVAGE, J., JOHANNES, C., GOEDECKE, W., JEPPESEN, P., NATARAJAN, A., MARTÍNEZ-LÓPEZ, W., FOLLE, G. & DRETS, M. (2002) Chromosomal aberrations: formation, identification and distribution. *Mutation Research/Fundamental and Molecular Mechanisms of Mutagenesis,* 504**,** 17-36.

OLOVNIKOV, A. (1973) A theory of marginotomy : The incomplete copying of template margin in enzymic synthesis of polynucleotides and biological significance of the phenomenon. *Journal of Theoretical Biology,* 41**,** 181-190.

OPRESKO, P., VON KOBBE, C., LAINE, J., HARRIGAN, J., HICKSON, I. & BOHR, V. (2002) Telomere-binding protein TRF2 binds to and stimulates the Werner and Bloom Syndrome helicases. *J. Biol. Chem.,* 277**,** 41110-41119.

PENG, Y., ZHANG, Q., NAGASAWA, H., OKAYASU, R., LIBER, H. & BEDFORD, J. (2002) Silencing expression of the catalytic subunit of DNA-dependent protein kinase by small interfering RNA sensitizes human cells for radiation-induced chromosome damage, cell killing, and mutation. *Cancer Research,* 62**,** 6400-6404.

POINSIGNON, C., MOSHOUS, D., CALLEBAUT, I., DE CHASSEVAL, R., VILLEY, I. & DE VILLARTAY, J.-P. (2004a) The Metallo-beta-lactamase/beta-CASP domain of Artemis constitutes the catalytic core for V(D)J recombination. *J. Exp. Med.,* 199**,** 315-321.

POINSIGNON, C., MOSHOUS, D., CALLEBAUT, I., DE CHASSEVAL, R., VILLEY, I. & DE VILLARTAY, J.-P. (2004b) Phosphorylation of Artemis following irradiation-induced DNA damage. *Eur. J. Immunol.,* 34**,** 3146-3155.

POWELL, S. & KACHNIC, L. (2003) Roles of BRCA1 and BRCA2 in homologous recombination, DNA replication fidelity and the cellular response to ionizing radiation. *Oncogene,* 22**,** 5784-5791.

RIBALLO, E., KOHNE, M., RIEF, N., DOHERTY, A., SMITH, G., RECIO, M., REIS, C., DAHM, K., FRICKE, A., KREMPLER, A., PARKER, A., JACKSON, S., GENNERY, A., JEGGO, P. & LOBRICH, M. (2004) A pathway of double-strand break rejoining dependent upon ATM, Artemis, and proteins locating to gamma-H2AX Foci. *Cell,* 16**,** 715-724.

ROONEY, S., ALT, F., LOMBARD, D., WHITLOW, S., ECKERSDORFF, M., FLEMING, J., FUGMANN, S., FERGUSON, D., SCHATZ, D. & SEKIGUCHI, J. (2003) Defective DNA repair and increased genomic instability in Artemis-deficient murine cells. *J. Exp. Med.,* 197**,** 553-565.

ROONEY, S., SEKIGUCHI, J., ZHU, C., CHENG, H., MANIS, J., WHITLOW, S., DEVIDO, J., FOY, D., CHAUDHURI, J., LOMBARD, D. & ALT, F. (2002) Leaky scid phenotype associated with defective V(D)J coding end processing in Artemis-deficient mice. *Molecular Cell,* 10**,** 1379-1390.

ROTHKAMM, K., KUHNE, M., JEGGO, P. & LOBRICH, M. (2001) Radiation-induced genomic rearrangements formed by nonhomologous end-joining of DNA double-strand breaks. *Cancer Research,* 61**,** 3886-3893.

ROTHKAMM, K. & LOBRICH, M. (2003) Evidence for a lack of DNA double-strand break repair in human cells exposed to very low x-ray doses. *Proc. Natl. Acad. Sci. (USA),* 100**,** 5057-5062.

RUFER, N., DRAGOWSKA, W., THORNBURY, G., ROOSNEK, E. & LANSDORP, P. (1998) Telomere length dynamics in human lymphocyte subpopulations measured by flow cytometry. *Nat. Biotech.,* 16**,** 743-747.

SAMPER, E., GOYTISOLO, F. A., SLIJEPCEVIC, P., VAN BUUL, P. P. W. & BLASCO, M. A. (2000) Mammalian Ku86 protein prevents telomeric fusions independently of the length of TTAGGG repeats and the G-strand overhang. *EMBO reports,* 1**,** 244.

SARETZKI, G., SITTE, N., MERKEL, U., WURM, R. & VON ZGLINICKI, T. (1999) Telomere shortening triggers a p53-dependent cell cycle arrest via accumulation of G-rich single stranded DNA fragments. *Oncogene,* 18**,** 5148-5158.

SCHOEFTNER, S. & BLASCO, M. (2009) A 'higher order' of telomere regulation: telomere heterochromatin and telomeric RNAs. *EMBO J.,* 28**,** 2323-2336.

SEKIGUCHI, J. & FERGUSON, D. (2006) DNA double-strand break repair: A relentless hunt uncovers new prey. *Cell,* 124**,** 260-262.

SFEIR, A., KOSIYATRAKUL, S., HOCKEMEYER, D., MACRAE, S., KARLSEDER, C., SCHILDKRAUT & DE LANGE, T. (2009) Mammalian telomeres resemble fragile sites and require TRF1 for efficient replication. *Cell,* 138**,** 90-103.

SHILOH, Y. (2003) ATM and related protein kinases: safeguarding genome integrity. *Nat Rev Cancer,* 3**,** 155-168.

SLIJEPCEVIC, P. (1998) Telomeres and mechanisms of Robertsonian fusion. *Chromosoma,* 107**,** 136-140.

SLIJEPCEVIC, P. (2006) The role of DNA damage response proteins at telomeres--an "integrative" model. *DNA Repair,* 5**,** 1299-1306.

SLIJEPCEVIC, P. (2008) DNA damage response, telomere maintenance and ageing in light of the integrative model. *Mech. Ageing Dev.,* 129**,** 11-16.

SLIJEPCEVIC, P., XIAO, Y., DOMINGUEZ, I. & NATARAJAN, A. (1996) Spontaneous and radiation-induced chromosomal breakage at interstitial telomeric sites. *Chromosoma,* 104**,** 596-604.
SMITH, S. & DE LANGE, T. (2000) Tankyrase promotes telomere elongation in human cells. *Current Biology,* 10**,** 1299-1302.
SMITH, S., GIRIAT, I., SCHMITT, A. & DE LANGE, T. (1998) Tankyrase, a Poly(ADP-Ribose) polymerase at human telomeres. *Science,* 282**,** 1484-1487.
SONG, K., JUNG, D., JUNG, Y., LEE, S. & LEE, I. (2000) Interaction of human Ku70 with TRF2. *FEBS Letters,* 481**,** 81-85.
SOUBEYRAND, S., POPE, L., DE CHASSEVAL, R., GOSSELIN, D., DONG, F., DE VILLARTAY, J.-P. & HACHÉ, R. (2006) Artemis phosphorylated by DNA-dependent protein kinase associates preferentially with discrete regions of chromatin. *Journal Molecular Biology,* 358**,** 1200-1211.
STIFF, T., O'DRISCOLL, M., RIEF, N., IWABUCHI, K., LOBRICH, M. & JEGGO, P. (2004) ATM and DNA-PK function redundantly to phosphorylate H2AX after exposure to ionizing radiation. *Cancer Research,* 64**,** 2390-2396.
SUMPTION, N., GOODHEAD, D. & ANDERSON, R. (2006) No increase in radiation-induced chromosome aberration complexity detected by m-FISH after culture in the presence of 5'-bromodeoxyuridine. *Mutation Research/Fundamental and Molecular Mechanisms of Mutagenesis,* 594**,** 30-38.
TAKAI, H., SMOGORZEWSKA, A. & DE LANGE, T. (2003) DNA damage foci at dysfunctional telomeres. *Cell,* 13**,** 1549-1556.
TAKATA, H., KANOH, Y., GUNGE, N., SHIRAHIGE, K. & MATSUURA, A. (2004) Reciprocal association of the budding Yeast ATM-related proteins Tel1 and Mec1 with telomeres in-vivo. *Molecular Cell,* 14**,** 515-522.
TOMMERUP, H., DOUSMANIS, A. & DE LANGE, T. (1994) Unusual chromatin in human telomeres. *Mol. Cell. Biol.,* 14**,** 5777-5785.
TOUVREY, C., COUEDEL, C., SOULAS, P., COUDERC, R., JASIN, M., DE VILLARTAY, J.-P., MARCHE, P., JOUVIN-MARCHE, E. & CANDÉIAS, S. (2008) Distinct effects of DNA-PKcs and Artemis inactivation on signal joint formation in vivo. *Molecular Immunology,* 45**,** 3383-3391.
URUSHIBARA, A., KODAMA, S., SUZUKI, K., DESA, M., SUZUKI, F., TSUTSUI, T. & WATANABE, M. (2004) Involvement of telomere dysfunction in the induction of genomic instability by radiation in scid mouse cells. *Biochemical and Biophysical Research Communications,* 313**,** 1037-1043.
VAN DER BURG, M. (2009) A DNA-PKcs mutation in a radiosensitive T-B SCID patient inhibits Artemis activation and nonhomologous end-joining. *The Journal of Clinical Investigation,* 119**,** 91-98.
VAN OVERBEEK, M. & DE LANGE, T. (2006) Apollo, an Artemis-related nuclease, interacts with TRF2 and protects human telomeres in S-phase. *Cell,* 16**,** 1295-1302.
VERDUN, R., CRABBE, L., HAGGBLOM, C. & KARLSEDER, J. (2005) Functional human telomeres are recognized as DNA damage in G2 of the cell cycle. *Molecular Cell,* 20**,** 551-561.
VILENCHIK, M. & KNUDSON, A. (2006) Radiation dose-rate effects, endogenous DNA damage, and signaling resonance. *Proc. Natl. Acad. Sci.,* 103**,** 17874-17879.

WANG, J., PLUTH, J., COOPER, P., COWAN, M., CHEN, D. & YANNONE, S. (2005) Artemis deficiency confers a DNA double-strand break repair defect and Artemis phosphorylation status is altered by DNA damage and cell cycle progression. *DNA Repair,* 4**,** 556-570.

WATSON, J. (1972) Origin of concatemeric T7 DNA. *Nature New Biology,* 239**,** 197-201.

WILLIAMS, E., KLINGLER, R., PONNAIYA, B., HARDT, T., SCHROCK, E., LEES-MILLER, S., MEEK, K., ULLRICH, R. & BAILEY, S. (2009) Telomere dysfunction and DNA-PKcs deficiency: characterization and consequence. *Cancer Research,* 69**,** 2100-2107.

WLODEK, D. & HITTELMAN, W. (1987) The repair of double-strand DNA breaks correlates with radiosensitivity of L5178Y-S and L5178Y-R cells. *Radiation Research,* 115**,** 566-575.

WONG, H. & SLIJEPCEVIC, P. (2004) Telomere length measurement in mouse chromosomes by a modified Q-FISH method. *Cytogenetics and Genome Research,* 105**,** 464-470.

WRIGHT, W., TESMER, V., HUFFMAN, K., LEVENE, S. & SHAY, J. (1997) Normal human chromosomes have long G-rich telomeric overhangs at one end. *Genes & Development,* 11**,** 2801-2809.

YE, J., HOCKEMEYER, D., KRUTCHINSKY, A., LOAYZA, D., HOOPER, S., CHAIT, B. & DE LANGE, T. (2004) POT1-interacting protein PIP1: a telomere length regulator that recruits POT1 to the TIN2/TRF1 complex. *Genes & Development,* 18**,** 1649-1654.

ZHANG, X., ZHU, Y., GENG, L., WANG, H. & LEGERSKI, R. J. (2009) Artemis is a negative regulator of p53 in response to oxidative stress. *Oncogene,* 28**,** 2196-204.

ZHANG, Y., ZHOU, J., CAO, X., ZHANG, Q., LIM, C. U. K., ULLRICH, R. L., BAILEY, S. M. & LIBER, H. L. (2007) Partial deficiency of DNA-PKcs increases ionizing radiation-induced mutagenesis and telomere instability in human cells. *Cancer letters,* 250**,** 63-73.

Appendix I

Table 3.3. Detail of CA experiments.
Two sets of experiments were carried out using Giemsa stained techniques. In each experiment at least 100 metaphases were analysed whenever possible.

Cytological Analysis	**Metaphase cells analyzed**
Experiment 1	759
Experiment 2	637
Total	1396

Table 3.4. Summary of spontaneous and induced chromosomal aberration Experiments using Telo-*FISH*.

		Metaphase cells Analysed
Experiment 1	Spontaneous	478
Experiment 2	Radiation Induced (0.5Gy and 1.0 Gy)	401
Experiment 3	Radiation Induced (0.5Gy and 1.0 Gy)	450
Experiment 4	Radiation Induced (0.5Gy and 1.0 Gy)	317
	Total:	1646 Metaphase Cells Analyzed

Table 4.4. Summary of Experiments on early passage cell lines induced with 1.0Gy of gamma radiation.

Name of Experiment	**Irradiation dose (Gy)**	**Repair Time (in Hour)**	**Cell lines and PD**	**Number of cells scored/cell line**
Experiment 1	1.0	0.5, 5, 24	CJ179 (PD16), F01-240 (PD12), GM08399 (PD16)	100 cells/point
Experiment 2	1.0	0.5, 5, 24	CJ179 (PD21, PD16), GM08399 (PD27, PD16)	100 cells/point

Table 5.11. TIF assay on DNA-PKcs inhibited Artemis and normal human primary cell lines induced with 1.0Gy of gamma radiation.

Cell line	Experiment Number	PD	Radiation dose and repair time point	Cell counts
GM08399 (WT)	1	16	1.0Gy 0.5hr, 5hr, 24hr	80 cells/time point
CJ179 (Art)	1	17	1.0Gy 0.5hr, 5hr, 24hr	
F01-240 (Art)	1	13	1.0Gy 0.5hr, 5hr, 24hr, 48hr	
GM08399 (WT)	2	16	1.0Gy 0.5hr, 5hr, 24hr	80 cells/time point
CJ179 (Art)	2	17	1.0Gy 0.5hr, 5hr, 24hr	
F01-240 (Art)	2	13	1.0Gy 0.5hr, 5hr, 24hr, 48hr	
GM08399 (WT)	3	21	1.0Gy 0.5hr, 5hr, 24hr	100 cells/time point
CJ179 (Art)	3	16	1.0Gy 0.5hr, 5hr, 24hr	
F01-240 (Art)	3	17	1.0Gy 0.5hr, 5hr, 24hr	

Table 6.6.Quantification of GAPDH mRNA knock-down.

Cell lines	Endogenous *GAPDH* Ct	Target *GAPDH* Ct	ΔCt	ΔCt SD	Cell Viability % (SD)
GM08399					
Control	21.88	21.85	0		97.5% (±0.95)
3 Days	21.76	21.66	-0.100	0.140	97% (±0.95)
5 Days	21.70	24.47	2.760	0.130	98% (±0.5)
7 Days	21.75	21.65	-0.100	0.050	98% (±0.5)
Scrambled	21.85	20.53	-1.320	0.060	99% (±0.5)
CJ179					
Control			-0.151		
3 Days			-0.207		
5 Days			2.160		
7 Days			0.741		
Scrambled					
F01-240					
Control					
3 Days			-0.431	0.150	
5 Days			4.067	0.170	
7 Days			5.218	0.146	
Scrambled			-1.144	0.139	

Appendix II

The conversion of the telomere fluorescence intensity (TFI) unit into base pairs was performed using the established formula y= 4.13 X + 2.56; where X=TFI (R^2 = 1)(Cabuy et al., 2004). This formula is based on correlation studies using the Q-FISH technique to measure telomere length and has previously been shown to be a valid formula in converting TFI units into base pairs when measuring telomere length using Flow-FISH (Cabuy et al., 2004, McIlrath et al., 2001).